LOADING AND RELEASE OF LARGE PROTEIN MOLECULES AND SEPARATION OF LANTHANIDES USING MESOPOROUS MATERIALS

By

Gauri Deodhar

A thesis submitted to the Faculty and the Board of Trustees of the Colorado School of Mines in partial fulfillment of the requirements for the degree of Doctor of Philosophy (Applied Chemistry).

Golden, Colorado

Date: _____

Signed: _____

Gauri V Deodhar

Signed: _____

Dr. Brian Trewyn
Thesis Advisor

Golden, Colorado

Date: _____

Signed: _____

Dr. Tom Gennett
Professor and Head
Department of Chemistry

ABSTRACT

Protein therapeutics are promising candidates for disease treatment due to their high specificity and minimal adverse side effects; however, targeted protein delivery to specific sites has proven challenging. Mesoporous silica nanoparticles (MSN) have demonstrated to be ideal candidates for this application, given their high loading capacity, biocompatibility, and ability to protect host molecules from degradation. These materials exhibit tunable pore sizes, shapes and volumes, and surfaces which can be easily functionalized. This serves to control the movement of molecules in and out of the pores, thus entrapping guest molecules until a specific stimulus triggers release. The benefits of using MSN as protein therapeutic carriers will be covered, demonstrating that there is great diversity in the ways MSN can be used to service proteins. Methods for controlling the physical dimensions of pores via synthetic conditions, applications of therapeutic protein loaded MSN materials in cancer therapies, delivering protein loaded MSN materials to plant cells using biolistic methods, and common stimuli-responsive functionalities will be discussed. New and exciting strategies for controlled release of proteins will also be covered.

Mesoporous silica nanoparticles (MSN) with enlarged pores were prepared and characterized, and reversibly dissociated subunits of large protein molecules such Concanavalin A were entrapped in the mesopores, as shown by multiple biochemical and material characterizations. When loaded in the MSN, we demonstrated protein stability from proteases and, upon release, the subunits re-associated into active proteins. We have demonstrated a versatile and facile method to load homomeric proteins into MSN with potential applications in enhancing the delivery of large therapeutic proteins.

Similarly dissociated Yeast alcohol dehydrogenase (ADH) can be loaded into MSN and regain activity upon release. This shows our method can be extended to multi-subunit enzymes as well as proteins.

Adjacent lanthanides are among the most challenging elements to separate, to the extent that current separations materials would benefit from transformative improvement. Ordered mesoporous carbon (OMC) materials are excellent candidates, owing to their small mesh size and uniform morphology. Herein, two OMC materials were physisorbed with bis-(2-ethylhexyl) phosphoric acid (HDEHP) and the relationships between surface areas, pore sizes, and recovery performance were explored using a $^{152/154}$Eu radiotracer. The HDEHP-OMC materials displayed higher distribution coefficients and loading capacities than current state-of-the-art materials.

TABLE OF CONTENTS

LIST OF FIGURES AND SCHEMES

LIST OF TABLES

ACKNOWLEDGMENTS

I would like to convey appreciation to all my colleagues, families, friends and well-wishers who have contributed to the dissertation in some way or another. They have provided me the constant encouragement and support in completion of my dream of achieving the doctorate degree.

I am grateful to my family, my sister Dr. Chaitra Deodhar, my brother in-law Dr. Mihir Date; and in-laws, who supported me in every way to complete my doctorate degree. Living away from home was not easy, but their constant support and moral boosting made the experience even more enjoyable. I would also like to thank my friends and colleagues here who have always guided me throughout my doctorate and made the transition phase of my life smooth.

To Prof. Brian Trewyn, for his stellar support, guidance and constant challenging throughout the graduate years, for having confidence and allowing me the freedom to explore and research the complex topic of Mesoporous Silica Nanoparticles in my own way. I would like to thank him for his guidance both academic and personal, during this tough tenure.

To my thesis committee members, Prof. Mathew Posewitz, Prof. Jennifer Shafer, Prof. Melissa Krebbs for their invaluable time and support. I am also thankful to Prof. Alan Sellinger for allowing me to use multiple instruments in his laboratory.

To my group members Megan Otting, Marisa Adams, Dr. Malcom Davidson, Tabitha Evans for their help and support. Special thanks to Dr. Fiona Davies, for her guidance during my graduate degree.

Dedicated to my parents, Ashwini and Vasant Deodhar, and my husband Rounak Kharait without whom it would be impossible to be where I am. And to my nieces Reva and Myra – may you also chase your dreams as I did.

CHAPTER 1 GENERAL INTRODUCTION

Dissertation organization

The Trewyn group at Colorado School of Mines researches on the synthesis of multifunctional high surface area, and porous inorganic and organic materials. The research is applied in development for electrocatalysis, heterogeneous catalysis, drug delivery and controlled release of proteins. One of the areas of focus is synthesis and characterization of Mesoporous Silica Nanoparticles (MSN). This thesis focuses on loading and release of large therapeutic proteins using MSN as delivery vehicle.

Chapter 2 in this dissertation focuses on literature review of benefits of using MSN for protein delivery. The review provides guidance on the synthesis of MSN, the importance of functionalization, pore morphology and pore size for controlled release of proteins. This chapter also covers applications of therapeutic protein loaded MSN materials in cancer therapies, delivering protein loaded MSN to plant cells using biolistic methods, and common stimuli-responsive functionalities. This chapter has been published in the Biotechnology journal in December 2017. I was the first author, while Marisa Adams, who is currently a graduate student at Colorado School of Mines Department of Chemistry, was the co-author for the publication. Dr. Trewyn was the corresponding author.

Chapter 3 and Chapter 4 include synthesis of pore expanded MSN and its potential to deliver large molecular weight active proteins. These chapters further include loading and release of multi-subunit proteins using MSN. Dissociation of large proteins, loading of subunits onto MSN followed by their release and reconstitution into active form has been covered.

Specifically, Chapter 3 has been published in ACS Langmuir Journal, where I was the first author. Dr. Trewyn was the corresponding author.

Chapter 5 focuses on synthesis and characterization of ordered mesoporous carbon materials (OMC) using for f-element separations. HDEHP physisorbed OMC materials has confirmed their potential as solid-phase sorbents for f-element recovery and separation. This report suggests OMC-based materials have the ability to complete chromatographic, intragroup lanthanide separations and, in some instances, could perform better than state-of-the-art materials.

CHAPTER 2 CONTROLLED RELEASE AND INTRACELLULAR PROTEIN DELIVERY FROM MESOPOROUS SILICA NANOPARTICLES

Modified from a paper published in

Biotechnology Journal

Gauri Deodhar, Marisa Adams, Brian Trewyn

2.1. Abstract

Protein therapeutics are promising candidates for disease treatment due to their high specificity and minimal adverse side effects; however, targeted protein delivery to specific sites has proven challenging. Mesoporous silica nanoparticles (MSN) have been demonstrated to be ideal candidates for this application, given their high loading capacity, biocompatibility, and ability to protect host molecules from degradation. These materials exhibit tunable pore sizes, shapes and volumes, and surfaces which can be easily functionalized. This serves to control the movement of molecules in and out of the pores, thus entrapping guest molecules until a specific stimulus triggers release. In this review, we will cover the benefits of using MSN as protein therapeutic carriers, demonstrating that there is great diversity in the ways MSN can be used to service proteins. Methods for controlling the physical dimensions of pores via synthetic conditions, applications of therapeutic protein loaded MSN materials in cancer therapies, delivering protein loaded MSN materials to plant cells using biolistic methods, and common stimuli-responsive functionalities will be discussed. New and exciting strategies for controlled release and manipulation of proteins are also covered in this review. While research in this area has advanced substantially, we conclude this review with future challenges to be tackled by the scientific community.

2.2. Introduction

Within biological systems, proteins play key roles in the development, growth, and regulation of most metabolic systems in the human body.[1] Consequently, protein therapeutics, such as those used in the treatment of diabetes type I and II provided by insulin, are extremely beneficial treatments.[2] There are many advantages of protein therapeutics over traditional low molecular weight pharmaceuticals. For instance, proteins do not interfere with normal biological processes at the same frequency as small molecule drugs due to the high reaction specificity of proteins. Proteins also possess a high intracellular activity compared to low molecular weight drugs, making them prime candidates for disease treatment. In the case of diseases caused by gene mutation or deletion, protein therapeutics are safer than gene therapy because detrimental side effects like random and permanent genetic changes are rarely observed with protein therapy.[3] In spite of all these advantages, effective delivery of proteins to target sites is a monumental challenge.[3-4] Proteins are rapidly cleared from the body and chemically fragile, unable to survive high and low pH environments or denaturing enzymes (proteases). Ideally, proteins escape from the delivery vehicle during early stages of the endolysosomal pathway after the target cell internalizes the carrier. This prevents degradation by low pH and denaturing enzymes in the lysosomes.[3-5] Transporting drugs and molecules through cell membranes has recently been the topic of a substantial amount of research in the area of drug delivery and controlled release. Several different types of drug carriers or "vehicles" have been developed and investigated for this task including polymers, liposomes, dendrimers, and inorganic nanoparticles. One of the main functions of delivery vehicles in these systems is to protect proteins from premature degradation in a biological environment. Protein-loaded vehicles enter the cell through endocytosis, during which the protein-vehicle composite enters early endosomes, which become late endosomes. Late endosomes further mature into lysosomes to

form endolysomes, which are characterized by low pH. Degradation of the protein-vehicle composite typically occurs here if it is unable to escape from the endolysosomal entrapment. Once it escapes, it travels through the cytoplasm where the proteins are released from the vehicle to interact with its specific target.[3-4, 6-11] One type of inorganic nanoparticle that has been successfully applied as a controlled-release drug delivery system for intracellular protein delivery is mesoporous silica nanoparticle (MSN) materials.[4, 12] MSN materials are particularly useful in a wide range of biological applications due to their biocompatibility and biodegradability.[13] The silicon oxide matrix is stable under biological conditions and consists of a hexagonal array of mesopores of various sizes. These pores are able to take on host molecules, sheltering them from the external environment until such time as unloading conditions are met (Section 2.4). This functionality has proven particularly useful in the delivery of small drug molecules.[11] Alternatively, the hosts can take up permanent residence within the pores, making the particles catalytically active, as was demonstrated by Wu and coworkers.[14] Small proteins with hydrodynamic diameters less than the pore size can also be loaded and delivered;[15] however, the delivery of large molecular weight proteins remains an ongoing challenge. In this review, we will cover the benefits of utilizing MSN materials for protein therapeutic delivery, the methods by which MSN can be synthesized to accommodate proteins, strategies for controlled release of proteins, and cover instances where MSN were successfully used to deliver proteins, DNA, and enzymes.

2.3. Mesoporous silica nanoparticles: Ideal candidates for protein delivery

Protein delivery has been explored using a wide variety of materials. In 2005, delivery of a cell membrane-impermeable protein, cytochrome *c* (*Cyt c*), using single-walled carbon nanotubes

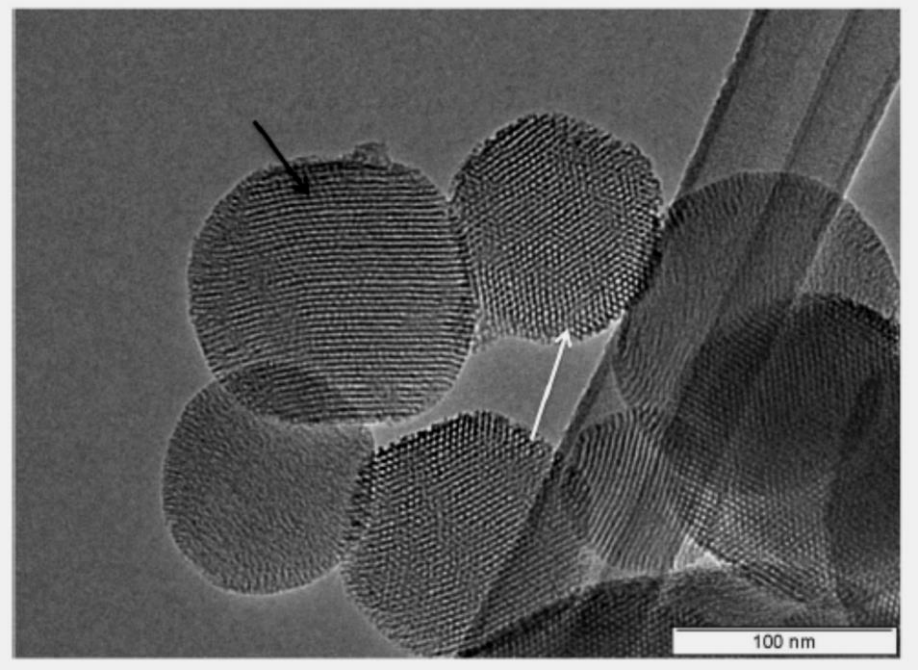

Figure 2.1 Transmission electron micrograph of MCM-41-type MSN materials. The honeycomb-like structure of the nanoparticles is visualized with the parallel stripes (black arrow) and the hexagonally packed pores visualized as light dots (white arrow)

was demonstrated by Kam et al. Though the protein-nanotube composite successfully entered the cells, as determined by confocal microscopy, they observed that it failed to escape the endolysosomes.[16] Thus, the protein was not delivered into the cytoplasm. The same year, Song et al. reported the controlled release of proteins using SBA-15 under non-physiological acidic conditions. Although these conditions are not applicable for intracellular delivery, this study demonstrated the potential of these mesoporous materials for protein delivery.[17] Mesoporous silica nanoparticle (MSN) materials are formed by condensation of silica around organic micelles, creating an ordered array of hexagonally arranged mesoporous channels with a spherical morphology as shown in Fig.2.1.[11, 18-22] The resulting structure makes them ideal nanovehicles for protein delivery and release because of their high surface area (>800m^2g^{-1}), large pore volume (≈1cm^3g^{-1}) and tunable pore diameters (2–10nm), which allows for the

loading of substantial amounts of protein.[11, 15, 21-27] Additionally, MSN materials possess a strong inorganic oxide framework that is biocompatible and protects the protein molecules entrapped inside the pores from exposure to harmful denaturation chemicals and conditions. They have the potential for substantial loading, zero premature release of proteins, and highly efficient cellular uptake.[10, 28-29] Finally, MSNs are able to aid in effective endosomal escape due to the pH buffering properties naturally found on silica nanomaterials which destabilizes the endosomal membrane (the proton sponge effect).[15, 20, 30-31]

2.4. Tuning the pore size, shape, and surface of MSNs

Within the MSN family, the two most commonly used in protein delivery are SBA-15 and MCM-41. SBA-15 materials are characterized by larger pore sizes (5–30 nm), allowing them to accommodate and deliver large, therapeutic molecules.[32] However, the particle sizes of SBA-15 are generally in the range of 800 nm to 2 μm, and small particle size (<200 nm) is required for efficient cellular uptake [11, 12]. These large particle sizes lead to some limitations of SBA-15, namely, large molecular diffusion and adsorption capacity. Therefore, to enhance the cellular delivery of large molecules, the development of small sized SBA-15 materials has become necessary.[33] On the other hand, MCM-41-type MSN materials possess tunable pore sizes (2–10 nm), with an average distribution centered at less than 5 nm. For the effective delivery of proteins in particular, special attention must be paid to the pore size. Indeed, depending on the size of the protein to be loaded, it can be necessary to enlarge the MCM-41 pores beyond what is achieved in basic synthesis. In order to understand how this control is accomplished, it is necessary to review the basic syntheses of MSN materials. Pore templates (frequently ionic, such as CTAB, or nonionic surfactants, such as the Pluronic family) self-assemble into micelles during the preparation of mesoporous silica materials, creating voids in the silica matrix.

Electrostatic interactions between the silicate species and ionic surfactants lead to the formation of the mesoporous structure of MCM-41. Hydrogen bonding between the surfactants for nonionic surfactants like triblock copolymers (Pluronics) and the silicate is considered to be the main driving force in the formation of mesoporous silica materials, such as SBA-15. For intracellular purposes, it is desirable to control the size of the MSN such that endocytosis remains viable. The synthetic process has a strong influence on the resulting MSN particles, pH in particular, allowing for fine control of particle size, etc.[34] Additionally, alcohols with long alkyl chains have been shown to affect MSN particle size by altering the tetraalkylsilicate hydrolysis kinetics.[35] The ratio of silica precursor to surfactant is also crucial for soft templated MSN, with ratios lower than 0.13 preventing the pores from extending through the entire particle.[36] Trialkylbenzenes have also proven effective reagents in controlling particle size and morphology.[37] Further summary of methods used to prepare MSN for biological applications has been presented in previously published works.[38-39] In all these cases, ordered structures with closely packed cylindrical pores result from templating surfactant agents, which can be employed to direct the pore size of MSN materials. These include: hydrothermal treatment, salt incorporation, utilizing pore expanding agents like mesitylene, co-surfactants, or tuning the reaction temperature.[11, 15, 32, 40] For example, when non-polar chemicals enter the hydrophobic cores of the pore-forming micelles, the pore size of the final MSN product has been shown to increase.[33] Slowing et al. demonstrated the synthesis and characterization of MCM-41 with a large average pore diameter (5.4 nm) and reported that the MSN with large pores were able to host *Cyt c*, then release the protein under physiological conditions.[15] This work was the first to demonstrate loading of a model protein into mesopores, in vitro cellular uptake, and intra-cellular release of proteins from the MSN.

2.5. Pore expanding agents

Pore expansion is crucial for the successful use of MSN in protein therapeutics. This was most notably demonstrated via the immobilization of lysozyme into pore expanded MSN (5.6 nm) and conventional MSN (2.5 nm). After comparing the results, it was observed that pore expanded MSN materials had larger adsorption capacity (420 mg lysozyme g^{-1} MSN) than the conventional MSN materials (340 mg lysozyme g^{-1} MSN).[41] These results indicated that the pore expanded MSN materials would make superior nanovehicles for proteins. There are a wide variety of agents that can be useful in expanding the pore size. Kao and Mou reported synthetic methods for pore expanded MSN materials using different alkanes (hexane, octane, decane, dodecane and hexadecane) as pore expanding agents in ethanol. Decane proved to be the most effective, yielding MSN materials with enlarged pores (5.6 nm) and well-ordered mesostructure. An alternate strategy for controlling the particle size, pore size, and pore structure is to tune the concentration of aqueous ammonia (NH_4OH) in ethanol. This method generated multiple combinations of pore-expanded MSN.[41] Gu et al. were able to synthesize large pore MSN (4.6 nm) materials with particle diameter less than 150 nm using a pore size mediator DMHA (N, N-dimethylhexadecylamine), the cationic surfactant CTAB (cetyltrimethylammonium bromide) acting as a templating agent, and the triblock copolymer Pluronic F127 as a particle growth inhibitor.[42] One proposed mechanism of large pore MSN synthesis with tunable pore size is illustrated in Fig.2.2. Attractive hydrophobic forces hold the DMHA inside the cationic surfactant (CS) micelle, which self-assembles into an inverted cylindrical micelle. At the same time, well-ordered mesostructures are constructed under basic conditions. As illustrated in Fig. 2, the steady self-assembly of negatively charged silicates was observed and positively charged composite micelles of CS and DMHA led to well-ordered mesostructures. The pore size is

dependent on the amount of DMHA and the selection of CS. These large MSNs successfully delivered *Cyt c* into human cervical HeLa cancer cells.[42]

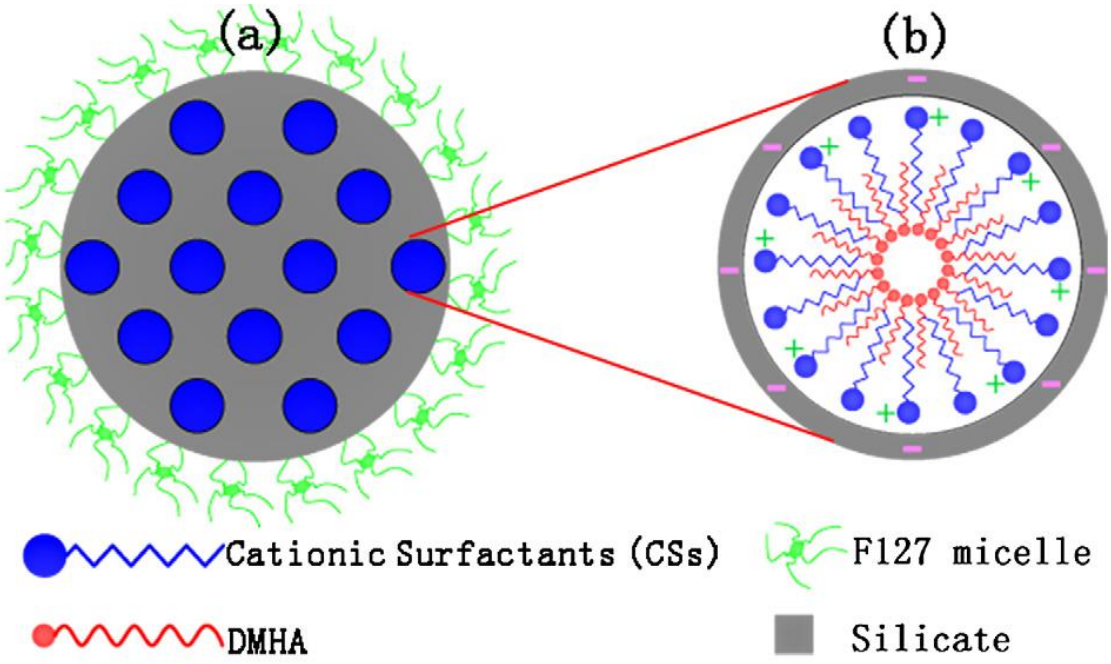

Figure 2.2 Schematic illustration of the proposed synthetic mechanism for the monodispersed large-pore MSNs with tunable pore and controlled particle sizes where (A) shows the whole particle and (B) shows micelle expansion due to DMHA. Adapted and reproduced with permission from [42]. Copyright 2013, Elsevier

Kim and coworkers synthesized MSN with enlarged pores by substituting CTAB with trioctylmethylammonium bromide (TOMAB), which acts as an auxiliary chemical for increasing the pore size from 2.6 nm to 17.4 nm. While micelle formation with the CTAB generates a nanoporous structure of silica nanoparticles, TOMAB molecules enter the interspaces of the micelles by means of ionic and hydrophobic interactions, causing micelles to enlarge due to outward expansion of the CTAB molecules. *Cyt c* was used as a model protein to investigate the feasibility of this system.[43] TOMAB was also used by Lee et al. to achieve large pore (16 nm) MSN, which were used to deliver nerve growth factor into PC12 cells and showed sustained

release over a week. When these nerve growth factor loaded MSN were embedded within a collagen matrix, protein release was more sustained. The release pattern, however, remained constant with and without the collagen matrix. Successful delivery of the protein into cells was confirmed through the observed upregulation of growth-associated protein gene expression. When the cells were cultured directly in a nerve growth factor loaded MSN-collogen hydrogel matrix, they were stimulated to undergo neuritogenesis, indicating a potential utility for this material in tissue engineering.[44]

2.6. Non-surfactant templates

Pore expansion can be accomplished during MSN synthesis without surfactants. Gao and Zharov demonstrated a one-pot synthesis for MSN with large interconnected tunable mesopores using tannic acid (TA) acting as a non-surfactant template. Tannic acid is inexpensive and non-toxic and TA-MSN materials had a high protein adsorption capacity of 77.1 mg for lysozyme (Lz) g^{-1} MSN, 397 mg for hemoglobin (BHb) g^{-1} MSN, and 130 mg for BSA g^{-1} MSN.[45] Shin et al. demonstrated the synthesis of ultra-large pore MSNs from as-synthesized MSNs using divalent cation salts (Ca $[NO_3]_2 \cdot 4H_2O$ or Mg $(NO_3)_2 \cdot 6H_2O$), which generated large mesopores (47.5 nm and 52.4 nm diameter, respectively) by selectively etching the silica. These were compared to calcined MSN (with a pore size of 3.5 nm) and it was observed that these ultra-large pore MSNs had superior absorption abilities for large proteins and antibodies such as bovine serum albumin (BSA) and immunoglobulin (IgG). Ca-MSN adsorbed 307 mg BSA g-1 MSN and 262 mg IgG g-1 MSN and Mg-MSN adsorbed 263 mg for BSA g-1 MSN and 115 mg for IgG g-1 MSN while calcined MSN adsorbed 250 mg for BSA and 162 mg for IgG g-1 MSN. In the case of IgG, it was found that Ca-MSN had a higher adsorption capacity than both Mg-MSN and calcined MSN.[46]

2.7. Non-spherical morphologies

Frequently, MSN materials display a spherical morphology, but certain alterations to the synthetic conditions can enhance the morphology types available to include rods and sheets. Yang et al. demonstrated the synthesis of small SBA-15 rods (80–200 nm in length, 18 ± 8 nm in width) and large pore size (8.3 nm). Often, the size of the hydrophobic core of block copolymer templates dictate the pore size. In this system, the hydrophobic core is enlarged as a result of decreases in the protonation degree of the block copolymer as pH increases. Thus, controlling the pH range from 3.40–3.88 resulted in small SBA-15 rods with 8.3 nm diameter pores, which demonstrated large protein adsorption capacity towards BSA (438 mg g-1 MSN) and lysozyme (417 mg g-1 MSN) and improved cellular uptake performance compared to traditional SBA-15 and MCM-41 silica materials.[47] Hao et al. synthesized micrometer sized MCM-41 with ordered perpendicular nanochannels using water and petroleum ether co-solvents in the presence of CTAB acting as a template and TEOS as the silica source. The first step of synthesis was to form CTAB micelles in the water phase. This was followed by the addition of silica in a petroleum ether phase, which led to the formation of silica-coated micelles. These further self-assembled to form sheet-like structures with ordered pore channels at the water/oil interface. This material showed high loading capacity for bovine serum albumin (598 mg protein g-1 MCM-41) and a controllable, sustained protein release profile in which almost all protein was released at a pH of 4.9 over 36 h.[48] Using a soft-hard templating method, in which a carbon nanosphere serves as the hard template and CTAB as the soft template, Zhang et al. were able to create hollow MSNs with a rough surface that exhibited a high adsorption capacity of *Cyt c*. This was accomplished through the use of a carbon nanosphere core, which was double coated in mesoporous silica that was synthesized using CTAB as the pore template. The carbon core and surfactant were removed

via calcination and the adsorption capacities of the material depended on the pH of the solution, with a maximum absorbance of 260 mg *Cyt c* g^{-1} hollow MSN at a pH of 9.6. This is illustrated in Fig.2.3. This dropped to only 90 mg g^{-1} at a pH of 3.0, thus it was concluded that this material had a pH responsive release. In vitro tests with L02 cells showed minimal cytotoxicity.[49]

A novel core-cone structure resembling the dahlia flower was successfully synthesized by Xu et al. These particles consisted of a spherical core with conical structures blooming off the surface. This unique morphology was created by synthesizing the materials in a chlorobenzene-water solvent emulsion using cetyltrimethylammonium chloride surfactant and triethanolamine base catalyst. Chlorobenzene diffused into the water phase with rapid, controlled stirring, generating closely packed silica lamellae encircling the core. This material exhibited a particle size of about 200 nm, an ultra large pore size and volume (45 nm and 2.59 cm^3g^{-1} MSN, respectively) and demonstrated the capacity to load two different high molecular weight proteins, IgG (150 kDa) and ß-galactosidase (119 kDa). A maximum of 560 mg IgG g^{-1} MSN and 190 mg ß-galactosidase g^{-1} MSN were loaded, and both retained their bioactivity upon delivery into mouse neuro-blastoma cells.[50]

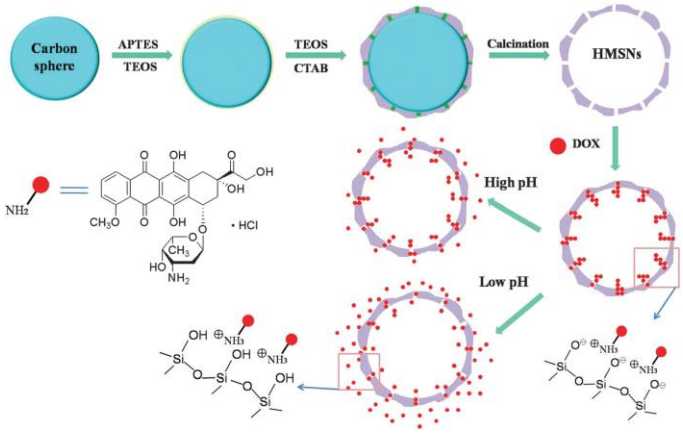

Figure 2.3 Schematic representation of the formation of hollow MSNs (HMSNs) using both carbon nanosphere hard templating and CTAB soft templating methods. Adapted and reproduced with permission from [49]. Copyright 2015, Royal Society of Chemistry

2.8. Surface functionalization of MSNs with stimuli-responsive tethers

Once MSN materials have been successfully loaded with protein therapeutics, it is important to ensure that the release occurs in a controlled and directed manner. To this end, the pore surfaces of MSNs can be covalently modified (exterior and interior pore surfaces) with organic or inorganic groups, which serve as gating devices that can regulate the release of guest molecules with different external stimuli.[40, 51] The removal of the gating device (cap) from the pores can be triggered either by an intracellular phenomenon, like enzymatic activity, or by external stimuli, such as a change in pH or temperature, ultra-sound, light, or an electromagnetic field. Additionally, in order to achieve cell or tissue specificity, the MSN surface can be decorated with cell directing moieties like peptides, antibodies or organic molecules. Recent studies on surface-functionalized MSNs have demonstrated controlled release of a variety of biogenic molecules like DNA, proteins, and pharmaceutical drugs.[27, 52-53] In order to fine-tune the chemical properties of MSN, organic functionalization must be controlled. Generally, two well-established methods, co-condensation and post-synthetic grafting, are applied. The external surface can be selectively functionalized via a post-synthetic grafting method.[24, 54] Different factors such as temperature, reaction time, type of solvent, and type of organoalkoxysilane (OAS) precursor can all be used to control the properties of the grafted materials. However, this method often leads to heterogeneously distributed functional groups; achieving complete, uniform surface functionalization via post-synthesis grafting is challenging. Contrarily, an in-situ co-condensation synthesis method typically leads to homogeneous surface coverage and better control over the amount of OAS groups incorporated on the MSN surface. However, unlike the post-synthesis grafting, this method will not allow for selective functionalization of the external

surface. The independent functionalization of the exterior and/or interior surface of MSNs can be achieved by using a combination of both methods.[40]

2.9. Magnetic and thermal stimuli responsive systems

Vallet-Regí and coworkers were able to demonstrate the release of both proteins and small molecules in response to an alternating magnetic field and changes in temperature.[55] Magnetic iron oxide nanocrystals were imbedded inside the silica matrix of MSN and the MSN surface was functionalized with the thermally responsive block copolymer poly(ethyleneimine)-b-poly(N-isopropylacrylamide) (PEI/PNIPAM). The hydrodynamic size of NIPAM polymers is known to shrink or swell in response to temperature changes. This system has a dual purpose: to retain proteins in the polymer shell through hydrogen bonding and electrostatic interactions of the polymer chains and to act as a temperature-responsive gatekeeper for the drugs trapped inside the MSN framework. Branched polyethyleneimine (PEI) chains (MW≈10 kDa) were grafted to the end of each of the PNIPAM chains. The copolymer was then cross-linked using N, N′-methylene-bis (acrylamide) (MBA), creating an extensive polymeric net-work that limited premature protein release via electrostatic interactions with entrapped proteins. When the temperature was maintained below the lower critical solution temperature (LCST), partial retention of macromolecules within the pores was achieved. As temperature increased above the LCST, the pores opened and a significant increase in protein release occurred due to polarity inversion (hydrophilic to hydrophobic transition) and three-dimensional polymeric changes in the network. Thus, the authors concluded that the phase transition of the polymer acted as the gatekeeper, allowing or preventing the release of macromolecules attached into the polymer branches.[55]

2.10. Photosensitive-responsive systems

Huang et al. functionalized MSN materials using a reductively cleavable photoreactive disulfide phenylazide (SPA) linker. After functionalization of MSNs with SPA, phenyl azide was photolyzed into phenyl nitrene, which can react with biocompatible dextran polymers and proteins.[28] The disulfide bridge present in SPA linker was cleaved upon exposure to glutathione (GSH) in the cytoplasm, thereby triggering the intracellular release of loaded proteins. The model protein, avidin, was success-fully loaded upon light irradiation and released when exposed to GSH, demonstrating the SPA-MSN to be an excellent nanocarrier. Liu and coworkers synthesized photo-degradable protein–polyelectrolyte complex (PPC)-coated MSNs to demonstrate co-release of proteins and model drugs such as rhodamine B.[56] Random copolymers composed of oligo (ethylene glycol) monomethyl ether methacrylate (OEGMA) and 5-(2′-(dimethylamino) ethoxy)-2-nitroben-zyl methacrylate (DENBMA) were synthesized, then anchored on MSN materials. The DENBMA included an o-nitrobenzyl containing monomer, which is unstable in the presence of light (330–420 nm). Further quaternary amination of tertiary amine moieties in DENBMA segments yielded positively charged polyelectrolyte P(OEGMA-co-TENBMA), which interacted with BSA to form a decomposable protein-polyelectrolyte complex (PPC). The PPC exhibited photo-induced charge conversion characteristics; thus, when used as a capping agent for MSNs, UV irradiation of the resulting particles led to the co-release of BSA and rhodamine B due to electrostatic repulsion.[56]

2.11. pH sensitive systems

Effective drug delivery requires that guest molecules be released in the intracellular space. Thus, for high delivery efficiency, it is desirable to design MSN delivery vehicles that facilitate the protein release when stimulated by factors in the intracellular environments.[15] That

is to say, to entrap proteins in the MSN pores and prevent premature protein release into the extracellular space. Park et al. demonstrated the synthesis of MSN with pore walls that convert from negatively to positively charged in endosomal environments. The surface of MSN was functionalized with citraconic amide, which has a pH responsive charge reversal property. At physiological pH, positively charged *Cyt c* can efficiently attach to the negatively charged citraconic amide functionalized MSN. Then, after endocytosis, the citraconic amide facilitates the protein release within the cells by responding to the intracellular endosomal pH.[57] The surface of unfunctionalized MSN is composed of silicates and is negatively charged at neutral pH, thus positively charged objects such as lysozymes adsorb on both the external and interior pore surface of the nanochannels at physiological pH (7.4). Kao et al. devised a scheme to intentionally prevent this via opposing electrostatic interactions with site-selective surface functionalization, which allowed them to load lysozyme exclusively in the nanochannels.[58] Mesoporous silica nanoparticles were first functionalized with 3-aminopropyltriethoxysilane (APTES) such that the amines on the external surfaces became positively charged in a buffer solution at pH 3.2, giving the MSN surface a net positive charge. This caused a strong electrostatic repulsive force to be exerted on similarly charged lysozymes, leading to desorption from the aminopropyl-functionalized silica external surfaces. The isoelectric point of MSN can be tuned depending on the amount of APTES grafted, hence allowing for control of these electrostatic forces. It was observed that APTES could not perforate into the nanochannels of MSNs at low temperature (25°C) and therefore was only grafted on the external surfaces. As illustrated in Scheme 2, through electrostatic interactions or hydrogen bonding between peptides and MSN silanol groups (Si–OH), lysozymes inside or on the pore openings of MSNs were still adsorbed; the pore entrances of the MSN were not blocked by this post synthesis

functionalization method. The stability and activity of lysozyme immobilized in MSN of various pore sizes were studied and correlated to spectroscopic data. It was found that the confinement of lysozyme within 5.6 nm pores limited unfolding and hence increased the thermal stability of the protein. Additionally, this study showed superior catalytic activity by enzymes within the nanochannels as compared to those in the cytoplasm.[58]

Alternatively, the MSN surface can be decorated with a pH responsive macromolecule that changes conformation in response to a decrease in pH, resulting in an opening of the pores. Gan et al. were able to generate this type of system using chitosan cross-linked by glycidoxypropyltrimethoxysilane. Dexamethasone was loaded into the pores, and then the particles were dispersed in a solution with 1% chitosan and cross-linking agent. The chitosan MSN showed superior dexamethasone loading to nonfunctionalized MSN (35 mg g^{-1} MSN vs. 29 mg g^{-1} MSN). Bone morphogenetic protein-2 was incorporated into the chitosan network via stirring of the previously prepared nanoparticles in a solution containing the protein at a 1:5 weight ratio. The chitosan-decorated particles again showed better loading than non-functionalized MSN (248 μg g^{-1} MSN vs. 120 μg g^{-1} MSN, respectively). Uptake into rat bone marrow stromal cells was observed to occur in the first 4 h, thus the majority of bioactive protein was released into the extracellular space (over 80% released within 6 h). The released protein was able to bind to the cell surface and underwent endocytosis. When the pH dropped to 5.0–6.0, loaded dexamethasone was released from the uncapped pores. This dual-drug delivery system was shown to enhance osteoblast differentiation in vitro as well as bone formation in vivo.[59]

2.12. Biolistic Method

Biolistics is a technique of using a particle bombardment to deliver high-density particles coated with genomic material into cells. This technique is particularly useful for delivery into

plant cells since the particle in question is able to penetrate the cell wall. In 2012, Martin-Ortigosa et al. reported the co-delivery of proteins and plasmid DNA to plant tissues (onion) using a biolistic particle delivery system based on a gold nanoparticle functionalized MSN (Au-MSN) platform [60]. The Au-MSN materials were much denser than unfunctionalized MSN, allowing for MSN delivery into plant cells through the biolistic method. Fluorescently-labeled BSA and enhanced green fluorescent protein (eGFP) loaded Au-MSNs were coated with plasmid DNA and, passing through the plant cell wall upon bombardment, the in vitro uptake and release profiles were investigated. Au-MSN with large average pore diameters (10 nm) was shown to deliver and subsequently release proteins and plasmid DNA to the same cell.[60] Later in 2014, the same team explored direct delivery of *Cre* recombinase protein into maize cells using MSN carriers.[61] This study was of particular interest for genome editing since *Cre* recombinase can avoid DNA (transgene) integration into the genome and generate precise modifications without creating transgenic plants. The pores of gold-plated MSNs were loaded with *Cre* recombinase and delivered via the biolistic method to maize cells, which contained the loxP sites integrated into chromosomal DNA. Biochemical analysis of the resulting genome modifications was possible due to the successful delivery of the protein into plant cells.

2.13. Applications

Proteins have significant potential as therapeutic molecules; however, the size and/or charge of these macromolecules restrict cell membrane penetration, and once inside cells, the low pH environment in lysosomes easily degrades proteins. The biocompatibility, stability, and ability to undergo efficient endocytosis make MSN appealing protein carriers into cells. When proteins are sheltered in the pores of MSN, premature degradation of proteins within the biological environment can be minimized, and MSN materials with large pores have assisted in

the delivery of cell membrane impermeable proteins and polysaccharides.[23, 62-63] The release of these cargos can be controlled, and if the system is properly designed, cargo release can be triggered remotely with nontoxic and penetrating stimuli like an alternating magnetic field. The synergic effect associated with chemotherapy and hyperthermia make MSNs promising candidates for oncology therapy.[55] Below are several choice examples describing the potential of MSNs for therapeutic protein delivery.

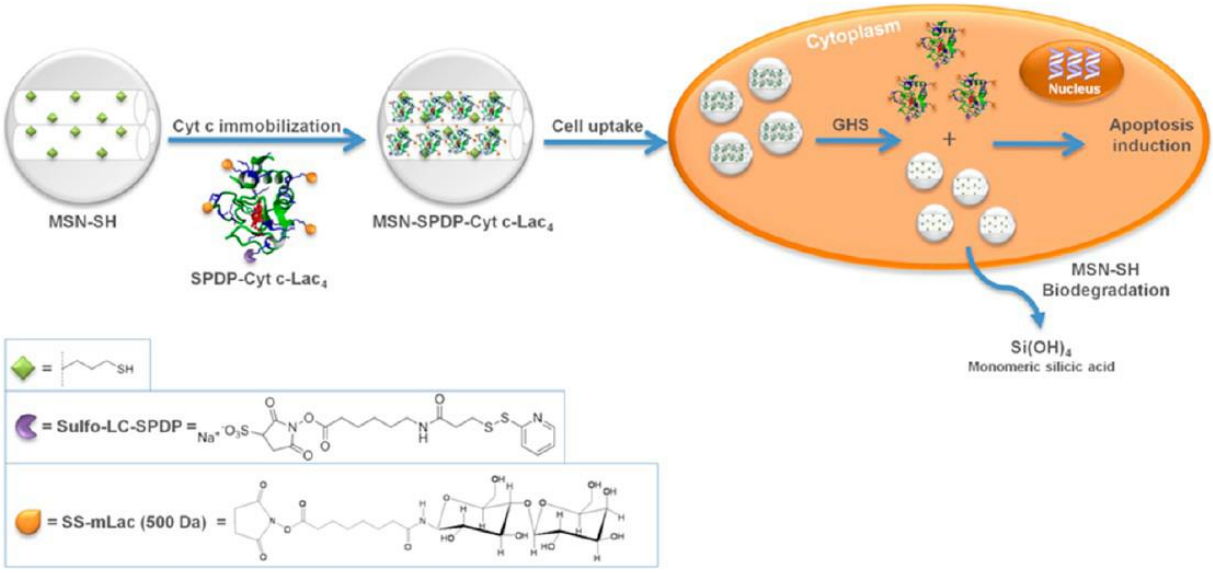

Figure 2.4 Schematic illustration of the immobilization of *Cyt c*-Lac4 into MSN-SH via redox-sensitive smart bonds followed by its intracellular delivery into cancer cells. Adapted and reproduced with permission from [66]. Copyright 2014, American Chemical Society

Mou and coworkers enhanced the transmembrane delivery of the key antioxidant enzyme Cu, Zn superoxide dismutase by embedding the protein in MSN. In this study, the superoxide dismutase was fused with human immunodeficiency virus 1 transactivator protein in E. coli using isopropyl ß-D-1 thiogalactopyranoside induction. This protein was then bound to MSN functionalized with both Ni-nitrilotriacetic acid and fluorescein isothiocyanate through a histidine tag. The protein was dissociated prior to delivery into HeLa cells and refolded upon

cellular uptake as determined via Western blot of the cell lysate. The enzyme was also found to be active within the cells.[64] More recently, the same group was able to deliver superoxide dismutase and glutathione peroxidase at the same time using similarly functionalized MSN material. Dissociating the proteins prior to delivery into HeLa cells was found to increase the penetration efficiency and, once inside, both proteins were able to refold and regain their enzymatic activity. The transactivator protein conjugation leads to cellular uptake through a non-endocytosis mechanism and escape from the endosomes, allowing the MSN material to line up along the cytoskeleton.[65] *Cyt c* is an apoptosis-inducing, membrane impermeable protein that has been successfully delivered into HeLa cells by MSNs. Slowing et al. synthesized a MCM41-type MSN with a large pore diameter (5.4 nm), demonstrating MSNs can serve as efficient transmembrane carriers by escaping endosomal entrapment into the cytoplasm.[15] *Cyt c* remained active even after its release from MSN and induced apoptosis in human cancer cells. Mendez et al. improved the use of MSN as a protein drug carrier by first covalently immobilizing the model protein carbonic anhydrase on a thiolated surface. In this system, protein discharge occurred under intracellular conditions through the cleavage of the redox-sensitive disulfide bond that linked the protein and MSN.[53]

In 2013, Mendez et al. addressed the potential instability of *Cyt c* during encapsulation, storage and release. They generated a smart delivery system for intracellular drug delivery by covalently immobilizing *Cyt c* into MSNs. *Cyt c* was bio-conjugated with sulfosuccinimidyl-6-[3′-(2- pyridyldithio)-propionamido] hexanoate (SPDP) and covalently incorporated into SH-functionalized MSN by a thiol–disulfide interchange reaction (Fig.2.4). Unfortunately, the study revealed that the delivery of *Cyt c* from the MSN was not sufficient for the induction of apoptosis in HeLa cells. They also carried out experiments to confirm whether glycosylation of

Cyt c could be useful in overcoming the efficacy problems. This improved the thermodynamic and kinetic stability of *Cyt c* and also reduced proteolytic degradation.[66]

In order to take advantage of the low pH within lysosomes that accompanies endocytosis, aldehyde-displaying MSN materials (MSN-aldehyde) containing lysosome activated rhodamine-lactams were implemented. An imine bond that formed between the aldehyde functionality and loaded proteins was cleaved by a drop in pH and thus considered a lysosome-responsive protein delivery system. Loaded proteins, like arginase and eGFP were internalized into HepG2, HeLa and L929 cancer cells. Arginase catalyzed the hydrolysis of L-arginine, which is an important amino acid for cell growth, and is used in enzyme replacement therapy for argininemia and cancer treatment. For this application, it is important that the arginase be delivered into cytosol. The eGFP allowed for tracking of the MSN-aldehyde particle in order to evaluate whether or not this system proved useful in this endeavor. Host cells experienced autophagy (self-destruction via delivery of cytoplasmic contents into lysosomes), indicating that the arginase was successfully translocated from lysosomes and retained its enzymatic activity.[67]

Sullivan and coworkers investigated the incorporation of phosphate into the MSN matrix using dimethylphosphonatoethyltrimethoxysilane (DMPTMS) to form large pore phosphate mesoporous silica nanoparticles (PMSNs).[68] Phosphates are biocompatible in nature, thus their incorporation into MSNs is advantageous. Additionally, as a result of the large pore size (11.6 nm) and high surface area, large quantities of model protein membrane impermeable BSA were immobilized by PMSNs. No apparent cytotoxic effects were observed as the PMSN particles were readily internalized, and the BSA retained its secondary structure at physiological pH. These results were confirmed by circular dichroism analysis. Large pore PMSNs were labeled with rhodamine and used to deliver BSA into HeLa cells. The confocal images clearly

showed the presence of BSA (green channel) inside the cell membrane, demonstrating particle transport of BSA across the cell membrane (control experiments with free BSA showed no protein uptake). Successful delivery was partially attributed to the overexpressed folic acid receptors on the HeLa cell surfaces, showing PMSNs have potential for targeted drug delivery in cancer treatment.

2.14. Conclusions

It is clear that MSN materials hold great promise as nanovehicles for intracellular delivery of therapeutic proteins. Their inorganic framework is robust, biocompatible, and able to undergo endocytosis into cells. Pore size can be tuned through an assortment of methods and the synthetic conditions can be altered to generate non-spherical morphologies if desired. This creates a variety of environments in which choice proteins can be sheltered from degradation in biological conditions. It is also possible to functionalize the MSN surface such that the pores are blocked after protein loading, allowing for controlled delivery. In spite of all this, there remains work to be done. Though the MSN pores can be expanded to accommodate larger host molecules, there still remains a size limit. Only small proteins can be successfully loaded, since larger ones do not fit in the pores. As such, it remains vital to find novel ways to address this issue. Additionally, it often is desirable to deliver therapeutic molecules orally; thus, the ability of MSN materials to protect their host molecules even in the stomach environment should be investigated. Along these lines, surface modifications that encourage intestinal absorption, facile transport in the blood, and tissue directly could be topics of further research.

2.15. References

1. Carter, P. J., Introduction to current and future protein therapeutics: A protein engineering perspective. *Experimental Cell Research* **2011,** *317* (9), 1261-1269.

2. Leader, B.; Baca, Q. J.; Golan, D. E., Protein therapeutics: a summary and pharmacological classification. *Nature Reviews Drug Discovery* **2008,** *7* (1), 21-39.

3. Gu, Z.; Biswas, A.; Zhao, M.; Tang, Y., Tailoring nanocarriers for intracellular protein delivery. *Chemical Society Reviews* **2011,** *40* (7), 3638-3655.

4. Carboni, M.; Abney, C. W.; Taylor-Pashow, K. M. L.; Vivero-Escoto, J. L.; Lin, W. B., Uranium Sorption with Functionalized Mesoporous Carbon Materials. *Industrial & Engineering Chemistry Research* **2013,** *52* (43), 15187-15197.

5. Du, J.; Jin, J.; Yan, M.; Lu, Y., Synthetic nanocarriers for intracellular protein delivery. *Current drug metabolism* **2012,** *13* (1), 82-92.

6. Akash, M. S. H.; Rehman, K.; Chen, S., Polymeric-based particulate systems for delivery of therapeutic proteins. *Pharmaceutical development and technology* **2015,** (0), 1-12.

7. Chou, L. Y.; Ming, K.; Chan, W. C., Strategies for the intracellular delivery of nanoparticles. *Chemical Society Reviews* **2011,** *40* (1), 233-245.

8. Li, Z.; Barnes, J. C.; Bosoy, A.; Stoddart, J. F.; Zink, J. I., Mesoporous silica nanoparticles in biomedical applications. *Chemical Society Reviews* **2012,** *41* (7), 2590-2605.

9. Serda, R. E., *Mass Transport of Nanocarriers*. CRC Press: 2012.

10. Slowing, I.; Trewyn, B. G.; Lin, V. S.-Y., Effect of surface functionalization of MCM-41-type mesoporous silica nanoparticles on the endocytosis by human cancer cells. *Journal of the American Chemical Society* **2006,** *128* (46), 14792-14793.

11. Vivero,Äö√Ñ√∂,àö√ë,àö,àÇ,Äö√†√∂,àö√′,Äö√†√∂,Äö√ë¬¢Escoto, J. L.; Slowing, I. I.; Trewyn, B. G.; Lin, V. S. Ä. Ñ. à. ë. à. à. Ä. à. Ä. Ä. ë. Y., Mesoporous silica nanoparticles for intracellular controlled drug delivery. *Small* **2010,** *6* (18), 1952-1967.

12. Prokop, A.; Davidson, J. M., Nanovehicular intracellular delivery systems. *Journal of pharmaceutical sciences* **2008,** *97* (9), 3518-3590.

13. Trewyn, B. G.; Giri, S.; Slowing, I. I.; Lin, V. S. Y., Mesoporous silica nanoparticle based controlled release, drug delivery, and biosensor systems. *Chemical Communications* **2007,** (31), 3236-3245.

14. Lee, B.-S.; Huang, L.-C.; Hong, C.-Y.; Wang, S.-G.; Hsu, W.-H.; Yamauchi, Y.; Hsieh, C.-J.; Lai, J.-Y.; Wu, K. C. W., Synthesis of metal ion–histidine complex functionalized

mesoporous silica nanocatalysts for enhanced light-free tooth bleaching. *Acta Biomaterialia* **2011,** *7* (5), 2276-2284.

15. Slowing, I. I.; Trewyn, B. G.; Lin, V. S.-Y., Mesoporous silica nanoparticles for intracellular delivery of membrane-impermeable proteins. *Journal of the American Chemical Society* **2007,** *129* (28), 8845-8849.

16. Kam, N. W. S.; Dai, H., Carbon nanotubes as intracellular protein transporters: generality and biological functionality. *Journal of the American Chemical Society* **2005,** *127* (16), 6021-6026.

17. Song, S.-W.; Hidajat, K.; Kawi, S., Functionalized SBA-15 materials as carriers for controlled drug delivery: influence of surface properties on matrix-drug interactions. *Langmuir* **2005,** *21* (21), 9568-9575.

18. Angelos, S.; Johansson, E.; Stoddart, J. F.; Zink, J. I., Mesostructured silica supports for functional materials and molecular machines. *Advanced Functional Materials* **2007,** *17* (14), 2261.

19. Giri, S.; Trewyn, B. G.; Lin, V. S., Mesoporous silica nanomaterial-based biotechnological and biomedical delivery systems. **2007**.

20. Slowing, I. I.; Trewyn, B. G.; Giri, S.; Lin, V. Ä. Ñ. à. ë. à. Ñ. Y., Mesoporous silica nanoparticles for drug delivery and biosensing applications. *Advanced Functional Materials* **2007,** *17* (8), 1225-1236.

21. Trewyn, B. G.; Slowing, I. I.; Giri, S.; Chen, H.-T.; Lin, V. S.-Y., Synthesis and functionalization of a mesoporous silica nanoparticle based on the sol,Äö√Ñ√∂,àö√ë,àö¬®gel process and applications in controlled release. *Accounts of Chemical Research* **2007,** *40* (9), 846-853.

22. Vallet,Äö√Ñ√∂,àö√ë,àö,Ñ¢Reg,Äö√†√∂,Äö√¢,Ä†, M. Ä. Ä. Ä. a.; Balas, F.; Arcos, D., Mesoporous materials for drug delivery. *Angewandte Chemie International Edition* **2007,** *46* (40), 7548-7558.

23. Fang, I.-J.; Trewyn, B. G., 3 Application of Mesoporous Silica Nanoparticles in Intracellular Delivery of Molecules and Proteins. *Methods in enzymology* **2012,** *508*, 41.

24. Hoffmann, F.; Cornelius, M.; Morell, J. Ä. à. r.; Fr,Äö√†√∂,Äö√†√ába, M., Silica,Äö√Ñ√∂,àö√ë,àö,Ñ¢based mesoporous organic,Äö√Ñ√∂,àö√ë,àö¬®inorganic hybrid materials. *Angewandte Chemie International Edition* **2006,** *45* (20), 3216-3251.

25. Klabunde, K. J.; Richards, R. M., *Nanoscale materials in chemistry*. John Wiley & Sons: 2009.

26. Trewyn, B. G.; Whitman, C. M.; Lin, V. S.-Y., Morphological control of room-temperature ionic liquid templated mesoporous silica nanoparticles for controlled release of antibacterial agents. *Nano letters* **2004,** *4* (11), 2139-2143.

27. Vivero-Escoto, J. L., *Surface functionalized mesoporous silica nanoparticles for intracellular drug delivery*. 2009.

28. Huang, D.-M.; Hung, Y.; Ko, B.-S.; Hsu, S.-C.; Chen, W.-H.; Chien, C.-L.; Tsai, C.-P.; Kuo, C.-T.; Kang, J.-C.; Yang, C.-S., Highly efficient cellular labeling of mesoporous nanoparticles in human mesenchymal stem cells: implication for stem cell tracking. *The FASEB journal* **2005,** *19* (14), 2014-2016.

29. Lin, Y.-S.; Tsai, C.-P.; Huang, H.-Y.; Kuo, C.-T.; Hung, Y.; Huang, D.-M.; Chen, Y.-C.; Mou, C.-Y., Well-ordered mesoporous silica nanoparticles as cell markers. *Chemistry of Materials* **2005,** *17* (18), 4570-4573.

30. Giri, S.; Trewyn, B. G.; Stellmaker, M. P.; Lin, V. S. Ä. Ñ. à. ë. à. Ñ. Y., Stimuli,Äö√Ñ√∂,àö√ë,àö,Ñ¢responsive controlled,Äö√Ñ√∂,àö√ë,àö,Ñ¢release delivery system based on mesoporous silica nanorods capped with magnetic nanoparticles. *Angewandte Chemie International Edition* **2005,** *44* (32), 5038-5044.

31. Lai, C.-Y.; Trewyn, B. G.; Jeftinija, D. M.; Jeftinija, K.; Xu, S.; Jeftinija, S.; Lin, V. S.-Y., A mesoporous silica nanosphere-based carrier system with chemically removable CdS nanoparticle caps for stimuli-responsive controlled release of neurotransmitters and drug molecules. *Journal of the American Chemical Society* **2003,** *125* (15), 4451-4459.

32. Zhao, D.; Huo, Q.; Feng, J.; Chmelka, B. F.; Stucky, G. D., Nonionic Triblock and Star Diblock Copolymer and Oligomeric Surfactant Syntheses of Highly Ordered, Hydrothermally Stable, Mesoporous Silica Structures. *Journal of the American Chemical Society* **1998,** *120* (24), 6024-6036.

33. Johansson, E. M.; Córdoba, J. M.; Odén, M., The effects on pore size and particle morphology of heptane additions to the synthesis of mesoporous silica SBA-15. *Microporous and Mesoporous Materials* **2010,** *133* (1), 66-74.

34. Chiang, Y.-D.; Lian, H.-Y.; Leo, S.-Y.; Wang, S.-G.; Yamauchi, Y.; Wu, K. C. W., Controlling Particle Size and Structural Properties of Mesoporous Silica Nanoparticles Using the Taguchi Method. *The Journal of Physical Chemistry C* **2011,** *115* (27), 13158-13165.

35. Yamada, H.; Urata, C.; Ujiie, H.; Yamauchi, Y.; Kuroda, K., Preparation of aqueous colloidal mesostructured and mesoporous silica nanoparticles with controlled particle size in a very wide range from 20 nm to 700 nm. *Nanoscale* **2013,** *5* (13), 6145-6153.

36. Yamada, H.; Urata, C.; Higashitamori, S.; Aoyama, Y.; Yamauchi, Y.; Kuroda, K., Critical roles of cationic surfactants in the preparation of colloidal mesostructured silica nanoparticles: control of mesostructure, particle size, and dispersion. *ACS applied materials & interfaces* **2014,** *6* (5), 3491-3500.

37. Yamada, H., A multifunctional role of triakylbenzenes for the preparation of aqueous colloidal mesostructured/mesoporous silica nanoparticles with controlled pore size, particle diameter, and morphology *Nanoscale* **2015,** *7*, 19557-19567.

38. Wu, K. C. W.; Yamauchi, Y., Controlling physical features of mesoporous silica nanoparticles (MSNs) for emerging applications. *Journal of Materials Chemistry* **2012,** *22* (4), 1251-1256.

39. Yamauchi, Y., Templated synthesis for nanoarchitectured porous materials *Bull. Chem. Soc. Jpn* **2015,** *88*, 1171-1200.

40. Slowing, I. I.; Vivero-Escoto, J. L.; Trewyn, B. G.; Lin, V. S.-Y., Mesoporous silica nanoparticles: structural design and applications. *Journal of Materials Chemistry* **2010,** *20* (37), 7924-7937.

41. Kao, K.-C.; Mou, C.-Y., Pore-expanded mesoporous silica nanoparticles with alkanes/ethanol as pore expanding agent. *Microporous and Mesoporous Materials* **2013,** *169*, 7-15.

42. Yue, Y.; Sun, X.; Mayes, R. T.; Kim, J.; Fulvio, P. F.; Qiao, Z.; Brown, S.; Tsouris, C.; Oyola, Y.; Dai, S., Polymer-coated nanoporous carbons for trace seawater uranium adsorption. *Science China Chemistry* **2013,** *56* (11), 1510-1515.

43. Eltohamy, M.; Shin, U. S.; Kim, H.-W., Silica nanoparticles with enlarged nanopore size for the loading and release of biological proteins. *Materials Letters* **2011,** *65* (23), 3570-3573.

44. Lee, J. H.; Park, J.-H.; Eltohamy, M.; Perez, R.; Lee, E.-J.; Kim, H.-W., Collagen gel combined with mesoporous nanoparticles loading nerve growth factor as a feasible therapeutic three-dimensional depot for neural tissue engineering. *RSC Advances* **2013,** *3* (46), 24202-24214.

45. Gao, Z.; Zharov, I., Large Pore Mesoporous Silica Nanoparticles by Templating with a Nonsurfactant Molecule, Tannic Acid. *Chemistry of Materials* **2014,** *26* (6), 2030-2037.

46. Shin, H.-S.; Hwang, Y.-K.; Huh, S., Facile preparation of ultra-large pore mesoporous silica nanoparticles and their application to the encapsulation of large guest molecules. *ACS applied materials & interfaces* **2014,** *6* (3), 1740-1746.

47. Yang, Y.; Karmakar, S.; Zhang, J.; Yu, M.; Mitter, N.; Yu, C., Synthesis of SBA-15 rods with small sizes for enhanced cellular uptake. *Journal of Materials Chemistry B* **2014,** *2* (30), 4929-4934.

48. Hao, N.; Tang, F.; Li, L., MCM-41 mesoporous silica sheet with ordered perpendicular nanochannels for protein delivery and the assembly of Ag nanoparticles in catalytic applications. *Microporous and Mesoporous Materials* **2015,** *218*, 223-227.

49. Zhang, H.; Xu, H.; Wu, M.; Zhong, Y.; Wang, D.; Jiao, Z., A soft–hard template approach towards hollow mesoporous silica nanoparticles with rough surfaces for controlled drug delivery and protein adsorption. *Journal of Materials Chemistry B* **2015,** *3* (31), 6480-6489.

50. Chun, X.; Meihua, Y.; Owen, N.; Jun, Z.; Hao, S.; Hongwei, Z.; Chang, L.; Yuting, N.; Xiaodan, H.; Yannan, Y.; Chengzhong, Y., Core-Cone Structured Monodispersed Mesoporous Silica Nanoparticles with Ultra-large Cavity for Protein Delivery. *Small* **2015,** *11* (44), 5949-5955.

51. Slowing, I. I.; Vivero-Escoto, J. L.; Wu, C.-W.; Lin, V. S.-Y., Mesoporous silica nanoparticles as controlled release drug delivery and gene transfection carriers. *Advanced drug delivery reviews* **2008,** *60* (11), 1278-1288.

52. Kresge, C.; Leonowicz, M.; Roth, W.; Vartuli, J.; Beck, J., Ordered mesoporous molecular sieves synthesized by a liquid-crystal template mechanism. *Nature* **1992,** *359* (6397), 710-712.

53. Me,àö√â,àö√ñndez, J.; Monteagudo, A.; Griebenow, K., Stimulus-responsive controlled release system by covalent immobilization of an enzyme into mesoporous silica nanoparticles. *Bioconjugate chemistry* **2012,** *23* (4), 698-704.

54. Lin, V. S. Y.; Lai, C.-Y.; Huang, J.; Song, S.-A.; Xu, S., Molecular Recognition Inside of Multifunctionalized Mesoporous Silicas: Toward Selective Fluorescence Detection of Dopamine and Glucosamine. *Journal of the American Chemical Society* **2001,** *123* (46), 11510-11511.

55. Baeza, A.; Guisasola, E.; Ruiz-Hernández, E.; Vallet-Regí, M., Magnetically triggered multidrug release by hybrid mesoporous silica nanoparticles. *Chemistry of Materials* **2012,** *24* (3), 517-524.

56. Wan, X.; Liu, T.; Hu, J.; Liu, S., Photo-Degradable, Protein–Polyelectrolyte Complex-Coated, Mesoporous Silica Nanoparticles for Controlled Co-Release of Protein and Model Drugs. *Macromolecular rapid communications* **2013,** *34* (4), 341-347.

57. Park, H. S.; Kim, C. W.; Lee, H. J.; Choi, J. H.; Lee, S. G.; Yun, Y.-P.; Kwon, I. C.; Lee, S. J.; Jeong, S. Y.; Lee, S. C., A mesoporous silica nanoparticle with charge-convertible pore walls for efficient intracellular protein delivery. *Nanotechnology* **2010,** *21* (22), 225101.

58. Kao, K.-C.; Lin, T.-S.; Mou, C.-Y., Enhanced activity and stability of lysozyme by immobilization in the matching nanochannels of mesoporous silica nanoparticles. *The Journal of Physical Chemistry C* **2014,** *118* (13), 6734-6743.

59. Gan, Q.; Zhu, J.; Yuan, Y.; Liu, H.; Qian, J.; Li, Y.; Liu, C., A dual-delivery system of pH-responsive chitosan-functionalized mesoporous silica nanoparticles bearing BMP-2 and dexamethasone for enhanced bone regeneration. *Journal of Materials Chemistry B* **2015,** *3* (10), 2056-2066.

60. Martin,Äö√Ñ√∂,àö√ë,àö,Ñ¢Ortigosa, S.; Valenstein, J. S.; Lin, V. S. Ä. Ñ. à. ë. à. Ñ. Y.; Trewyn, B. G.; Wang, K., Gold functionalized mesoporous silica nanoparticle mediated protein and DNA codelivery to plant cells via the biolistic method. *Advanced Functional Materials* **2012,** *22* (17), 3576-3582.

61. Martin-Ortigosa, S.; Peterson, D. J.; Valenstein, J. S.; Lin, V. S.-Y.; Trewyn, B. G.; Lyznik, L. A.; Wang, K., Mesoporous Silica Nanoparticle-Mediated Intracellular Cre Protein Delivery for Maize Genome Editing via loxP Site Excision. *Plant physiology* **2014,** *164* (2), 537-547.

62. Hudson, S. P.; Padera, R. F.; Langer, R.; Kohane, D. S., The biocompatibility of mesoporous silicates. *Biomaterials* **2008,** *29* (30), 4045-4055.

63. Knežević, N. Ž.; Durand, J.-O., Large pore mesoporous silica nanomaterials for application in delivery of biomolecules. *Nanoscale* **2015,** *7* (6), 2199-2209.

64. Chen, Y.-P.; Chen, C.-T.; Hung, Y.; Chou, C.-M.; Liu, T.-P.; Liang, M.-R.; Chen, C.-T.; Mou, C.-Y., A New Strategy for Intracellular Delivery of Enzyme Using Mesoporous Silica Nanoparticles: Superoxide Dismutase. *Journal of the American Chemical Society* **2013,** *135* (4), 1516-1523.

65. Lin, Y.-H.; Chen, Y.-P.; Liu, T.-P.; Chien, F.-C.; Chou, C.-M.; Chen, C.-T.; Mou, C.-Y., Approach To Deliver Two Antioxidant Enzymes with Mesoporous Silica Nanoparticles into Cells. *ACS Applied Materials & Interfaces* **2016,** *8* (28), 17944-17954.

66. Méndez, J.; Morales Cruz, M.; Delgado, Y.; Figueroa, C. M.; Orellano, E. A.; Morales, M.; Monteagudo, A.; Griebenow, K., Delivery of chemically glycosylated cytochrome c immobilized in mesoporous silica nanoparticles induces apoptosis in HeLa cancer cells. *Molecular pharmaceutics* **2013,** *11* (1), 102-111.

67. Wu, X.; Wu, S.; Yang, L.; Han, J.; Han, S., Cytosolic delivery of proteins mediated by aldehyde-displaying silica nanoparticles with pH-responsive characteristics. *Journal of Materials Chemistry* **2012,** *22* (33), 17121-17127.

68. Maddala, S. P.; Mastroianni, G.; Velluto, D.; Sullivan, A. C., Intracellular delivery of BSA by phosphonate@ silica nanoparticles. *Journal of Materials Chemistry B* **2015,** *3* (29), 6057-6070.

CHAPTER 3 CONSERVED ACTIVITY OF RE-ASSOCIATED HOMOTETRAMERIC PROTEIN SUBUNITS RELEASED FROM MESOPOROUS SILICA NANOPARTICLES

Modified from a paper published in

ACS Langmuir

Gauri Deodhar, Marisa Adams, Sutapa Joardar, Madhura Joglekar, Malcolm Davidson, William Smith, Maddie Mettler, Sydney Toler, Fiona Davis, Kim Williams, Brian Trewyn

3.1. Abstract

Mesoporous silica nanoparticles (MSN) with enlarged pores were prepared and characterized, and reversibly dissociated subunits of concanavalin A were entrapped in the mesopores, as shown by multiple biochemical and material characterizations. When loaded in the MSN, we demonstrated protein stability from proteases and, upon release, the subunits re-associated into active proteins shown through mannose binding and o-phthalaldehyde fluorescence. We have demonstrated a versatile and facile method to load homomeric proteins into MSN with potential applications in enhancing the delivery of large therapeutic proteins.

3.2. Introduction

Within the human body, proteins perform numerous essential functions in the development, growth, and regulation of several key metabolic systems.[1] Protein therapeutics exploit these functions in order to improve human health; i.e., certain diseases are treated directly through changes in the functions of intracellular proteins such as the use of insulin to treat diabetes I and II. When compared to small molecule drugs, protein therapeutics possess several major advantages. Proteins are highly specific, decreasing the probability of interference with normal biological processes, and have a high intracellular activity when compared with small molecule drugs. In cases where a gene mutation or deletion is responsible for causing a disease, protein

therapeutics are safer than gene therapy because side effects like random or permanent genetic changes are rarely observed.[2] Still, the effective delivery of proteins to target sites poses a mammoth challenge. Proteins are rapidly cleared from the body and face degradation by low pH environments and certain enzymes, specifically within lysosomes. Once internalized by target cells, protein escape during early stages of the endolysosomal pathway is crucial.[2-4] Hence, strategies to successfully deliver therapeutic proteins into their target cells with their activity still intact are essential. To this effect, nanovehicles have been extensively employed to transport and release proteins to intracellular targets.[2, 5-12] Mesoporous silica nanoparticles (MSN) are able to not only carry more protein units than their nonporous counterparts, but if the protein is small enough to diffuse into the pores, it can also be sheltered from premature degradation in the biological environment.[13] For example, cytochrome C, a small (12 kDa) membrane impermeable protein, has been successfully entrapped inside the pores of MSN and delivered into HeLa cells.[14] A variety of other proteins have been immobilized in the pore network of MSN as well; however, those proteins are too large to fit into the pores (dimensions greater than the 4 nm pore size), only adsorbed onto the silica surface.[15] This was demonstrated by Diaz and Balkus, who found that horseradish peroxidase was not immobilized into the pores of MCM-41 because its average spherical size of 4.6 nm was greater than the 4 nm pore diameter.[16] On the particle surface, proteins would be exposed to harsh lysosomal conditions and degrade before achieving their intracellular therapeutic effect. Thus, delivering large molecular weight therapeutic proteins remains a challenge. Recently, research has focused on increasing the average pore size of MSN to accommodate larger proteins.[17-23] Perhaps an equally intuitive solution is to make the large proteins small enough to fit into the MSN pores. For proteins with quaternary structure, this is not such a far-fetched proposition. Certain proteins, including ribonuclease, lysozyme, α-

chymotrypsin, and β-lactoglobulin, can be reversibly dissociated through pH dependent mechanisms or upon exposure to a denaturant.[24-28] In particular, aqueous solutions of concentrated urea have been shown to successfully dissociate proteins, such as αm-crystallin (a heteromeric protein found in the ocular lens) and pyruvate decarboxylase (a homotetrameric protein).[24, 29] Upon dilution and a return to neutral pH, the urea diffuses out of the protein and allows the subunits to re-associate. This re-associated protein also regains its activity; hence, we can successfully make large proteins smaller. It should be noted that this is demonstrated on a homomeric protein and methods to dissociate, entrap, and release subunits from heteromeric proteins may be different. Herein, we use concanavalin A (Con A), a homotetrameric protein with a mass of 104 kDa, as a model therapeutic protein. Con A is a lectin, extracted from jack beans, that has been shown to possess a notable antihepatoma effect.[30] The tetramers were dissociated into dimer and monomer units using a urea solution, and subsequently loaded into pore expanded MSN (PEMSN) pores. When released in appropriate physiological buffer, these subunits re-associated into their active form, thus demonstrating the utility of this method in the delivery of larger molecular weight proteins (Scheme 3.1).

3.3. Materials and methods

3.3.1. Materials

Concanavalin A (from jack beans), mesitylene, cetyltrimethylammonium bromide (CTAB), 98% tetraethyl orthosilicate (TEOS), 14.5 M NH4OH (28% w/w NH3), urea, and sodium acetate were purchased from Sigma-Aldrich and used as received.

3.3.2. Pore Expanded MSN

A solution of 2.08 mM cetyltrimethylammonium bromide (CTAB) in nanopure water (1 g of CTAB in 480 mL of nanopure water) was mixed with 3.5 mL of 2 M NaOH(aq) and 7.0 mL of

mesitylene. This mixture was stirred vigorously at 80 °C for 2 h before 5 mL of tetraethyl orthosilicate was added dropwise at approximately 1 mL min−1.

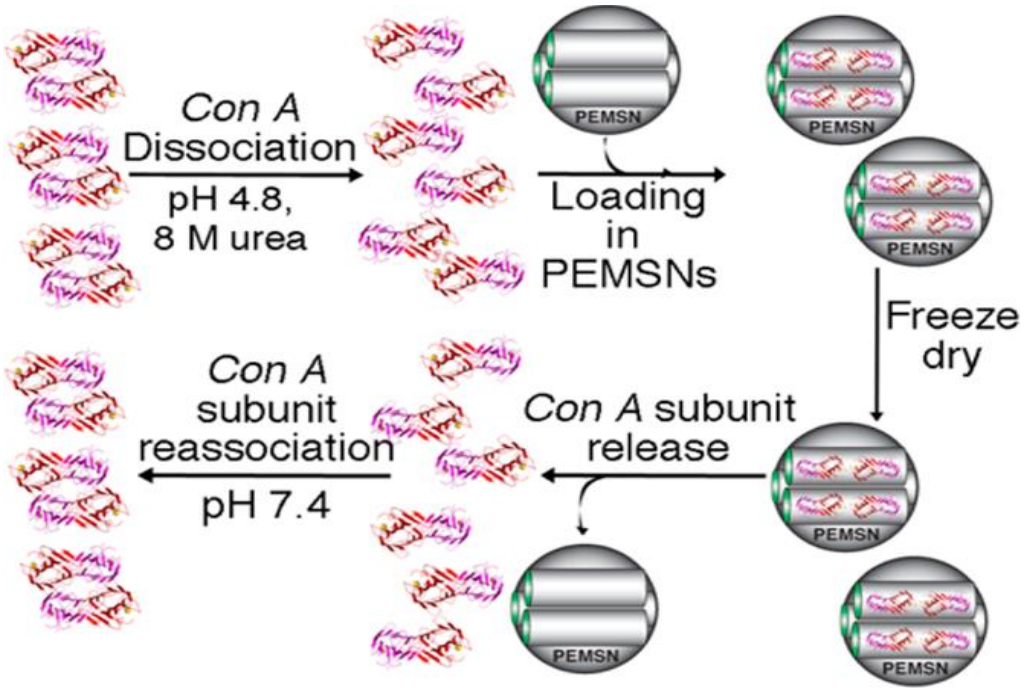

Scheme 3.1 Illustration of the Dissociation, Loading of Con A Subunits into the Expanded Pores of MSN, Release, and Reassociation Process of Con A Tetramers

The reaction was allowed to continue for another 2 h, and the resulting white precipitate was filtered, washed with abundant methanol, and dried for 12 h at 100 °C. Residual CTAB was removed via an acid extraction in which a suspension of 1g as-synthesized material was stirred at 50 °C for 6 h in 100 mL of methanol with 0.75 mL of concentrated hydrochloric acid. The product was filtered again, rinsed with methanol, and dried under a vacuum for 12 h at room temperature.

3.3.3. Protein Dissociation, Loading, and Release

Concanavalin A was dissociated and re-associated as reported previously [30]. Dissociation into dimer units was accomplished using 8 M urea in a sodium acetate buffer (2 μM protein in 20 mM buffer, pH 5.2, with 0.15 M NaCl, 1 mM Mn^{2+}, and 1 mM Ca^{2+}). This mixture was stirred at 25 °C with a constant pH of 4.8 for 18 h. The solution was then centrifuged, and the resulting pellet washed with phosphate buffer saline solution (10 mM with a pH of 7.4) and lyophilized. The dissociated protein was loaded into MSN by stirring the protein solution at a mass:volume ratio of 1:5 for 6 h at room temperature with PEMSN. Protein subunits were successfully released from the PEMSN, and the subunits were reconstituted by diluting the loaded particle solution with 10 mM PBS buffer at a pH of 7.4 until the concentration of urea was negligible. This solution was sampled every 4 h for 24 h, and the absorbance at 280 nm was measured.

3.3.4. Fluorescence Studies

Fluorescence measurements were recorded on a Horiba Jobin Yvon NanoLog using an excitation wavelength of 280 nm and a scanning range of 290−400 nm. The native protein was found to have an emission wavelength of 337 nm, while the dissociated protein emission peak was red-shifted to 352 nm.

3.3.5. Gel Electrophoresis

Gel electrophoresis was run in Tris buffer (pH 8) at 160 V for approximately 45 min using Bio Rad precast gels. The gel was soaked in Coomassie Brilliant Blue R250 staining solution for 2 h, then transferred to a 50:40:10 water methanol:acetic acid by volume destaining solution, and left overnight to visualize protein bands.

3.3.6. Activity Quantification of Released Con A

The activity of re-associated Con A was tested, as has been previously reported.[31-32] A Sephadex G-100 column with a 2 mL bed volume was equilibrated overnight with 20 mM sodium acetate buffer (pH 5.2 with 0.15 M NaCl, 1 mM Mn^{2+}, and 1 mM Ca^{2+}) and then loaded with a 1 mL aliquot of released protein (before and after the particles were exposed to pepsin). Unbound protein was collected within 2 min, and the bound protein was eluted using a 0.2 M glucose solution in the 20 mM sodium acetate buffer. The amount of protein in each fraction was quantified using an o-phthalaldehyde fluorescent method.

3.3.7. Stöber Silica (Nonporous Silica Particles)

Stöber silica was synthesized by measuring out 150 mL of ethanol and 50 mL of 14.5 M NH4OH (28% w/w NH3) in a 250 mL round-bottom flask. To this mixture, 12.5 mL of TEOS was added. The reaction mixture was stirred overnight at room temperature. Solutions were then centrifuged, washed with copious amounts of ethanol, and stored in ethanol. Silica particles were collected as needed for use and dried in a vacuum oven at 550 °C for 5 h.

3.3.8. Nitrogen Physisorption Analysis

Nitrogen adsorption−desorption measurements were carried out on a Micrometrics TriStar II surface area and porosity analyzer. Samples (60−100 mg) were dried under nitrogen at 100 °C for 6 h before analysis. BET surface area, pore volume, and pore diameter measurements were recorded at −196 °C using nitrogen gas, and the BJH model was used to calculate pore volume and diameter values from the adsorption−desorption isotherms.

3.3.9. Small Angle X-ray Scattering

Small angle X-ray scattering (SAXS) measurements were acquired using a PANalytical X-ray generator with a Cu target and an Anton-Paar SAXSess system, which is an updated model of the Kratky camera.[33] The signal was acquired by exposing a phosphor image plate detector, which was digitized using a PerkinElmer Cyclone readout system and Anton-Parr SAXSquant software. The latter was used to perform the desmearing operation (15 iterations) to correct for the slit geometry of the SAXSess system and also to perform some particle size analyses. Data analysis was conducted on SAXSquant1D and the Irena SAXS package for Igor Pro.[34] For absolute intensities (cross section per unit volume, cm−1), methods were developed to measure the transmission of the Cu Kα X-rays and thickness of each sample. Transmission values for samples were acquired on a Siemens D500 X-ray diffractometer using Cu Kα X-rays diffracted from a LaB6 standard. The attenuation of the (110) peak from the LaB6 was measured with and without the sample placed in the beam on the diffracted side. Samples were prepared by taking a finely divided and homogenized powder consisting of PEMSN and placing it on a commercial acetate adhesive tape. After mounting the sample film onto an aluminum plate with a 3 mm × 30 mm slot, excess powder was gently tapped from the holder assembly. Data processing was performed by extracting the corrected absolute intensity data with SAXSQuant1D. A density of 0.34 $g \cdot cm^{-3}$ was assigned to the PEMSN sample based on commercial data from Sigma-Aldrich. SAXS measurements were made on the commercial acetate tape (which exhibited some scattering, albeit much weaker than sample) and used to correct the intensity.

3.3.10. Batch Dynamic Light Scattering (DLS)

A DAWN HELEOS II (Wyatt Technology Corporation, Santa Barbara, CA) was used for determination of diffusion coefficients in batch mode. The light scattering setup is equipped with a 60-mW laser with an emission wavelength of 658 nm. The DLS detector attachment was connected by replacing detector 8 at an angle of 61.1°. The sample compartment is kept at an operating temperature of 25.0 ± 0.2 °C. Native and dissociated Con A samples were prepared in 10 mM PBS buffer and 8 M urea, respectively (as above), at a concentration of 2 μM in 5 mL. Re-associated Con A samples were prepared in reassociation buffer (as described) which was assumed to be both isorefractive and isoviscous with 10 mM PBS. Each sample was then passed through a 0.2 μm Nylon filter into a dust free scintillation vial. A 5 min batch mode DLS experiment was then performed for each sample. One correlation function per second is averaged over a collection interval of 5 s for a total of 60 independent measurements. For each measurement, the average correlation function is fit with an exponential decay using ASTRA 6.1 analysis software to determine a translational diffusion coefficient. Solution refractive indices used in the fitting process were 1.330 for 10 mM PBS and 1.470 for 8 M urea. The mean hydrodynamic radius of the analytes (R_h) is then calculated from the translational diffusion coefficient (D) via the Stokes−Einstein equation for Brownian motion

$$D = \frac{k_B T}{6\pi\eta R_h}$$

where k_B is the Boltzmann constant, η is the viscosity of the medium, and T is the temperature. The viscosities of 10 mM PBS and 8 M urea are 0.8945 and 1.5124 cP, respectively, at 25 °C.

3.4. Results and discussion

3.4.1. Pore Expanded MSN

To accommodate the 52 kDa protein dimer and 26 kDa protein monomer subunits formed from the dissociation of Con A, PEMSN was synthesized using mesitylene as a pore expanding agent.[14]

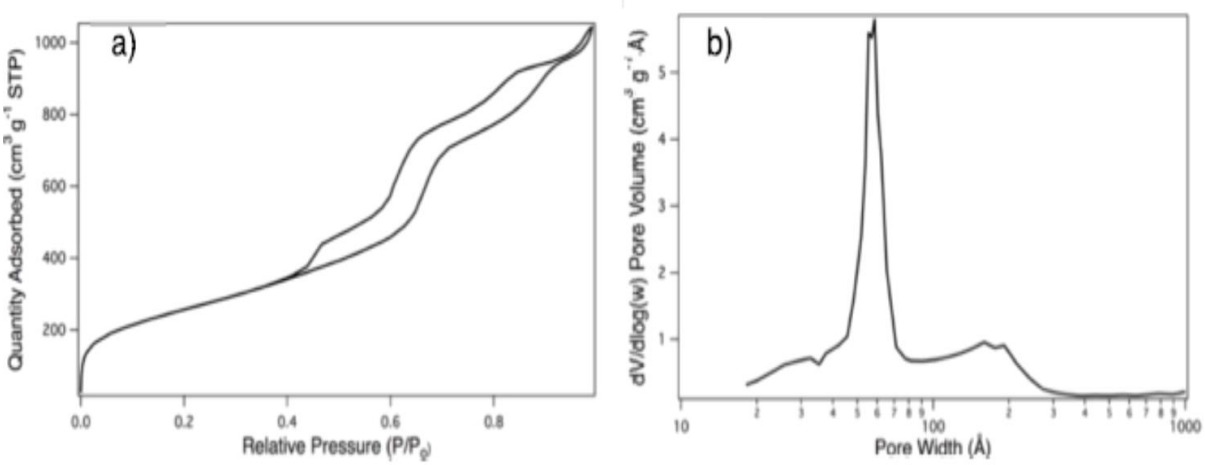

Figure 3.1 a) Nitrogen sorption isotherm of PEMSN synthesized using mesitylene pore expanding agent using BET calculation, b) BJH pore size distribution of PEMSN showing two pore size distributions centered on 5.8 nm (major peak) and 15.9 nm (minor peak)

Nitrogen sorption analysis shows a type IV isotherm with high surface area (726 m^2 g^{-1}) and a pore volume of 1.34 cm^3 g^{-1}. The double plateau shape of the isotherm is consistent with previously reported isotherms of PEMSN and is indicative of heterogeneous pore expansion.[14] Barrett−Joyner−Halenda (BJH) pore width distributions calculated from the desorption isotherm of nitrogen sorption data show a bimodal pore size distribution: a major peak at 5.8 nm and a minor peak at 15.9 nm, also consistent with previously reported materials[13] Small angle X-ray scattering (SAXS) was used to further characterize the particles (Figure 3.2).

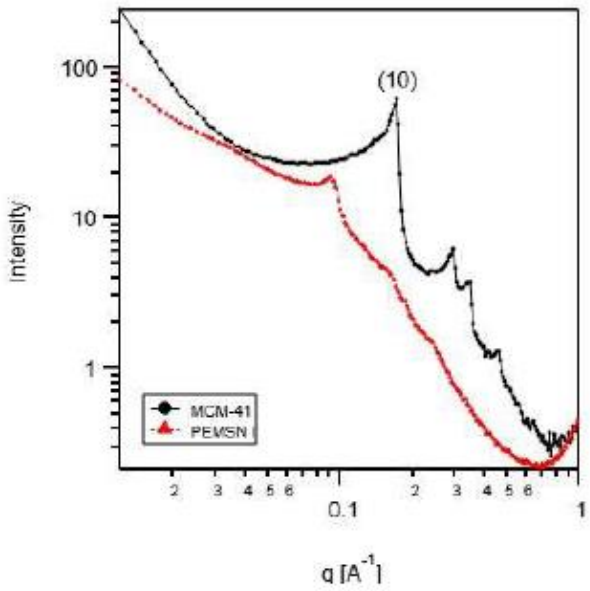

Figure 3.2 Diffraction peaks present in SAXS data acquired for MCM-41 prepared with (red) and without mesitylene (black)

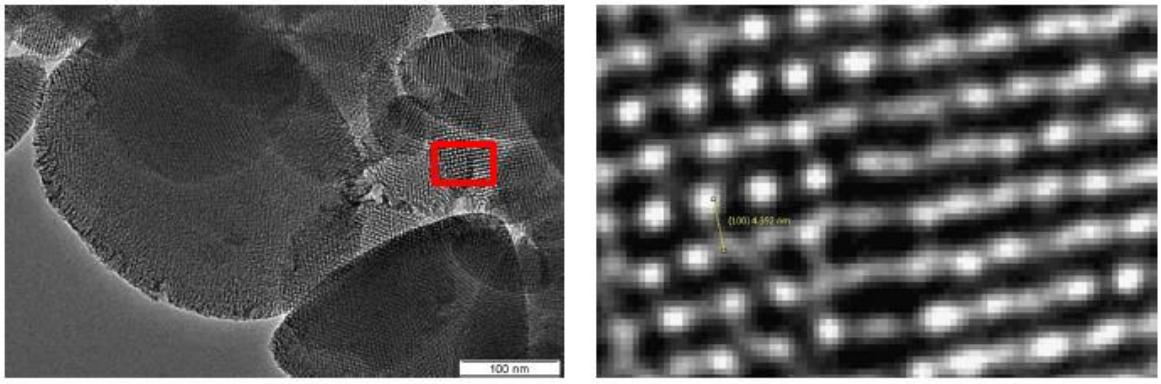

Figure 3.3 TEM images of the PEMSN. The right images are a magnification of the inset depicted on the box outlined in the image on the left. d (100) was measured by imageJ as 4.4 nm

We observed diffraction from the (100) plane of hexagonally ordered pores common to MCM-41.[35] The d (100) was measured to be 4.4 nm by TEM (Figure 3.3).

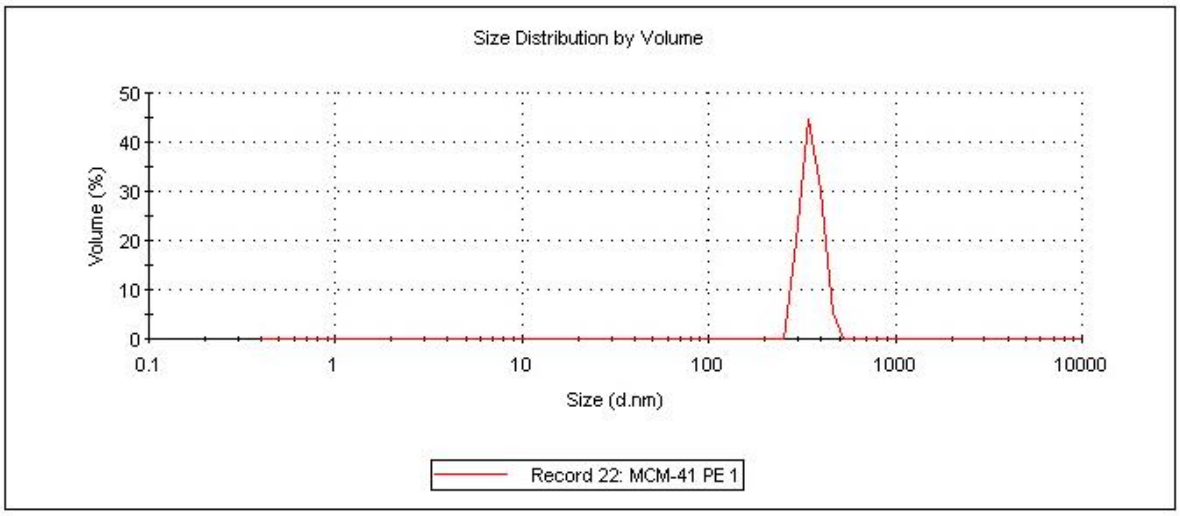

Figure 3.4 Dynamic light scattering measurement of particle size distribution of PEMSN suspended in 10mM PBS pH 7.4 showing an average size of 300 nm

For MSN prepared with and without mesitylene, the magnitude of Q at the (100) peak yields an interplanar spacing of 7.3 and 13.5 nm, respectively.[36] The particle size of the PEMSN was determined to be 300 ± 60 nm by dynamic light scattering (DLS) in a PBS suspension (Figure 3.4).

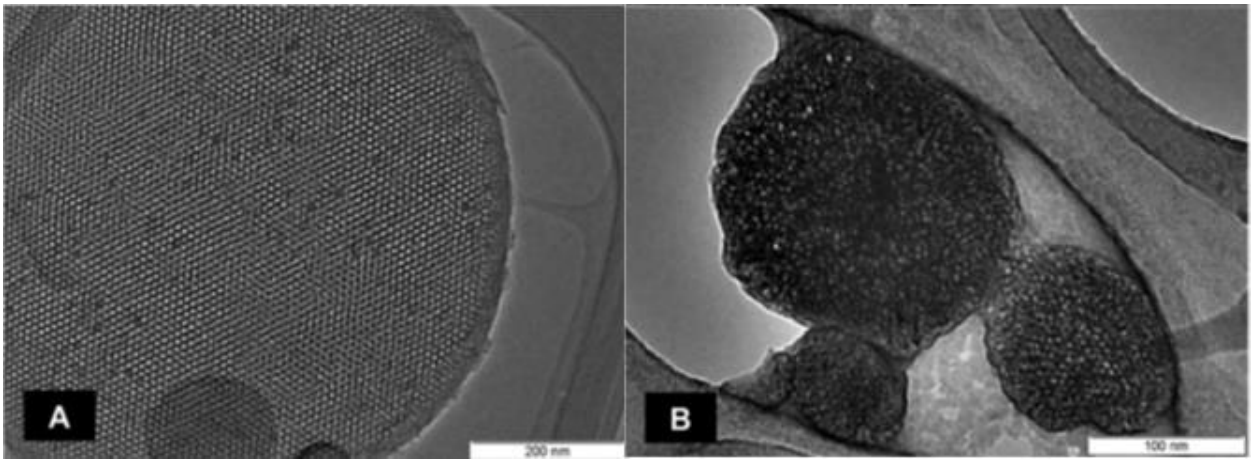

Figure 3.5 Transmission electron micrographs of (a) pore-expanded MSN and (b) Con A subunit loaded PEMSN (protein stained with 2% uranyl acetate)

The characteristic TEM image shows the characteristic ordered hexagonal packing of the pore channels in PEMSN. Additional TEM images of protein loaded PEMSN before staining with uranyl acetate are located in the Supporting Information (Figure 3.6)

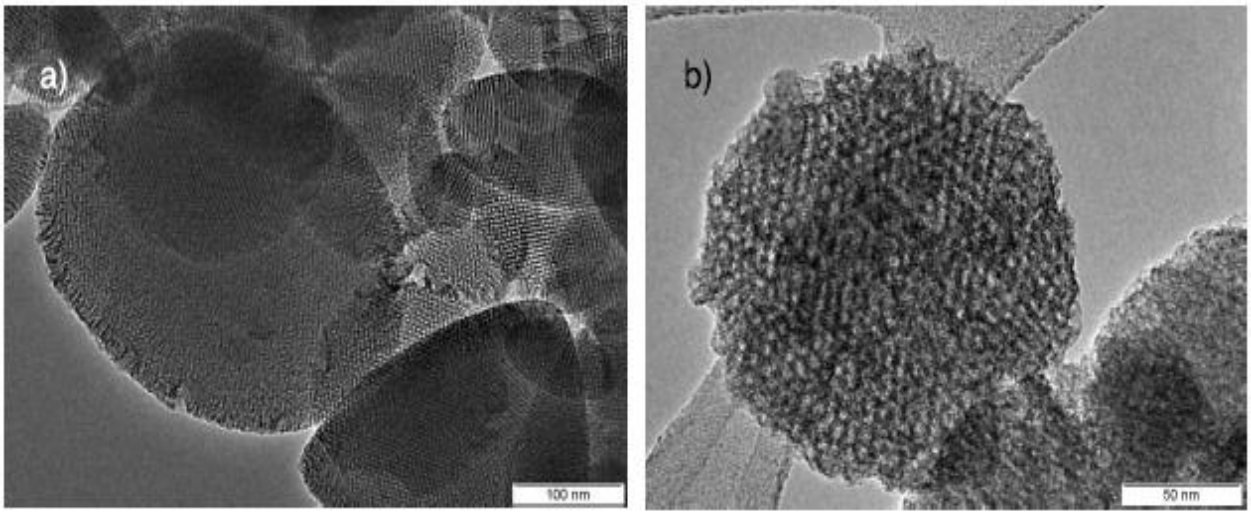

Figure 3.6 TEM images of PEMSN before (a) and after (b) and Con A loading

3.4.2. Protein Dissociation and Loading

Protein dissociation was accomplished using 8 M urea in a sodium acetate buffer (2 μM protein in 20 mM buffer) and confirmed through fluorescence studies using an excitation wavelength of 280 nm.

Dissociated protein shows a red shift from 337 nm to 352 nm. Re-associated Con A after diffusing out of the mesopores of MSN showing a blue shift from 352 nm back to the 337 nm characteristic of the native Con A (Figure 3.7). Fluorescence intensity of the re-associated Con A is very low because this sample was diluted until the urea concentration was negligible such that

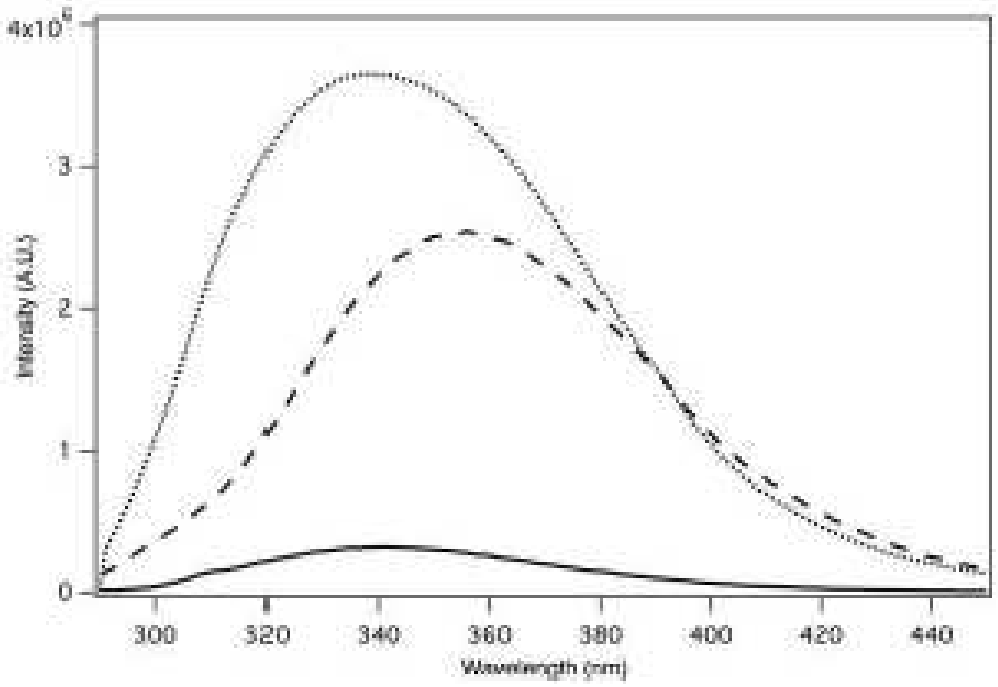

Figure 3.7 Fluorescence measurements at an excitation wavelength of 280 nm of native Con A (dotted line), dissociated Con A (dashed line), and re-associated Con A (solid line)

the protein concentration was 0.7 μM. Measurements were taken on samples that had not been exposed to pepsin. The native protein was found to have an emission wavelength (λmax) of 337 nm, while the dissociated protein emission peak was red-shifted to 352 nm, which is consistent with previously reported fluorescence studies of Con A.[26] Successful dissociation was also confirmed using gel electrophoresis. A band corresponding to the dimer unit was observed at ~50 kDa vs the ~100 kDa band from the native protein. These data fit well with the known masses of 52 and 104 kDa for the dimer and native protein, respectively (Figure 3.9). Batch DLS studies corroborate dissociation to dimer, with measured hydrodynamic radii (Rh) of 4.5 ± 0.6 nm for native and 2.2 ± 0.3 nm for dissociated, in their respective buffers (Figure 3.8).

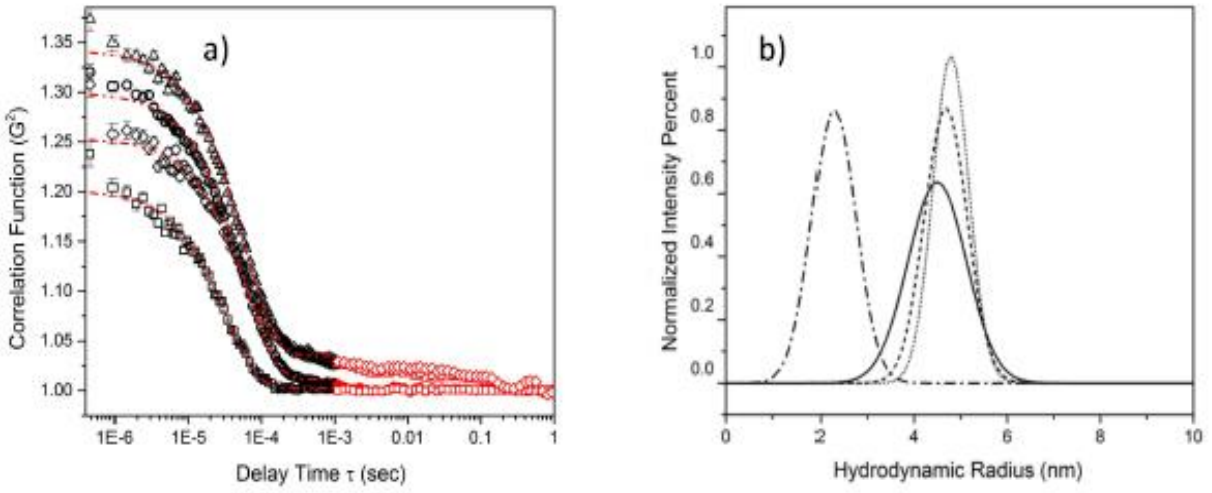

Figure 3.8 Con A size measurements from dynamic light scattering in respective buffers. The figures are a) correlation functions for native Con A (circles), dissociated Con A (squares), re-associated Con a post pepsin digestion (diamonds), and re-associated Con A without exposure to pepsin (triangles) and b) dynamic light scattering size measurements for Con A showing dissociation and reassociation to approximate size of native protein

The solid line represents data for native Con A, the alternating dots and dashed line for dissociated Con A, the dashed line for re-associated Con A, and the fine dotted line for reassociated Con A post pepsin digestion. For similarly sized particles the y-intercept, the initial ratio of scattering intensity, is proportional to the concentration of analytes, though not quantitatively, a decrease is shown for the post pepsin digest sample. Reassociation of subunits is also validated by batch DLS, as seen in Figure 8b, with Rh for the reassociated Con A of 4.7 ± 0.5 and 4.8 ± 0.4 nm with and without the pepsin digestion procedure, respectively. Hydrodynamic sizes show no statistical difference between native and reassociated Con A. These values are in agreement with hydrodynamic sizes of tetrameric and dissociated Con A as reported in the literature.[37]

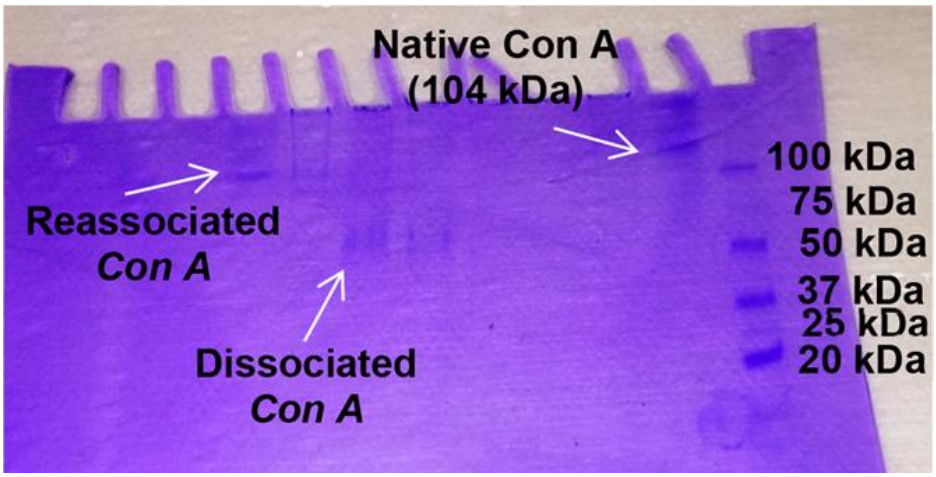

Figure 3.9 Gel electrophoresis of native, dissociated, and reassociated Con A released from PEMSN not exposed to pepsin

The dissociated protein was stirred with the PEMSN at a mass:solution volume ratio of 1:5 for 6 h at room temperature and then centrifuged. The pellet was washed with 10 mM PBS to remove weakly adsorbed protein subunits from the surface, and lypholized.

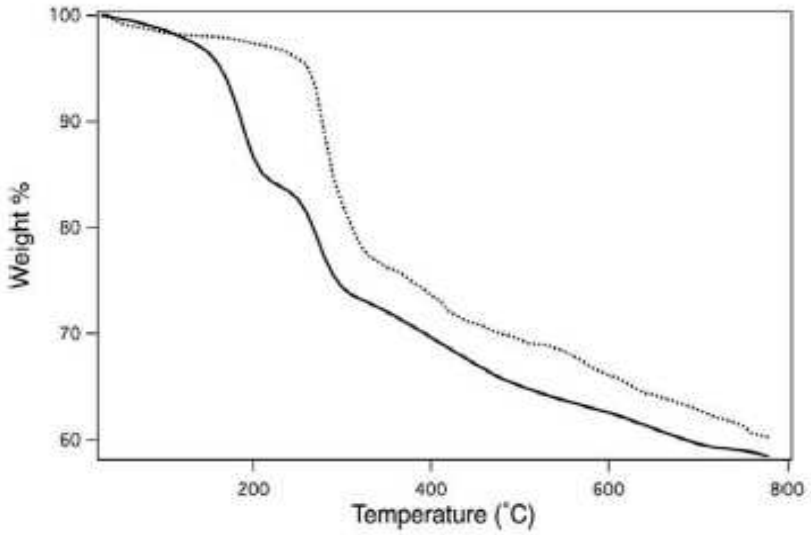

Figure 3.10 Thermogravimetric analysis (TGA) of buffer loaded (dotted line) indicating a 39.8 wt% loss and buffer with Con A loaded (solid line) PEMSN indicating a 42 wt% loss by 800°C

The weight percent difference between the buffer loaded blank final mass and the protein loaded PEMSN final mass was taken to determine how many milligrams of protein were loaded per gram (22 mg g^{-1} PEMSN). The weight loss due to silanol condensation is accounted for in the blank. From this and the molecular weight of Con A (54,000 g/mol), a loading in micromoles protein per gram PEMSN can be determined (0.407 μmol/g PEMSN). This was then compared to the original concentration to which the particles were exposed to determine what percentage was loaded (50.9%). This was further verified using thermogravimetric analysis relative to a blank in which PEMSN was treated in the same manner without any protein (Figure 3.10, calculation methodology is discussed), which indicated a loading of 0.4 μmol g^{-1} PEMSN (50.9% of the protein to which the PEMSN was exposed). In contrast, control experiments using nonporous Stöber silica particles (TEM, Figure 3.11) and MCM 41 with comparable surface area to the PEMSN showed only 6% of the protein solution was adsorbed onto the surface of nonporous silica and 27.5% onto MCM-41 (Figure 3.12).

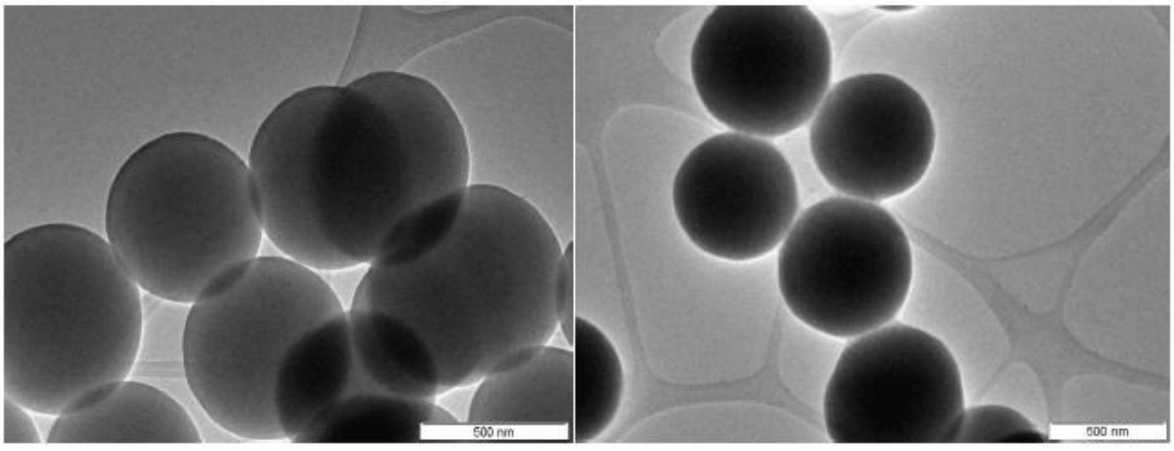

Figure 3.11 TEM images of nonporous silica nanoparticles (Stöber process)

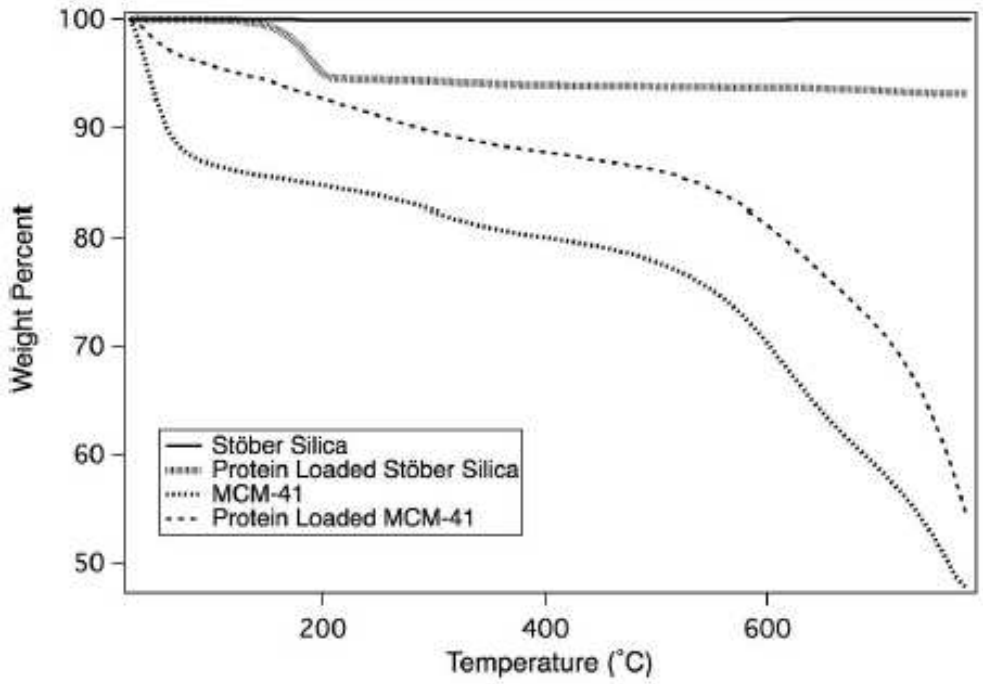

Figure 3.12 Thermogravimetric analysis (TGA) of nonporous silica (Stöber silica), Con A loading on nonporous silica nanoparticles, MCM-41 type mesoporous silica, and Con A loading onto MCM-41

The weight loss before 200°C is attributed to water loss/silanol condensation and accounted for in the blanks. Calculations were done as described in Figure 3.10. These data show a loading of 6% onto nonporous silica and 27.5% onto the MCM-41.

The low loading onto MCM-41 specifically suggests that the primary factor in achieving high protein loading is the expanded pore size of the PEMSN, not the surface area. That is to say, protein loading is more effective when the subunits have access to the pore volume through larger pore openings. To visualize the protein units, a 2% uranyl acetate negative staining solution was used. The uranyl cation binds biological material, specifically staining carboxylic acid and phosphate groups, which makes it an ideal stain for proteins and DNA in TEM imaging.[38] Con A possesses several carboxylic acid containing residues, including aspartic acid residues coordinated to the Ca^{2+} and Mn^{2+} ions in the active site. Thus, the dark areas in the

PEMSN shown in Figure 6B can be attributed to protein ionically bound to UO_2^{2+}.[39] Additionally, the spotting pattern indicates that the proteins are localized around the pores.

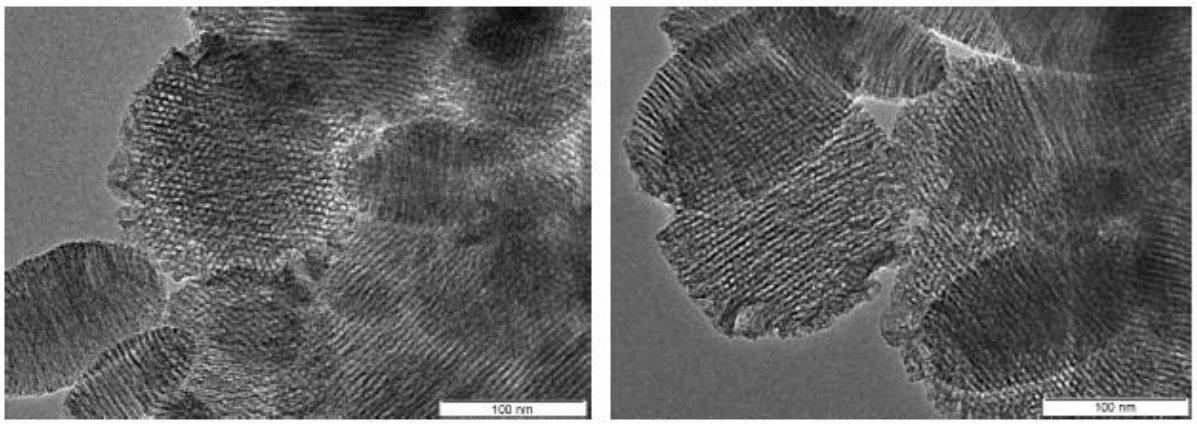

Figure 3.13 TEM images of PEMSN without protein loading stained with uranyl acetate

Staining of the bare PEMSN by the uranyl cation was not observed (Figure 3.13). To further illustrate the pores of the PEMSN protect the protein subunits from environmental factors, the loaded PEMSN were incubated in a 1:0.5 protein:pepsin solution for 1 h at 37 °C. Pepsin is a common digestive enzyme (protease) that breaks down exposed proteins into smaller peptides via hydrolysis of the amide bonds. Hence, decreases in pore volume relative to the unloaded MSN and darkened areas in the TEM can be attributed to protein subunits which were sheltered from pepsin digestion within the PEMSN pores. Nitrogen sorption analysis of these particles showed a small increase in pore volume (0.14 to 0.2 $cm^3\ g^{-1}$) and surface area (53.7 to 118 $m^2\ g^{-1}$), suggesting most of the protein subunits remained in the pore framework (Figure 3.14).

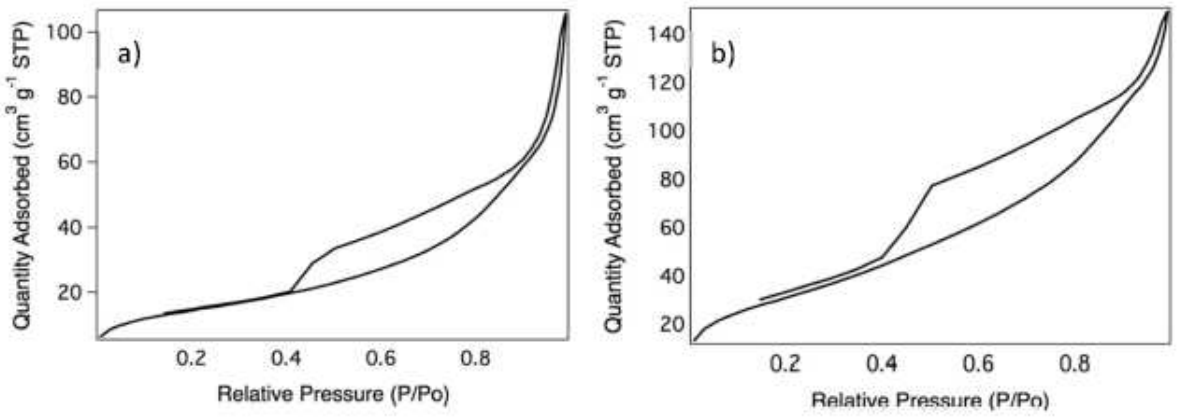

Figure 3.14 BET of a) PEMSN after loading Con A subunits and b) pore expanded, Con A loaded PEMSN after pepsin digestion.

The pore volume ($0.14 cm^3 g^{-1}$ to $0.2 cm^3 g^{-1}$) and surface area ($53.7 m^2 g^{-1}$ to $118 m^2 g^{-1}$) are relatively unchanged between the two, which indicated Con A within the PEMSN pores were not digested by pepsin

However, it should be noted that peptide fragments from digested protein would produce similar results. Therefore, the activity of protein released from the PEMSN that underwent digestion was tested and is addressed later. The TEM image (Figure 3.15) of protein subunit loaded PEMSN post pepsin exposure suggests protein persists within the pores. These data indicate that the protein subunits which were loaded into the PEMSN pores were protected from the pepsin digestion. Gel electrophoresis of the proteins unloaded from these digested particles showed clear bands corresponding to Con A dimers (data not shown), indicating that the proteins were additionally undamaged by the digestion. Thus, it can be concluded that dissociated protein was successfully loaded into the PEMSN pores.

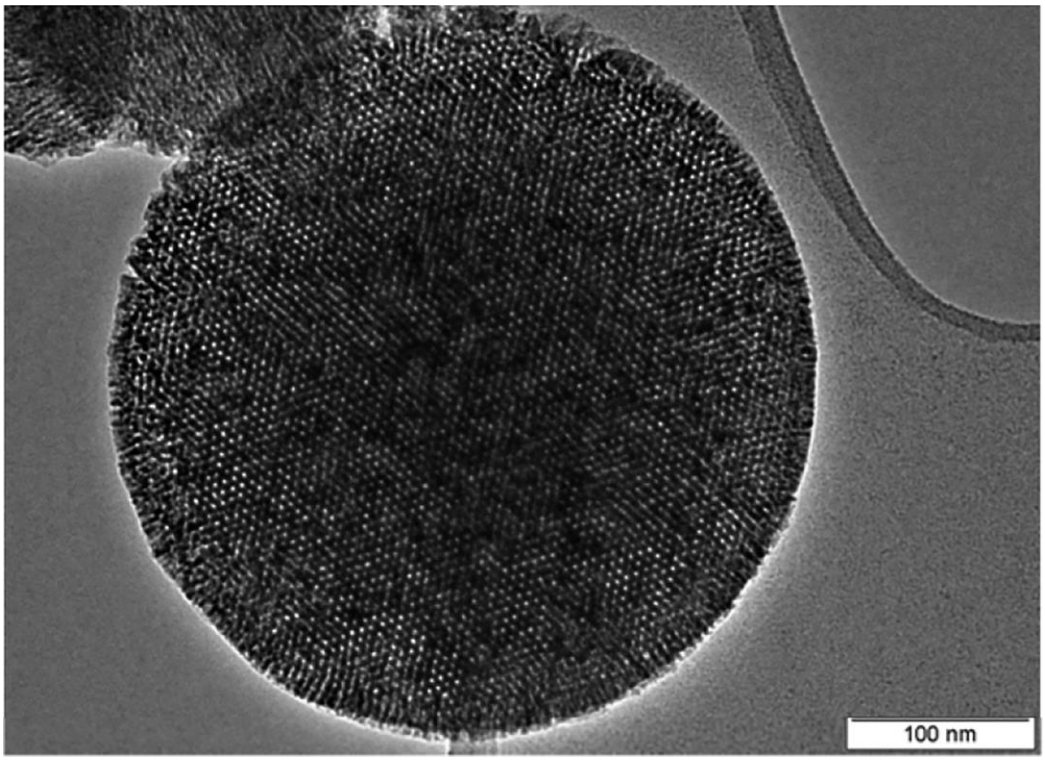

Figure 3.15 Transmission electron micrographs of protein loaded PEMSN after pepsin digestion (protein stained with 2% uranyl acetate)

3.4.3. Protein Release and Reassociation

Protein subunits were released, and the proteins were reconstituted by suspending the protein subunit loaded PEMSN in a solution of 10 mM PBS, pH 7.4 buffer (1 mg of MSN:15 mL of buffer). This solution was sampled every 4 h for 24 h, and the absorbance at 280 nm was measured. After one full 24 h cycle, 60% of the protein successfully diffused from the mesopores (Figure 3.16).

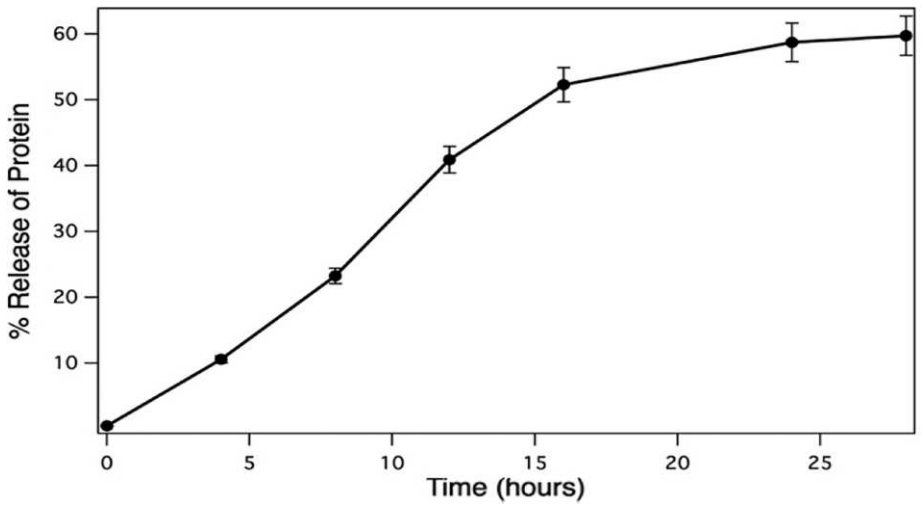

Figure 3.16 Protein release profile of Con A at pH 7.4 in PBS buffer. Error bars correspond to ±5% of the measured value. Experiments were done on protein released from PEMSN without pepsin digestion

Fluorescence measurements showed a blue shift of the 352 nm peak back to 337 nm (Figure 3.7), indicating that the subunits successfully reassociated with the tetramer. This was confirmed via gel electrophoresis, which showed the disappearance of the ~50 kDa band and reemergence of the ~100 kDa band (Figure 3.9). The activity was tested by binding the reassociated protein to a nylon membrane and adding horseradish peroxidase (HRP).[40] Con A binds to the mannose group in HRP without affecting enzymatic activity; thus, the activity of the protein can be visualized through the colored product created when HRP and Con A bind and react with ABTS substrate on the membrane. These binding experiments with the reassociated protein produced a characteristic pink spot (Figure 3.17), indicating that the Con A remains active after it is released from the PEMSN and reassociated. This experiment was done with protein released from PEMSN that had not been exposed to pepsin.

Figure 3.17 Binding activity of (a) native, (b) dissociated, and (c) reassociated Con A bound to a nylon membrane. The color is the product of active Con A bound horseradish peroxidase reacting with ABTS

The amount of active Con A after release from PEMSN and PEMSN exposed to pepsin was quantified using o-phthalaldehyde fluorescence, which has been shown to detect as little as 100 ng of protein. This was done relative to a calibration curve constructed using native Con A (Figure 3.18).

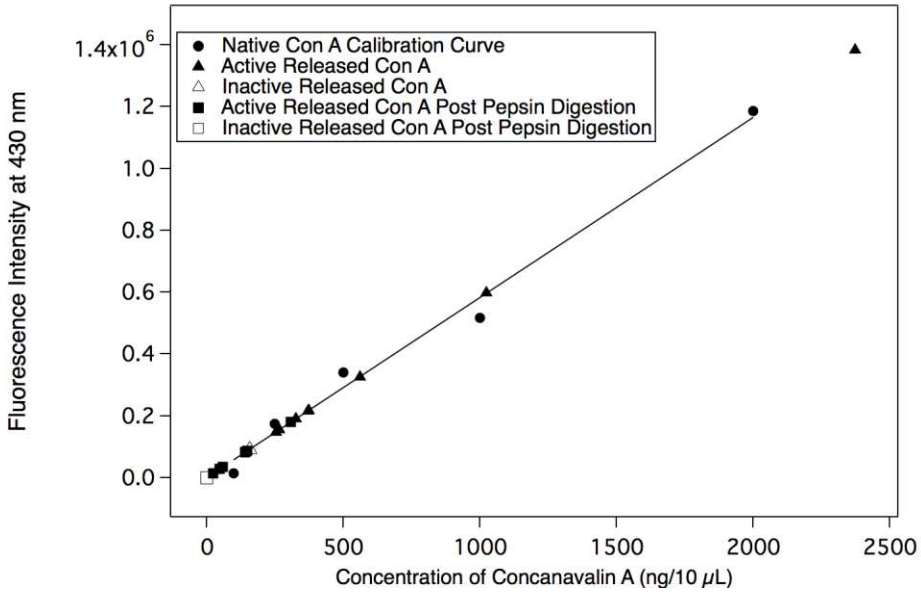

Figure 3.18 Native *Con A* calibration curve for the *o*-phthalaldehyde fluorescence quantification of released *Con A* activity showing: 3% unbound protein and 97% bound protein for the *Con A* released from PEMSN, and negligible unbound protein and nearly 100% bound protein for the *Con A* released from PEMSN that was exposed to pepsin

One milliliter of *Con A* solution was added to a 2 mL Sephadex G- 100 column, the inactive protein was collected over 2 min, and the bound protein was collected in 2 min increments for 20 min where each fraction consisted of 4 mL. The excitation wavelength was 340 nm and emission was monitored at 430 nm. First, the protein solution was run through a Sephadex G-100 column, which consists of cross-linked dextrose. Any active Con A would bind to the sugars on the column, while inactive protein would pass through. The active Con A was then eluted with a glucose solution. It was determined that 97% of the released protein (99% in the case of the sample digested with pepsin) was bound to the column and thus active. It is possible that the protein released from pepsin digested PEMSN shows higher activity because the pepsin removed any improperly reassociated or otherwise inactive Con A from the silica surface. None of the free, dissociated Con A showed activity after exposure to pepsin, and Con A on nonporous silica did not survive the digestion. This shows that the vast majority of Con A released from PEMSN reassociates properly, even after the PEMSN was digested with pepsin. Additionally, the inactivity of the free protein and that released from nonporous silica indicates that loading into the PEMSN pores is indeed necessary to preserve the Con A.

3.5. Conclusion

We have demonstrated the successful synthesis of pore enlarged MSN and its potential to deliver large molecular weight, active therapeutic proteins. Con A was shown to dissociate into smaller subunit groups which were successfully loaded into the expanded pores of MSN. These loaded subunits were sheltered from pepsin degradation and, upon a controlled, diffusion-based release, re-associated into the active protein. This was demonstrated through both gel electrophoresis and mannose binding experiments. This method of therapeutic protein delivery may be expanded to include heteromeric proteins and larger, multi-subunit enzymes in the

future. Heteromeric proteins could prove challenging due to variable adsorption and desorption rates between different subunits from the silica surface; however, it may still be possible to recover active protein. Further experimentation is necessary.

3.6. References

1. Carter, P. J., Introduction to current and future protein therapeutics: A protein engineering perspective. *Exp Cell Res* **2011,** *317* (9), 1261-1269.

2. Gu, Z.; Biswas, A.; Zhao, M.; Tang, Y., Tailoring nanocarriers for intracellular protein delivery. *Chem. Soc. Rev.* **2011,** *40* (7), 3638-3655.

3. Vivero-Escoto, J. L., Nanovehicles for Intracellular Protein Delivery. *J. Biotechnol. Biomater.* **2013,** *3*, e117.

4. Du, J.; Jin, J.; Yan, M.; Lu, Y., Synthetic nanocarriers for intracellular protein delivery. *Curr. Drug Metab.* **2012,** *13* (1), 82-92.

5. Carboni, M.; Abney, C. W.; Taylor-Pashow, K. M. L.; Vivero-Escoto, J. L.; Lin, W. B., Uranium Sorption with Functionalized Mesoporous Carbon Materials. *Industrial & Engineering Chemistry Research* **2013,** *52* (43), 15187-15197.

6. Akash, M. S. H.; Rehman, K.; Chen, S., Polymeric-based particulate systems for delivery of therapeutic proteins. *Pharm. Dev. Technol.* **2015,** *21* (3), 1-12.

7. Chou, L. Y.; Ming, K.; Chan, W. C., Strategies for the intracellular delivery of nanoparticles. *Chem. Soc. Rev.* **2011,** *40* (1), 233-245.

8. Li, Z.; Barnes, J. C.; Bosoy, A.; Stoddart, J. F.; Zink, J. I., Mesoporous silica nanoparticles in biomedical applications. *Chem. Soc. Rev.* **2012,** *41* (7), 2590-2605.

9. Serda, R. E., *Mass Transport of Nanocarriers*. CRC Press: 2012.

10. Slowing, I.; Trewyn, B. G.; Lin, V. S.-Y., Effect of surface functionalization of MCM-41-type mesoporous silica nanoparticles on the endocytosis by human cancer cells. *J. Am. Chem. Soc.* **2006,** *128* (46), 14792-14793.

11. Vivero-Escoto, J. L.; Slowing, I. I.; Trewyn, B. G.; Lin, V. S., Mesoporous silica nanoparticles for intracellular controlled drug delivery. *Small* **2010,** *6* (18), 1952-1967.

12. Deodhar, G. V.; Adams, M. L.; Trewyn, B. G., Controlled release and intracellular protein delivery from mesoporous silica nanoparticles. *Biotechnol J* **2017,** *12* (1).

13. Fang, I.-J.; Trewyn, B. G., Application of Mesoporous Silica Nanoparticles in Intracellular Delivery of Molecules and Proteins. *Methods Enzymol.* **2012,** *508*, 41.

14. Slowing, I. I.; Trewyn, B. G.; Lin, V. S.-Y., Mesoporous silica nanoparticles for intracellular delivery of membrane-impermeable proteins. *J. Am. Chem. Soc.* **2007,** *129* (28), 8845-8849.

15. Hudson, S.; Cooney, J.; Magner, E., Proteins in mesoporous silicates. *Angew. Chem. Int. Ed.* **2008,** *47* (45), 8582-8594.

16. Diaz, J. F.; Balkus, K. J., Enzyme immobilization in MCM-41 molecular sieve. *J. Mol. Catal. B: Enzym.* **1996,** *2* (2), 115-126.

17. Tu, J.; Boyle, A. L.; Friedrich, H.; Bomans, P. H.; Bussmann, J.; Sommerdijk, N. A.; Jiskoot, W.; Kros, A., Mesoporous Silica Nanoparticles with Large Pores for the Encapsulation and Release of Proteins. *ACS Appl. Mater. Interfaces* **2016,** *8* (47), 32211-32219.

18. Kwon, D.; Cha, B. G.; Cho, Y.; Min, J.; Park, E. B.; Kang, S. J.; Kim, J., Extra-Large Pore Mesoporous Silica Nanoparticles for Directing in Vivo M2 Macrophage Polarization by Delivering IL-4. *Nano Letters* **2017,** *17* (5), 2747-2756.

19. Kao, K.-C.; Mou, C.-Y., Pore-expanded mesoporous silica nanoparticles with alkanes/ethanol as pore expanding agent. *Microporous Mesoporous Mater.* **2013,** *169*, 7-15.

20. Eltohamy, M.; Shin, U. S.; Kim, H.-W., Silica nanoparticles with enlarged nanopore size for the loading and release of biological proteins. *Mater. Lett.* **2011,** *65* (23), 3570-3573.

21. Lee, J. H.; Park, J. H.; Eltohamy, M.; Perez, R.; Lee, E. J.; Kim, H. W., Collagen gel combined with mesoporous nanoparticles loading nerve growth factor as a feasible therapeutic three-dimensional depot for neural tissue engineering. *RSC Adv.* **2013,** *3* (46), 24202-24214.

22. Gao, Z.; Zharov, I., Large Pore Mesoporous Silica Nanoparticles by Templating with a Nonsurfactant Molecule, Tannic Acid. *Chem. Mater.* **2014,** *26* (6), 2030-2037.

23. Shin, H.-S.; Hwang, Y.-K.; Huh, S., Facile preparation of ultra-large pore mesoporous silica nanoparticles and their application to the encapsulation of large guest molecules. *ACS Appl. Mater. Interf.* **2014,** *6* (3), 1740-1746.

24. Thomson, J.; Augusteyn, R., On the structure of alpha m-crystallin. The reversibility of urea dissociation. *J. Biol. Chem.* **1984,** *259* (7), 4339-4345.

25. Schlesinger, M. J.; Barrett, K., The Reversible Dissociation of the Alkaline Phosphatase of Escherichia coli I. Formation and Reactivation of Subunits. *J. Biol. Chem.* **1965,** *240* (11), 4284-4292.

26. Rao, M. V. R.; Atreyi, M.; Rajeswari, M. R., Fluorescence studies on concanavalin-A. *J. Biosci.* **1984,** *6* (6), 823-828.

27. Weber, K.; Kuter, D. J., Reversible denaturation of enzymes by sodium dodecyl sulfate. *J. Biol. Chem.* **1971,** *246* (14), 4504-4509.

28. Varon, S.; Nomura, J.; Shooter, E. M., Reversible dissociation of the mouse nerve growth factor protein into different subunits. *Biochemistry* **1968,** *7* (4), 1296-1303.

29. Martina, P.; Joachim, G.; Axel, W.; Maria-Regina, K., Reversible Dissociation and Unfolding of Pyruvate Decarboxylase from Zymomonas mobilis. *European Journal of Biochemistry* **1994,** *224* (2), 651-661.

30. Lei, H. Y.; Chang, C. P., Lectin of Concanavalin A as an anti-hepatoma therapeutic agent. *J. Biomed. Sci.* **2009,** *16* (1), 1.

31. Chatterjee, A.; Mandal, D. K., Quaternary association and reactivation of dimeric concanavalin A. *Int. J. Biol. Macromolec.* **2005,** *35*, 103–109

32. Peterson, G. L., [12] Determination of total protein. In *Methods in Enzymology*, Academic Press: 1983; Vol. 91, pp 95-119.

33. Glatter, O., Kratky, O., *Small Angle X-ray Scattering: A Survey*. Academic Press: United Kingdom, 1982.

34. Ilavsky, J.; Jemian, P. R., Irena: tool suite for modeling and analysis of small-angle scattering. *Journal of Applied Crystallography* **2009,** *42* (2), 347-353.

35. Hoffmann, F.; Cornelius, M.; Morell, J.; Froba, M., Silica-based mesoporous organic-inorganic hybrid materials. *Angew. Chem. Int. Ed.* **2006,** *45* (20), 3216-3251.

36. Hudson, S. P.; Padera, R. F.; Langer, R.; Kohane, D. S., The biocompatibility of mesoporous silicates. *Biomaterials* **2008,** *29* (30), 4045-4055.

37. Mangold, S. L.; Cloninger, M. J., Binding of monomeric and dimeric Concanavalin A to mannose-functionalized dendrimers. *Organic & Biomolecular Chemistry* **2006,** *4* (12), 2458-2465.

38. Estandarte, A. K. C. A review of the different staining techniques for human metaphase chromosomes. University of London, 2012.

39. Becker, J. W.; Reeke, G.; Wang, J. L.; Cunningham, B. A.; Edelman, G. M., The covalent and three-dimensional structure of concanavalin A. III. Structure of the monomer and its interactions with metals and saccharides. *J. Biol. Chem.* **1975,** *250* (4), 1513-1524.

40. Company, T. B. E. Affinity Chromatography of Glucose Binding Protein.

CHAPTER 4 CONTROLLED RELEASE OF YEAST ALCOHOL DEHYDROGENASE SUBUNITS FROM LARGE PORE MESOPOROUS SILICA NANOPARTICLE

4.1 Introduction

After proving the successful loading and release of multi-subunits of concanavalin A (*Con A)* using pore expanded MSN,[1] controlled release of yeast alcohol dehydrogenase (ADH) was demonstrated at two different pH. Alcohol dehydrogenase is part of oxidoreductase family which catalyzes the oxidation of alcohols using NAD+ as the electron acceptor.[2] ADH is a homotetramer with a single zinc atom on each subunit, which is responsible for enzymatic activity, ADH has a molecular mass of 150 kDa.[3-8] Alcohol dehydrogenase plays a key role in alcohol metabolism involving two separate, subsequent steps. First, in a reversible reaction, ADH oxidizes alcohol to acetaldehyde and in a second step, acetaldehyde is further oxidized into acetate in the liver. The oxidation of acetate is completed by converting to carbon dioxide and water. Step 2 is catalyzed by the enzyme aldehyde dehydrogenase (ALDH). Acetaldehyde is oxidized to acetate; NAD+ is the enzymatic cofactor and is reduced to NADH. The ALDH reaction is essentially irreversible. Much of the acetaldehyde produced from the oxidation of alcohol is oxidized in the liver to acetate; leading to low levels of circulating acetaldehyde under normal conditions.[2, 6, 9-11] Most internalized and bio-produced alcohol is oxidized in the liver, which makes an oral delivery of an enzyme the size of ADH quite a difficult task. Unprotected, the enzyme will quickly be protonated in the acidic pH of the stomach, as well as degraded by proteases. Therefore, ADH needs to be protected for oral deliver, one technology to protect enzymes is by impregnating into mesoporous silica nanoparticles.[12-13] The molecular size of the intact, homotetramer of ADH is too large to fit into the pores of traditional MSN (mesopore size ~2-3.5 nm) or pore-expanded MSN (mesopores size ~5-6 nm). However, large proteins that

consist of quaternary structures of multiple smaller components can be chemically or physically dissociated in individual subunits to produce particles appropriately sized for loading into mesopores of pore-expanded MSN.[1] Chemical reagents that have been demonstrated to reversibly dissociate ADH include urea, guanidine hydrochloride (GnHCl) and dithiothreitol (DTT).[14-17]

Herein, we report the reversible dissociation of ADH in presence of guanidine hydrochloride. ADH has been dissociated into smaller subunits in presence of 6 M guanidine hydrochloride (GnHCl) and 0.5 mM dithiothreitol (DTT) which can be loaded inside the pores of pore expanded MSN. Release of ADH subunits was carried out at two different pH 5.5 and 7.4. Several studies have been demonstrated on pH responsive release of protein or drug molecules using mesoporous silica nanoparticles. In 2007, I. Slowing and coworkers successfully demonstrated release of cytochrome c from MSN at acidic (5.2) and physiological (7.4) pH.[18] Yang and coworkers studied release of DOX using pH responsive system of poly (glutamic acid) grafted MSN (MSN-PGLA). The release behavior was studied at different pH values (5.5, 6.8 and 7.4). Decreasing pH attributed to the protonation of poly (glutamic acid), which facilitated release of positively charged DOX from mesoporous material.[19]

Synthesis of pore expanded MCM-41 and amine functionalized MSN has been demonstrated and characterized. The amount of loading of dissociated ADH on PEMCM-41, positively charged NH2-MSN and stober silica particles acting as a control was determined using thermogravimetric analysis. Higher loading was observed on PEMCM-41 compared to NH2-MSN and stober silica material. The dissociation and re-association were verified using fluorescence, dynamic light scattering (DLS) and field flow fractionation (FFF)studies. More amount of ADH was released from PEMCM-41 at acidic conditions than at physiological pH due

to electrostatic repulsion between MSN and dissociated ADH. After release and reconstitution of ADH subunits, the activity of re-associated enzyme was studied using UV spectroscopy at wavelength 340 nm which monitors reduction of NAD+ to NADH.

4.2 Materials, Instrumentation and Methods

4.2.1 Materials and Instrumentation

Alcohol dehydrogenase (ADH) from yeast, mesitylene, 98% tetraethyl orthosilicate, cetyltrimethylammonium bromide (CTAB), Guanidine hydrochloride (GnHCl), dithiothreitol (DTT), 14.5 M NH_4OH (28% w/w NH_3) and β-NAD hydrate were purchased from Sigma-Aldrich. All other chemicals and materials were used as received.

4.2.2 Nitrogen sorption analysis

Nitrogen sorption analysis was conducted on a Micrometrics TriStar II surface area and porosity analyzer. Before analysis all the samples (80-100 mg) were degassed under nitrogen at 100 °C for 6 h. In presence of nitrogen gas (-196 °C), all measurements were recorded. From the adsorption-desorption isotherms, pore volume and diameter of samples were calculated using BJH model. Fluorescence studies were done using Horiba Jobin Yvon NanoLog. The measurements were taken with an excitation wavelength at 280 nm and emission wavelength ranging from 290 – 450 nm.

4.2.3 Synthesis of pore enlarged MSN

A solution of 1 g CTAB in 480 mL nanopure water was mixed with 3.5 mL of 2 M NaOH(aq) and 7.0 mL of mesitylene. This mixture was stirred vigorously at 80 °C for 2 h before 5 mL of tetraethyl orthosilicate was added dropwise at approximately 1 mL min^{-1}. The reaction was allowed to continue at the same temperature and stir rate for another 2 h, and the resulting white precipitate was filtered, washed with abundant methanol, and dried for 12 h at 100 °C.

Residual CTAB was removed via an acid extraction in which a suspension of 1 g of as-synthesized material was stirred at 50 °C for 6 h in 100 mL of methanol with 0.75 mL of concentrated hydrochloric acid. The product was filtered again, rinsed with methanol, and dried under a vacuum for 12 h at room temperature.[18]

4.2.4 Synthesis of amine functionalized MSN (NH_2-MSN)

NH_2-MSN was synthesized by co-condensation method.CTAB (1.0 g) was dissolved in 480 mL of nanopure water. NaOH (aq) (2.0 M, 3.5 ml) and 7.0 mL mesitylene was introduced to the CTAB solution at 80 °C. Tetraethyl orthosilicate (TEOS, 5.0 ml, 22.4 mmol) and 3-aminopropyltrimethoxysilane (APTMS, 1.0 ml) was added dropwise to the CTAB solution under vigorous stirring. The mixture was allowed to continue at the same temperature and stir rate for 2 h to generate a white precipitate. This solid crude product was filtered, washed with nanopure water and methanol, and dried under high vacuum to yield the as-synthesized NH_2-MSN. Surfactant was then removed by acid extraction as previously described.[20] Amino groups were quantified to be 12 wt % by thermogravimetric analysis (TGA).

4.2.5 Synthesis of Stöber Silica (Nonporous Silica Particles)

In a 250 mL round-bottom flask, mixture of ethanol (150 mL, 95%), 14.5 M NH_4OH (50 mL, 28% w/w NH_3) and TEOS (12.5 mL) was taken. The reaction mixture was stirred for 24 hours at room temperature followed by centrifugation and washings with abundant amounts of ethanol. The silica particles were stored in ethanol and collected as required by drying in a vacuum oven for 5 h at at 550 °C.[21]

4.2.6 Enzymatic activity of ADH

The enzymatic reactivity of alcohol dehydrogenase catalyzed conversion of ethanol to acetaldehyde was determined based on a method developed and published by Vallee and Hoch.[21] Typically, an alcohol dehydrogenase enzyme stock solution was prepared by dissolving the enzyme in a phosphate buffer (10 mM, pH 7.4) to reach an enzyme concentration of 1 mg ml^{-1}. The enzyme stock solution was further diluted to the enzyme working solution, with an enzyme concentration of 0.2 mg ml^{-1} in sodium phosphate buffer (10 mM with 0.1 % w/v Bovine Serum Albumin). A 15 mM solution of β-nicotinamide adenine dinucleotide (NAD+) was prepared by dissolving NAD+ (0.5 g) in deionized water (50 ml). In a cuvette, 3.2% (v/v)ethanol, 7.5 mMNAD+ solution and 0.1 mL enzyme working solution was pipetted and sodium pyrophosphate buffer solution (50 mM, pH 8.8) was added until a total volume of 3 mL was reached. The mixture was immediately measured for UV-Vis absorbance at 340 nm for 6 min Beckmann Coulter DU800 spectrophotometer.[22-24]

4.2.7 ADH dissociation, loading and release

Native enzyme (1 mg mL^{-1}) was dissolved in 0.1 M phosphate buffer, pH 7.5. Dissociation of native ADH (4 μM) was accomplished in 0.1 M phosphate buffer, pH 7.4 in the presence of 6 M guanidine hydrochloride and 0.5 mM DTT.[15] The reaction mixture was stirred at room temperature for 18 h. The loading of dissociated enzyme subunits into the mesopores was accomplished by stirring enzyme solution with pore expanded MSN (mass: volume ratio of 1:5) at room temperature for 6 h.[18] The mixture was then centrifuged at 75000 rpm and washed with 0.1 M phosphate buffer (pH 7.4) and lyophilized. The release profile of ADH subunits from mesoporous material was studied at two different pH 7.4 and 5.5. Successful release of enzyme subunits was carried out by suspending enzyme subunit loaded MSN in 0.1 M phosphate buffer

in presence of 1 mM $ZnCl_2$ (20-fold dilution) at pH 7.4 and 5.0. The mixture was centrifuged (6000 rpm) and the solution was sampled every 4 h for one full 24 h cycle. The absorbance of all the aliquots was recorded at 280 nm.

MCM-41 with enlarged pores synthesized by using a pore-expanding agent (mesitylene) was comprised of regular parallel mesoporous channels as shown in the transmission electron micrographs (TEM) image (Figure 4.1).

4.3 Results and Discussion

4.3.1 MSN characterization

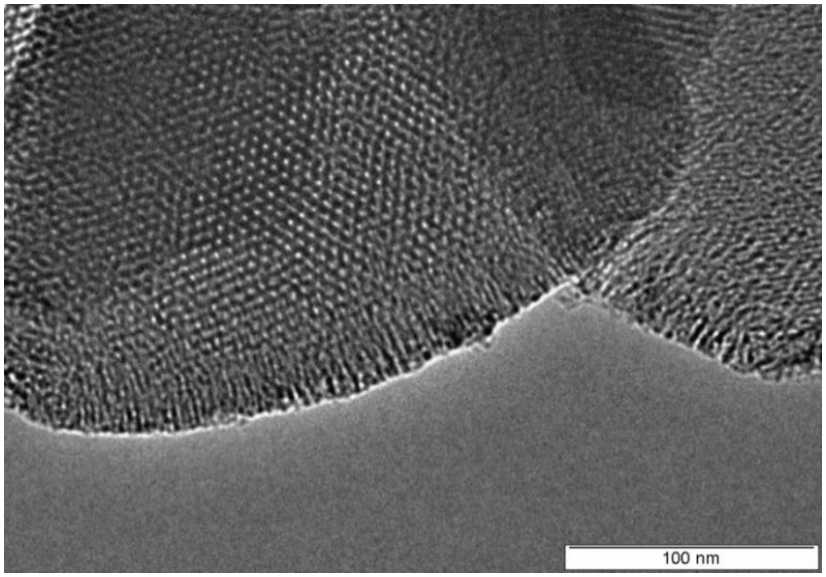

Figure 4.1 Transmission electron micrograph of pore expanded MCM-41

The surface area was calculated by the Brunauer-Emmett-Teller (BET) method. The pore size distribution was calculated by the Barrett-Joyner-Halenda (BJH) method using the desorption branch of isotherm Figure 4.2.

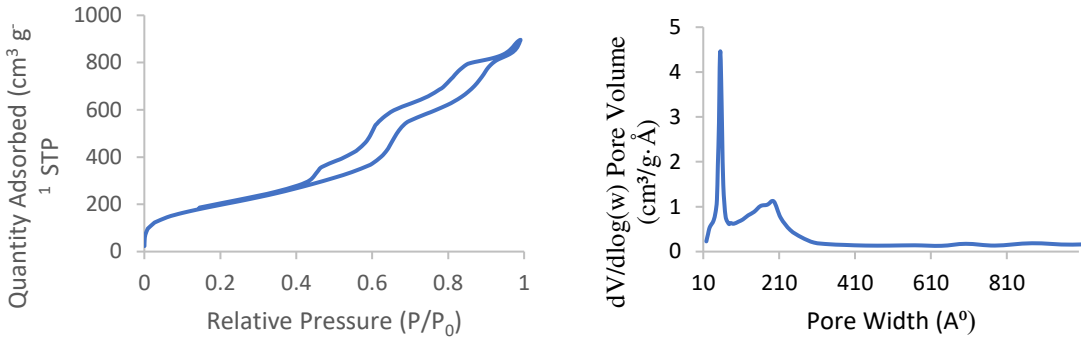

Figure 4.2 Nitrogen sorption analysis of pore expanded MCM-41 (PEMCM-41)

The nitrogen sorption analysis of the material exhibited a type IV isotherm characteristic of mesoporous material with a BET surface area of 726 m^2 g^{-1} and a pore volume of 1.0 cm^3 g^{-1} as shown in Table 4.1 The BJH method gave two pore size distributions centered on 5.6 nm (major peak) and 15.5 nm (minor).

Table 4.2 Nitrogen sorption analysis of before and after loading of dissociated ADH on pore expanded MCM-41

Material	BET Surface Area (m^2/g)	Pore volume (cm^3/g)
Pore expanded MCM-41	726	1.0
ADH loaded-MCM-41	119	0.2

4.3.2 Dissociation ADH and loading ADH into the pores of MSN

The dissociation and re-association of the enzyme was confirmed through fluorescence studies using an excitation wavelength of 280 nm and emission wavelength range of 290 – 450 nm. The native enzyme emission peak was observed at 337 nm while an emission peak for

dissociated enzyme was red-shifted to 354 nm (shown in Figure 4.3) indicating complete exposure of the buried tryptophan residues to the solvent.

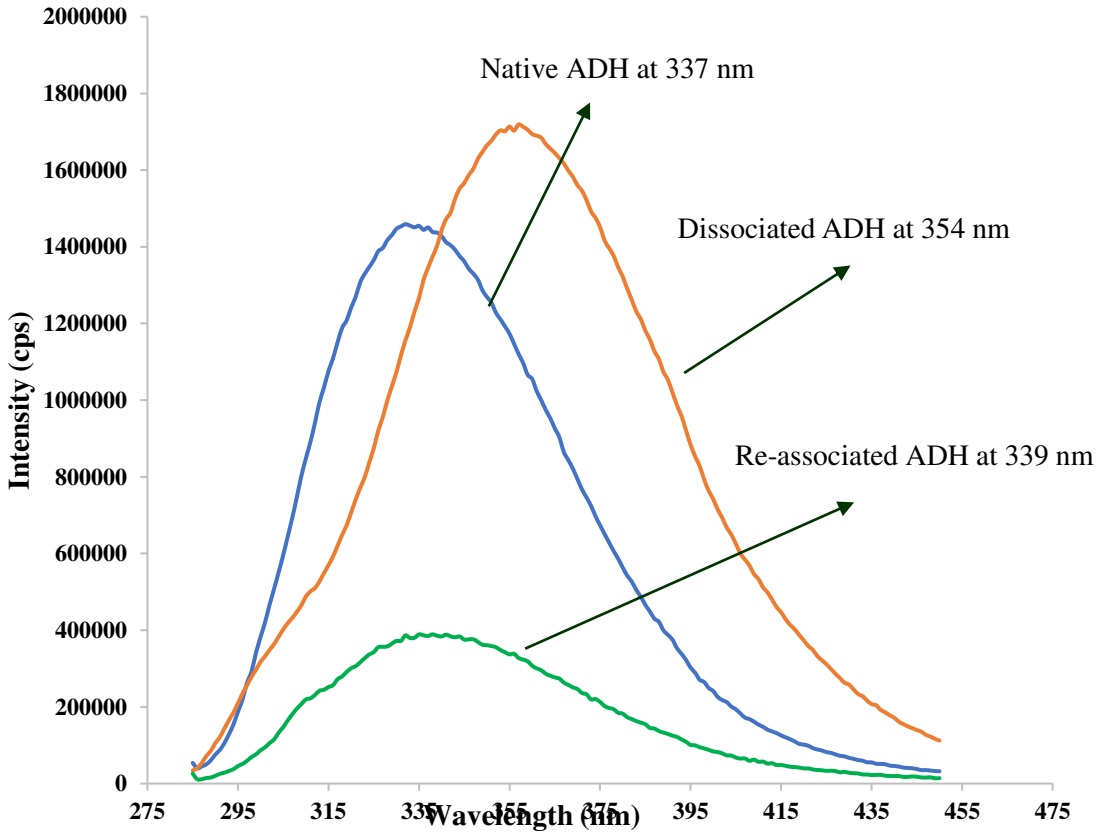

Figure 4.3 Fluorescence measurements at an excitation wavelength of 280 nm of native ADH (blue), dissociated ADH (red), and re-associated ADH (green)

Upon re-association, the dissociated enzyme emission peak at 354 nm was blue shifted back to 339 nm which was in accordance with the native enzyme emission wavelength peak.[25]

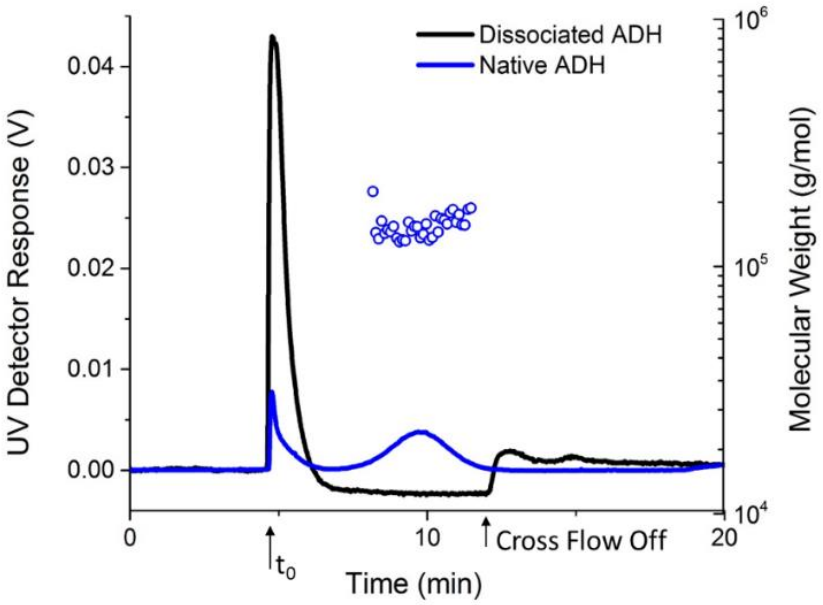

Figure 4.4 AF4 fractogram of native and dissociated ADH

The molecular weight and size were determined using asymmetrical flow field-flow fractionation with multiangle and dynamic light scattering (AF4-MALS-DLS). As is seen in Figure 4.4, the native ADH protein elutes at 10 min corresponding to hydrodynamic radius of 4.5 nm with a molecular weight of 143 kDa. Dissociated ADH co-elutes with the void peak in these flow conditions corresponding to a size approximately 1 nm. From monitoring of the cross-flow the dissociated ADH also appears to be passing through the AF4 regenerated cellulose membrane. The membrane molecular weight cut-off is nominally 30 kDa as determined by the manufacturer using globular protein standards. To confirm hydrodynamic radius, batch DLS was conducted on native and dissociated ADH in 0.1 M phosphate buffer with 8 M guanidine hydrochloride added to the dissociated experiment set-up The hydrodynamic radius of dissociated ADH is 1.25 nm while that of native is 4.7 nm.

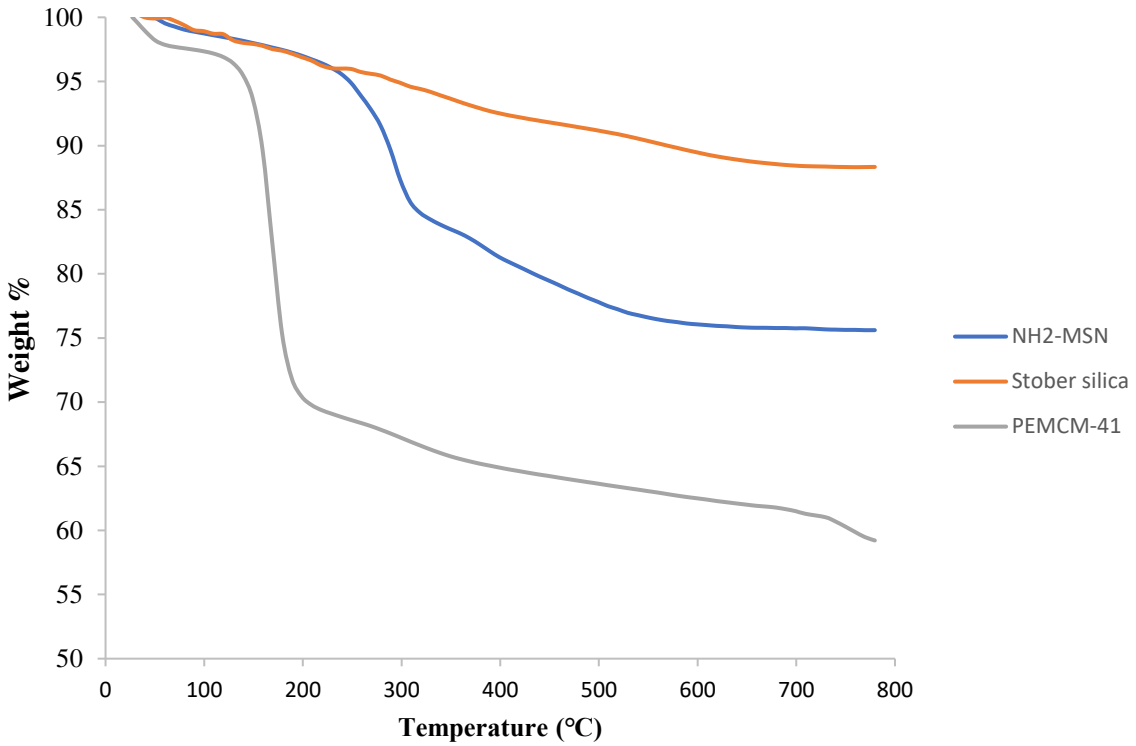

Figure 4.5 Thermogravimetric analysis (TGA) of ADH loading on NH_2-MSN, Pore expanded MCM-41 and stöber silica.

The amount of dissociated ADH loaded into the pores of PEMCM-41 was determined by thermogravimetric analysis (Figure 4.5). Controlled experiments were carried out using non-porous silica. It was observed that 40% of the enzyme was loaded on pore expanded MCM-41 and 24% on NH_2-MSN while only 8% of the enzyme was adsorbed on Stöber non-porous silica. This result suggests that loading of dissociated ADH subunits is more effective on negatively charged PEMCM-41 as compared to positively charged NH_2-MSN and nonporous silica. The loading of ADH on MSN was also confirmed by nitrogen sorption analysis. The BET surface area decreased from 726 to 118 m^2/g and pore volume from 1.0 to 0.2 cm^3/g upon ADH loading.

4.4 Enzyme release profile

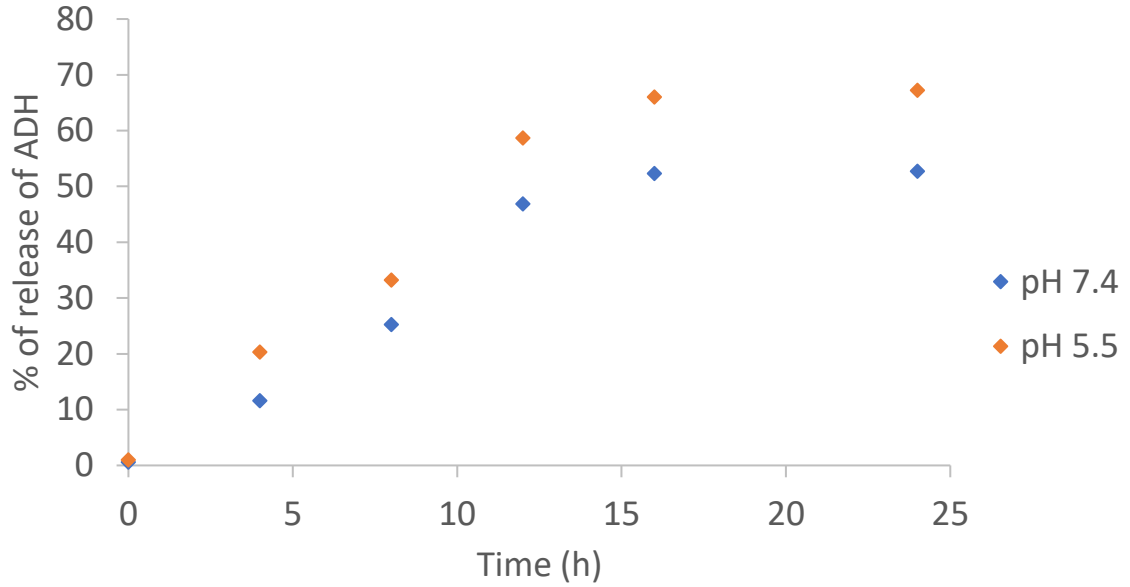

Figure 4.6 Release profile of dissociated ADH from pore expanded MCM-41 at different pH 7.4 and 5.5

The release of ADH subunits from the MSN material was studied by measuring UV absorption at 280 nm wavelength. ADH subunits were released from MSN material via diffusion in 0.1 M phosphate buffer at two different pH values. The release profiles were measured at cytoplasmic pH (pH 7.4) and at an endosomal pH (pH 5.5). The total percent of loaded proteins that were released was 52% and 67% at pH 7.4 and pH 5.5, respectively. The dissociated ADH is expected to be positively charged, whereas the MSN (pKa around 3) would be negatively charged at both pH values. At neutral pH, MSN will have more negative charges on the pore surface due to a greater number of deprotonated silanols than it would at acidic pH. Therefore, due electrostatic repulsion the percent release of dissociated ADH is greater at acidic medium.18 (Figure 4.6).

Table 4.3 Zeta potential of MSN and dissociated ADH at pH 7.4 and 5.5

	Zeta potential (mV)	
pH	7.4	5.5
Pore expanded MCM-41	-20.1	-2.02
Dissociated ADH	+1.14	+1.96

The observed difference in the rates of release at these two pH values could be attributed to the different amount of negative charges on the MSN surface. It was confirmed by measuring zeta potential of dissociated and MSN as a function of pH. The zeta potential of dissociated ADH was observed at between +1 mV and +2 mV at neutral and acidic pH, while the zeta potential of MSN dropped from -20 mV at pH 7.4 to -2 mV at pH 5.5 (Table 4.4). This confirmed the surface charge property of MSN was affected by the change in pH.

4.5 Enzymatic activity of re-associated ADH

The enzymatic activity of re-associated ADH was measured by means of ADH enzyme assay tests as described in the experimental section. The enzyme assay test is based on the different UV-Vis absorption behaviors of NAD+ and its reduced form, NADH. The strong absorption of NADH is observed at wavelength of 340 nm due to nicotinamide moiety but only when it is in reduced form. In an ADH enzyme catalyzed alcohol oxidation reaction, the production of NADH is proportional to the consumption of NAD+ and the generation of aldehyde. Therefore, we can monitor the reaction kinetics by measuring the UV-vis light absorbance values. At zero time, add 0.1 ml of appropriately diluted enzyme to the cuvette and record the A340 for 3-4 minutes. The enzymatic activity of native and re-associated ADH

calculated from the ΔA340/minute from the initial linear portion of the curve was 320 and 272 mg/units respectively.

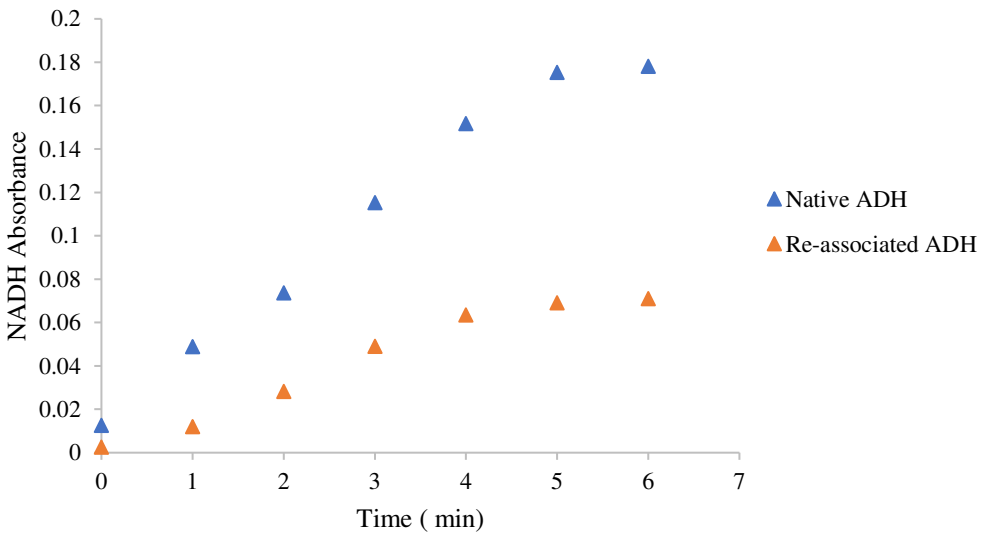

Figure 4.7 Enzymatic activity of native and re-associated ADH using UV-Vis spectroscopy

4.6 Conclusion

In summary we have demonstrated the loading and controlled release of ADH using MSN with enlarged pores. Successful dissociation and re-association of ADH was confirmed through fluorescence studies, FFF and DLS. The higher amount of enzyme loading (40 %) was observed on pore expanded MCM-41 as compared to positively charged APMSN and non-porous silica. Controlled release of ADH from mesoporous material was carried out at neutral and acidic pH and was further re-associated back into active form. The enzymatic activity of re-associated ADH was investigated by calculating the rate of absorbance at 340 nm resulting from the reduction of NAD + using UV-vis spectroscopy.

ADH breaks down alcohol to acetaldehyde, a highly toxic substance. Acetaldehyde can be further metabolized to acetate by another enzyme aldehyde hydrogenase (ALDH). Thus, further

experimentation is necessary in order to complete the cycle of alcohol metabolism. It can be achieved by controlled release of multiple enzymes from mesoporous materials.

4.7 References

1. Deodhar, G. V.; Adams, M. L.; Joardar, S.; Joglekar, M.; Davidson, M.; Smith, W. C.; Mettler, M.; Toler, S. A.; Davies, F. K.; Williams, S. K. R., Conserved Activity of Reassociated Homotetrameric Protein Subunits Released from Mesoporous Silica Nanoparticles. *Langmuir* **2017,** *34* (1), 228-233.

2. Edenberg, H. J., The genetics of alcohol metabolism: role of alcohol dehydrogenase and aldehyde dehydrogenase variants. *Alcohol Research & Health* **2007,** *30* (1), 5.

3. Drum, D. E.; Harrison, J. H.; Li, T.-K.; Bethune, J.; Vallee, B. L., Structural and functional zinc in horse liver alcohol dehydrogenase. *Proceedings of the National Academy of Sciences* **1967,** *57* (5), 1434-1440.

4. Raj, S. B.; Ramaswamy, S.; Plapp, B. V., Yeast alcohol dehydrogenase structure and catalysis. *Biochemistry* **2014,** *53* (36), 5791-5803.

5. Vallee, B. L.; Hoch, F. L., ZINC, A COMPONENT OF YEAST ALCOHOL DEHYDROGENASE. *Proceedings of the National Academy of Sciences* **1955,** *41* (6), 327.

6. Twu, J.-S.; Chin, C. C.; Wold, F., Active-site sulfhydryl groups of yeast alcohol dehydrogenase. *Biochemistry* **1973,** *12* (15), 2856-2862.

7. Leskovac, V.; Trivić, S.; Peričin, D., The three zinc-containing alcohol dehydrogenases from baker's yeast, Saccharomyces cerevisiae. *FEMS yeast research* **2002,** *2* (4), 481-494.

8. Ganzhorn, A.; Plapp, B., Carboxyl groups near the active site zinc contribute to catalysis in yeast alcohol dehydrogenase. *Journal of Biological Chemistry* **1988,** *263* (11), 5446-5454.

9. Frezza, M.; di Padova, C.; Pozzato, G.; Terpin, M.; Baraona, E.; Lieber, C. S., High blood alcohol levels in women: the role of decreased gastric alcohol dehydrogenase activity and first-pass metabolism. *New England Journal of Medicine* **1990,** *322* (2), 95-99.

10. Dickinson, F. M.; Monger, G. P., A study of the kinetics and mechanism of yeast alcohol dehydrogenase with a variety of substrates. *Biochemical Journal* **1973,** *131* (2), 261-270.

11. Racker, E., [79] Alcohol dehydrogenase from baker's yeast: RCH2OH+ DPN+⇄ RCHO+ DPNH+ H+. **1955**.

12. Deodhar, G. V.; Adams, M. L.; Trewyn, B. G., Controlled release and intracellular protein delivery from mesoporous silica nanoparticles. *Biotechnology journal* **2017,** *12* (1), 1600408.

13. Liao, M.-H.; Chen, D.-H., Immobilization of yeast alcohol dehydrogenase on magnetic nanoparticles for improving its stability. *Biotechnology letters* **2001,** *23* (20), 1723-1727.

14. Le, W.-P.; Yan, S.-X.; Zhang, Y.-X.; Zhou, H.-M., Acid-induced folding of yeast alcohol dehydrogenase under low pH conditions. *The Journal of Biochemistry* **1996,** *119* (4), 674-679.

15. GERSCHITZ, J.; RUDOLPH, R.; JAENICKE, R., Refolding and reactivation of liver alcohol dehydrogenase after dissociation and denaturation in 6M guanidine hydrochloride. *European journal of biochemistry* **1978,** *87* (3), 591-599.

16. OHTA, T.; OGURA, Y., Effects of urea on the activity and structure of yeast alcohol dehydrogenase. *The Journal of Biochemistry* **1965,** *58* (1), 73-89.

17. LE, W. P.; YAN, S. X.; LI, S.; ZHONG, H. N.; ZHOU, H. M., Alkaline unfolding and salt-induced folding of yeast alcohol dehydrogenase under high pH conditions. *International journal of peptide and protein research* **1996,** *47* (6), 484-490.

18. Slowing, I. I.; Trewyn, B. G.; Lin, V. S.-Y., Mesoporous silica nanoparticles for intracellular delivery of membrane-impermeable proteins. *Journal of the American Chemical Society* **2007,** *129* (28), 8845-8849.

19. Yang, K.-N.; Zhang, C.-Q.; Wang, W.; Wang, P. C.; Zhou, J.-P.; Liang, X.-J., pH-responsive mesoporous silica nanoparticles employed in controlled drug delivery systems for cancer treatment. *Cancer biology & medicine* **2014,** *11* (1), 34.

20. Yokoi, T.; Yoshitake, H.; Tatsumi, T., Synthesis of amino-functionalized MCM-41 via direct co-condensation and post-synthesis grafting methods using mono-, di-and tri-amino-organoalkoxysilanes. *Journal of Materials Chemistry* **2004,** *14* (6), 951-957.

21. Ibrahim, I. A.; Zikry, A.; Sharaf, M. A., Preparation of spherical silica nanoparticles: Stober silica. *J. Am. Sci* **2010,** *6* (11), 985-989.

22. Kägi, J. H.; Vallee, B. L., The role of zinc in alcohol dehydrogenase V. The effect of metal-binding agents on the structure of the yeast alcohol dehydrogenase molecule. *Journal of Biological Chemistry* **1960,** *235* (11), 3188-3192.

23. Harris, I., Structure and catalytic activity of alcohol dehydrogenases. *Nature* **1964,** *203* (4940), 30.

24. Vanni, A.; Anfossi, L.; Pessione, E.; Giovannoli, C., Catalytic and spectroscopic characterisation of a copper-substituted alcohol dehydrogenase from yeast. *International journal of biological macromolecules* **2002,** *30* (1), 41-45.

25. Gafni, A.; Brand, L., Fluorescence decay studies of reduced nicotinamide adenine dinucleotide in solution and bound to liver alcohol dehydrogenase. *Biochemistry* **1976,** *15* (15), 3165-3171.

CHAPTER 5 MICRO-COLUMN RARE EARTH SEPARATION USING HDEHP/ORDERED MESOPOROUS CARBON MATERIALS

5.1 Abstract

Adjacent lanthanides are among the most challenging element to separate, to the extent that current separations materials would benefit from transformative improvement. Ordered mesoporous carbon (OMC) materials are excellent candidates, owing to their small mesh size and uniform morphology. Herein, OMC materials were physisorbed with bis-(2-ethylhexyl) phosphoric acid (HDEHP) and sorption of Eu^{3+} was investigated under static and dynamic conditions. The HDEHP-OMC materials displayed higher distribution coefficients and loading capacities than current state-of-the materials. Using a small, unpressurized column, a separation between Eu^{3+} and Nd^{3+} was achieved. Based on these experimental results, HDEHP-OMC have shown potential as a solid phase sorbent for chromatographic intragroup, lanthanide separations.

5.2 Introduction

The most difficult elemental separations on the periodic table center on separating trivalent *f*-elements from each other. The separation of *f*-elements by a variety of solid sorbents has been broadly considered in the literature.[1-5] Both pristine and functionalized mesoporous carbon (MC) materials are a subcategory of solid sorbents that have been investigated for *f*-elements recovery.[4, 6-15] Ordered MC (OMC) materials are an attractive alternative to conventionally used polymeric resins due to their high surface areas, regular ordered mesopores, tunable pore size and morphology, large pore volumes, low reactivity, thermal and mechanical stability, and the potential for surface functionalization. The ability to utilize OMC materials for metal ion separations could have significant benefits since the smaller particle size should limit longitudinal diffusion of a given analyte and increase the number of theoretical plates in a given

column based on such materials ultimately improving the resolution of a given separation. The high surface area of the OMCs could allow for a higher ligand loading capacity as well. Considering the ongoing challenge of intragroup, trivalent *f*-element separations, and the potential improvements in resolution and loading capacity associated with OMC materials, the use of OMC materials to complete f-element separations is a logical step.

Despite all the potential benefits of using MC materials in a chromatographic configuration, all studies considering *f*-element separations to date have examined the batch mode (i.e. single separation stage) separation capability of *f*-element separation or recovery by MCs. Perrault et al. recently demonstrated that a column could be prepared from CMK-8 type MCs functionalized with diglycolamide-based ligand for the recovery of lanthanides.[16] However, no studies have demonstrated the ability to use MCs in a chromatographic, *f*-element separation. This is an important question to address since backpressure issues arising from the tight packing of submicron particles could prevent the application of a chromatographically-based approach for metal ion separation. To test these hypotheses, ordered mesoporous carbon nanomaterials physiorbed with bis-(2-ethylhexyl) phosphoric acid (HDEHP) have been prepared to complete intragroup, trivalent lanthanide separations.

While the general principles of completing chromatographic separations using a smaller footprint has broad applicability, one area that could significantly benefit from this advance is the nuclear forensics. Broadly, nuclear forensics is the term used to describe the analysis of material collected in pre- or post-detonation events. Frequently, the separation of post-detonation debris is necessary to assess the elemental or isotopic signatures of a sample. The relative presence of lanthanides, produced in significant quantities during the fission of either ^{235}U or ^{239}Pu, can give insight into the type of fuel used in the device, the age and history of the nuclear

material, and the device design.[17-18] Due to their predominant trivalent oxidation states and similar chemical properties, the separation of adjacent lanthanides presents a unique challenge. Typically, the separation of lanthanides is achieved by exploiting the decreasing atomic or ionic radii across the series and subsequent subtle changes in their binding strengths.[19] The organophosphorus extractant HDEHP has shown a high selectivity of five orders of magnitude across the lanthanide series in solvent extraction systems.[20] As such, the HDEHP physisorbed polyacrylic ester-based resin (LN Resin) from Eichrom is commonly used for the separation of lanthanides.[21-24] The separations efficacy of HDEHP-physisorbed OMC materials is compared to the commercially available LN resin.

Herein, OMC materials were synthesized and characterized for *f*-element separations. Two OMC materials, OMC-*l*-MSN and CMK-3 type OMC, were considered initially. The two OMC materials were then physisorbed with HDEHP and their recovery and separation performance were compared against LN Resin. Batch distribution studies were completed using a $^{152/154}Eu^{3+}$ radiotracer. While the HDEHP-CMK-3 type OMC provided the highest uptake of Eu^{3+}, particularly at higher acid concentrations, it was not further studied due to having a more irregular morphology that would be undesirable for chromatographic applications. Batch Eu^{3+} Langmuir adsorption isotherms show the HDEHP-OMC-*l*-MSN provides a greater maximum adsorption capacity, 0.35 ± 0.06 mmol Eu^{3+} g^{-1} adsorbent, relative to the LN Resin, 0.17 ± 0.07 mmol Eu^{3+} g^{-1} adsorbent. In contrast to the LN resin, the HDEHP-OMC-*l*-MSN maximum Eu^{3+} loading in the batch mode also agrees with the maximum adsorption capacity of 0.32 ± 0.04 mmol Eu^{3+} g^{-1} adsorbent obtained by column breakthrough analysis. Improved separation was also observed for the HDEHP-OMC-*l*-MSN materials, where the resolution for the chromatographic separation of Nd^{3+} and Eu^{3+} by the HDEHP-OMC-*l*-MSN is 0.58 ± 0.02

whereas the LN Resin provided no separation. This report suggests OMC-based materials have the ability to complete chromatographic, intragroup lanthanide separations and, in some instances, could perform better than state-of-the-art materials.

5.3 Experimental

5.3.1 Materials and Instrumentation

OMC materials were synthesized using tetramethylorthosilicate (TMOS, Sigma-Aldrich, 98%), Pluronic P104 (BASF), Pluronic P123 (BASF), ACS grade hydrochloric acid (MACRON Fine Chemicals), ACS grade methanol (MACRON Fine Chemicals), ACS grade hexane (Fisher Scientific), sucrose (Sigma-Aldrich, BioXtra ≥99.5% GC), and ACS grade sulfuric acid (EMD). These materials were used as received. The HDEHP was obtained from Sigma-Aldrich with 97% purity and was subsequently purified using the copper purification method.[16] Aqueous solutions were prepared using ultrapure (18 MΩ) deionized water, ACS grade nitric acid (MACRON Fine Chemicals), and sodium nitrate (Fisher Scientific).

A Philips CM200 with a 200 kV LaB6 cathode and a JOEL JSM-700F Field Emission SEM were used for TEM and SEM imaging, respectively. Nitrogen sorption data was collected using a Micrometrics TriStar II. A TA TGA Q500 was used for TGA measurements. For XRD data, a PANalytical Empyrean XRD was utilized.

LN Resin (20-50 μm bulk mesh) was obtained from Eichrom and 0.2 μm syringe filters were purchased from Thermo Scientific. Batch Eu^{3+} sorption and isotherm studies were conducted using a Labnet AccuTherm for all contacts and a BD Clay Adams Compact II Centrifuge was used for centrifugation. Gross $^{152/154}Eu^{3+}$ gamma activity for batch studies and breakthrough curves was monitored using a Packard Cobra II NaI(Tl) solid scintillation auto-gamma counter.

Column studies were done using a Mobicol "F" column with a 35 μm filter, a Pump II Elite syringe pump from Harvard Apparatus, and a Model 2110 Fraction Collector (Bio-Rad), 1.6 mm diameter tygon tubing (Bio-Rad), and BD 3 mL syringes. The activities of $^{147}Nd^{3+}$ and $^{152}Eu^{3+}$ for chromatographic separations were monitored using a Canberra HPGe well detector for column separation studies.

5.3.2 Synthetic procedures

Synthesis of *l*-MSN. The synthesis of large-pore mesoporous silica nanoparticles (*l*-MSN) was conducted according to a previously reported method.[25-26] The nonionic surfactant Pluronic P104 (7 g) was added to 1.6 M HCl (273.0 g) in an Erlenmeyer flask and stirred at 55 °C for 1 h, at which point TMOS (10.6 g) was added. This mixture was stirred at 55 °C for an additional 24 h, followed by a hydrothermal treatment at 150 °C for 24 h in a Teflon-lined autoclave. Finally, the mixture was cooled rapidly, filtered, and washed with water and methanol to obtain a white powder. This powder was lyophilized overnight and calcined at 550 °C for 6 h at a ramp rate of 1.5 °C min^{-1} to remove the surfactant.

Synthesis of SBA-15. In a 250 mL polypropylene bottle, Pluronic P123 (4 g) was dissolved in 30 mL of nanopore water at 40 °C for 3 h, after which 70 mL of 0.286 M HCl (in nanopore water) were added. The mixture was stirred for an additional hour before the dropwise addition of TMOS (9.89 g). This mixture was stirred for 24 h at 40 °C before undergoing a hydrothermal treatment at 100 °C for 48 h. Finally, the sample was filtered, washed extensively with water and methanol, and calcined at 550 °C in air for 8 h.[27-28]

Synthesis of OMC-*l*-MSN/CMK-3 type OMC material. Approximately 1 g of *l*-MSN (or SBA-15 for the CMK-3 type OMC materials) with a pore volume of 1 cm^3 g^{-1} was mixed with

sucrose (1.07 g), 2 drops of H_2SO_4 (0.12 g) and 5 mL of water (4.23 g) in a ceramic dish, adding the water slowly and mixing for 7 min such that the mixture remains homogeneous. The mixture was heated for 6 h at 100 °C, after which the temperature was raised to 160 °C and heated for an additional 6 h. This process was repeated three more times such that the amount of sugar was changed to 0.68 g, 0.10 g, and 0.18 g each time. This mixture was then transferred to a quartz boat and pyrolized in a tube furnace under nitrogen at 900 °C for 6 h. A HF digestion was employed to remove the silica hard template. Approximately half a gram of the silica-carbon material was added to 30 mL of a 10% HF solution and allowed to sit for 24 h. The mixture was then centrifuged and washed with copious amounts of ethanol.

HDEHP physisorption. HDEHP was physisorbed on the OMC material using a simple diffusion method. Generally, 0.5 mL of HDEHP in hexanes was added to 62.5 mg of OMC material in a microcentrifuge tube and allowed to sit for 18 h. Different HDEHP loading concentrations were examined by altering the HDEHP to hexane ratio, resulting in solutions containing 6.7% and 20% (v/v) HDEHP in hexanes. The loading behavior was also examined using multiple additions of the 20% (v/v) HDEHP solution. Here, the previously described loading method was applied three times with only a third of volume added each time and the hexanes removed between each addition. The material was then washed once with water, centrifuged, and freeze dried overnight to drive physisorption to the carbon surface.

5.4 Characterization of OMC materials

Nitrogen adsorption and desorption isotherms for the OMC materials were measured in air at 100 °C for 6 h prior to HDEHP physisorption. Surface areas were calculated using the Brunauer-Emmett-Teller (BET) method, while pore size distributions were obtained using the Barrett-

Joyner-Halenda (BJH) method. X-ray diffraction (XRD) patterns were used to determine the success of the templating procedure.

Transmission and scanning electron microscopy (TEM and SEM) were emplyed to observe the structure and porosity of OMC-*l*-MSN and CMK-3 materials before HDEHP physisorption. Samples for TEM were sonicated for 10 min in ethanol prior to drop-casting a single drop onto carbon-coated, 300 mesh copper grids. SEM samples were mounted on an aluminium stub with conductive carbon tape adhesive.

Quantification of HDEHP loading was measured using thermogravimetric analysis (TGA) to determine the mass percent content of the ligand. Data was obtained both before and after HDEHP physisorption to obtain the wt% HDEHP adsorbed to the OMC materials.

5.5 Radiochemical analyses

Batch distribution experiments. All aqueous solutions for batch and column studies were prepared at 1 M ionic strength using $NaNO_3$. An aliquot of 0.495 mL of the appropriate acid solution, ranging from about 0.1 to 0.8 M HNO_3, was added to approximately 5 mg of LN Resin or OMC material. A 5 µL spike of an approximately 3.2 mM $^{152/154}Eu^{3+}$ radiotracer in 0.001 M HNO_3, prepared as previously described by Drader, et al.,[29] was added to the aqueous phase, bringing the total volume to 0.5 mL. Contacts were done at 25 °C and shaken at 1500 rpm for 30 min. After contacting, the samples were centrifuged at 1163 *xg* for 15 min. The phase separation from the LN Resin was acccomplished by using transfer pipettes to collect the aqueous phases while 0.2 µm syringe filters were used to separate the aqueous phase from the OMC materials. A 200 µL aliquot of each aqueous phase was taken for gross gamma counting. The activity of the solid material was determined by difference. Triplicate samples were taken

for LN Resin and HDEHP-CMK-3 type OMC materials and errors denote a ±3σ of the triplicate analysis. Due to the limited quantity of HDEHP-OMC-*l*-MSN material available at that time, contacts were completed once at each acid concentration. Errors presented for the HDEHP-OMC-*l*-MSN represent ±3σ using propagation of error in the counting statistics.

Distribution coefficients for each sample were calculated using:

$$K_d = \left(\frac{A_0 - A}{A}\right)\left(\frac{V}{m}\right) \tag{5.1}$$

where A_0 and A are the activities (cpm) of the aqueous phase before and after equilibrium, respectively, V is the volume of the aqueous phase (mL), and m is the mass of the solid phase (g). For the batch distribution studies, the mass was normalized for the wt% HDEHP the material contained.

Europium adsorption isotherms. Isotherm studies were completed to determine the maximum Eu^{3+} loading capacity, q_{max}, of the extraction material. Aqueous solutions were prepared using $Eu(NO_3)_3$ and 0.5 M HNO_3. The $Eu(NO_3)_3$ concentrations ranged from 0.5 μM to 40 mM. The aqueous solutions were spiked with the $^{152/154}Eu^{3+}$ radiotracer so that 0.5 mL of solution contained 4.95 μL of the radiotracer. Approximately 5 mg of LN Resin or OMC material were contacted with 0.5 mL of the approprate aqueous phase. All contacts and activity determinations were done as in the batch sorption experiments and were completed in triplicate.

The concentration of analyte extracted was plotted against the analyte concentration remaining in the aqueous phase at equilibrium using the following equations:

$$C = \left(\frac{A}{A_0}\right) C_0 \tag{5.2}$$

$$q_e = \left(\frac{A_0 - A}{A_0}\right)\left(\frac{V}{m}\right) C_0 \quad (5.3)$$

where C_0 and C are the molar concentrations of analyte in the aqueous phase before and after equilibrium, respectively, q_e is moles of analyte sorbed per gram of material at equilibrium, V is the volume of the aqueous phase (L), and m is the mass of the chromatographic material (g). Using QtiPlot,[30] the data was then fit using the Langmuir isotherm equation:

$$q_e = \frac{q_{max}(a_L C)}{1+(a_L C)} \quad (5.4)$$

where q_{max} is the maxiumum adsorption capacity (mol g^{-1}) and a_L is the Langmuir constant (L mol^{-1}). Errors reported are ±3σ from the triplicate analysis.

Europium breakthrough curves. The maximum adsorption capacity under dynamic conditions was found using:

$$Q(m) = \frac{V(50) - V_0}{m_s} \times C_0 \quad (5.5)$$

where $Q(m)$ is the maximum adsorption capacity (mol g^{-1}), $V(50)$ is the elution volume at 50% breakthrough, and V_0 is the free column volume. If the batch and dynamic systems are under equilibrium, the maximum adsorption capacity values should be the same within error.[31] The breakthrough curves were obtained using 0.5 M HNO_3 containing 30 mM Eu^{3+}. The full column height (~1.5 cm) was used for the LN Resin, while half column height (~0.75 cm) for the OMC-*l*-MSN material was used. The chromatographic materials were dry packed to enable determination of chromatographic material mass and the free column volume (FCV). The dry packing also ensured that backpressure would not be an issue with the nanoparticle material. The FCV was determined gravimetrically using water. Each column was preconditioned with 10 FCVs of 0.5 M HNO_3. Approximately 10 FCVs of the Eu^{3+} solution was eluted from the

columns at a flow rate of 50 μL min^{-1}. Fractions were collected every two minutes so that about 100 μL were contained in each fraction. The breakthrough curves were completed in duplicate and the error in *Q(m)* reflects the relative difference between the two.

Europium/neodymium separations. LN Resin and HDEHP-OMC-*l*-MSN colums were prepared at half column height (~0.75 cm) for Eu^{3+} and Nd^{3+} separations. The LN Resin was packed via the slurry method. Because of the hydrophobicity of the HDEHP-OMC-*l*-MSN material, the slurry method did not produce a well-packed column. To obtain sufficient packing, the OMC material was dampened with just enough water to form a paste-like substance. Approximately one-fourth of the column height was filled with the OMC paste. With the stopcock open, the column was then placed into a microcentrifuge tube and centrifuged for two minutes at 1163 *xg*. The process was completed once more to fill the column half full. The LN Resin and HDEHP-OMC-*l*-MSN materials were both topped with a frit to prevent material distruption.

Each column was preconditioned with 2 mL of 0.001 M HNO_3. A loading solution was prepared as to initially contain approximately 100,000 cpm for both $^{147}Nd^{3+}$ (91 keV monitored gamma ray emission) and $^{154}Eu^{3+}$ (123 keV monitored gamma ray emission). Aliquots of $Nd(NO_3)_3$ and $Eu(NO_3)_3$ stock solutions were added to obtain a final concentration of 2 mM for each metal. The final loading solution contained 0.001 M HNO_3. Each column was loaded with 1.5 mL of the resulting solution. After loading, the columns were washed with 1.5 mL of 0.001 M HNO_3. Complete metal stripping from the columns was done using 1.5 mL of 2 M HNO_3. The flow rate for each step was 50 μL min^{-1}. Bulk loading and washing fractions were collected and counted to monitor metal breakthrough during load and wash steps. Stripping

fractions were collected every one minute and counted for 5 min on an HPGe well detector. The resolution of the separations was calculated using:

$$\text{Resolution} = \frac{0.589 \times \Delta V_r}{0.5 \times (w_{h/2,1} + w_{h/2,2})} \quad (5.6)$$

where ΔV_r is the difference in retention volume at the peak height maximums and $w_{h/2,n}$ is the width of the peak at half the peak manimum height.

After eluting the metals, the columns were dried to determine the mass of material each contained. The FCV was found gravimetrically using water.

Neodymium irradiations. A 0.01 M HNO_3 solution containing 0.110 M Nd^{3+} was irradiated for 3 hours in the Lazy Susan position at the U.S. Geological Survey TRIGA Reactor at the Denver Federal Center with a neutron flux of 4×10^{12} cm^{-1}. The irradiated solution was used directly as a ^{147}Nd source for separation studies.

5.6 Results and Discussion

5.6.1 OMC surface and material properties

Nitrogren physisorption isotherms and BJH pore width distributions. Nitrogen physisorption isotherms and BJH pore width distributions of the OMC materials are shown in Figure 1. The OMC-*l*-MSN isotherm is of type IV with H2 hysteresis, typical of ordered mesoporous materials,[26-27] and a BET surface area of 980 m^2 g^{-1}. However, there are two distinct inflection points attributed to the phenomenon of capilary condensation. This bimodal adsorption behavior is confirmed in the pore width distribution with averages of 7.1 nm and 45 nm. The CMK-3 type OMC material is characterized as having a pseudo type II isotherm with H4 hysteresis, yielding a BET surface area of 630 m^2 g^{-1} and pore diameters of 3.5 nm based on the

BJH distribution. In the case of CMK-3 type OMC, H4 hysteresis is common among activated carbons and often arises from low pore-curvature. This suggests that the majority of porosity arises from relatively rectangular inter pore regions and not the larger and more radial vertices where three pores arrayed within the p6mm space group intersect.[32] Based on the OMC-*l*-MSN isotherm, the material likely consists of cylindrical pores of a variety of widths. A summary of the surface area and pore diameters of OMC-l-MSN and CMK-3 type OMC can be found in Table 5.1

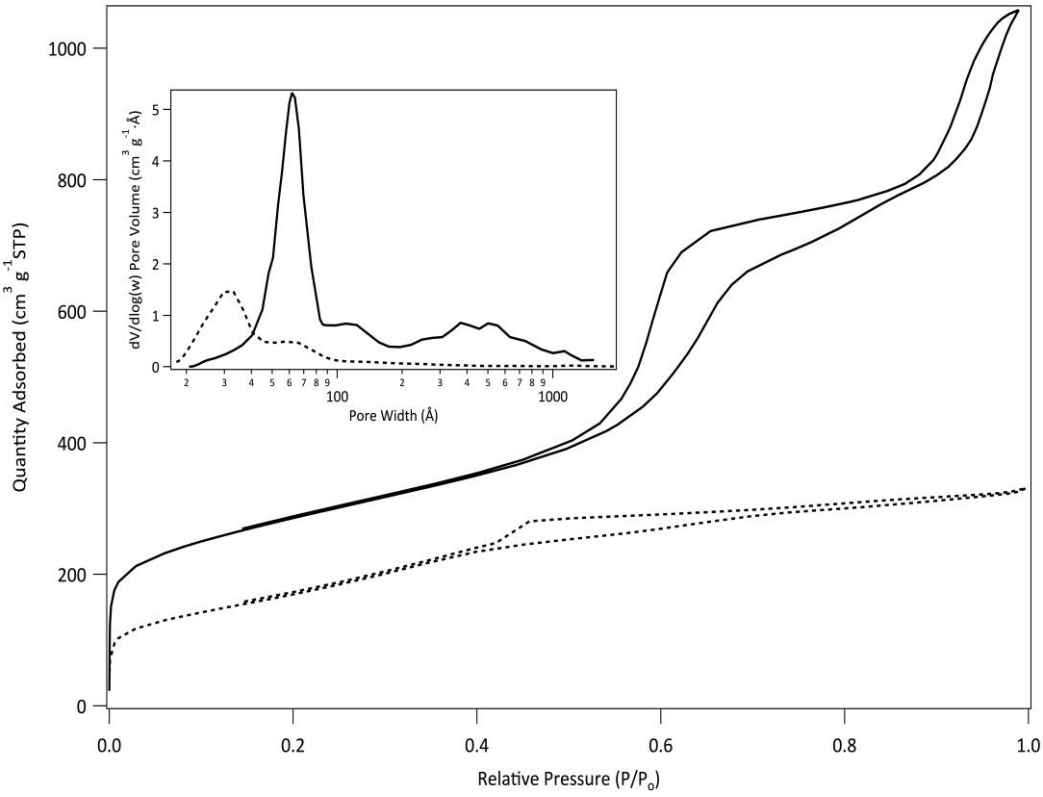

Figure 5.1 N_2 physisorption isotherm and BJH pore width distributions (inset) of prepared OMC materials: OMC-l-MSN (solid lines) and CMK-3 type OMC (dotted lines)

Table 5.1 BET and BJH data of OMC samples

Carbon Sample	BET surface area (m^2 g^{-1})	BJH pore diameter (nm)
OMC-*l*-MSN	980	7.1
CMK-3 type OMC	630	3.5

TEM and SEM surface analysis. TEM and SEM images show the mesoporous carbon synthesis from silica hard-templating techniques yielded OMC-*l*-MSN and CMK-3 type OMC materials with consistent pore and particle morphology (Figure 2). OMC materials synthesized from l-MSN templates exhibited uniform particle structure with regular, parallel pores (Figure 5.2). In contrast CMK-3 type OMC materials exhibit a rope-like morphology typical of such carbons,[27, 33-34] with pores running parallel along the particle length (Figure 5.2). In both cases, the carbon material mimicked the morphology of the silica template. A greater polydispersity also exists in the CMK-3 morphologies as compared with OMC-*l*-MSN. Particle sizes typically varied between 500-1000 nm in diameter for OMC-*l*-MSN and 1-5 μm for CMK-3 type OMC materials. OMC materials synthesized from l-MSN templates exhibited uniform particle structure with regular, parallel pores. The carbon material mimicked the morphology of the silica template. A greater polydispersity also exists in the CMK-3 morphologies as compared with OMC-*l*-MSN. The mesoporous carbon synthesis from silica hard-templating techniques yielded OMC-*l*-MSN and CMK-3 type OMC materials with consistent pore and particle morphology.

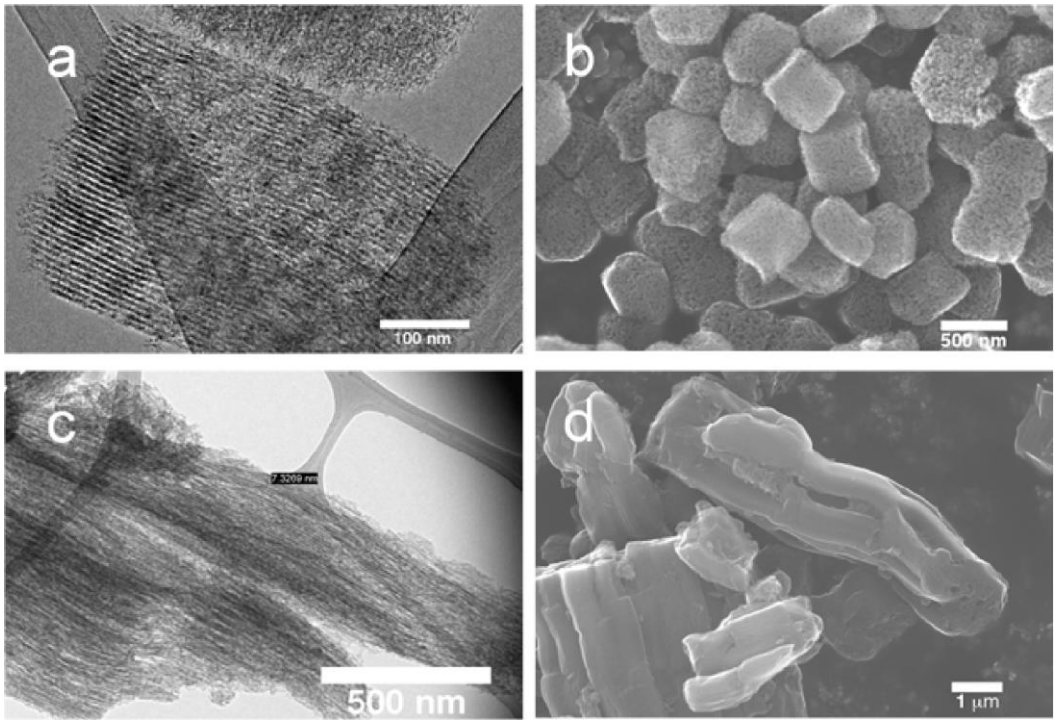

Figure 5.2 Representative TEM and SEM images of OMC materials synthesized using l-MSN (a and b) and SBA-15 (c and d) mesoporous silica templates

Low angle XRD. Low angle XRD patterns were obtained from 0.5 to 5 degrees (2θ) operating in transmission mode (Figure 5.3). Both materials show diffraction from the (100) plane of the hexagonally arrayed pores. The amount of long range order is low due to the lack of the (110) and (200) peaks. This is reasonable for the prepared OMC materials since the template is not always perfectly transcribed during the carbonization process. CMK-3 type OMC (dotted line, Figure 3) has $d_{(100)}$ of 8.68 nm while OMC-*l*-MSN (solid line, Figure 5.3) has a slightly condensed pore spacing along [100] at 8.56 nm.

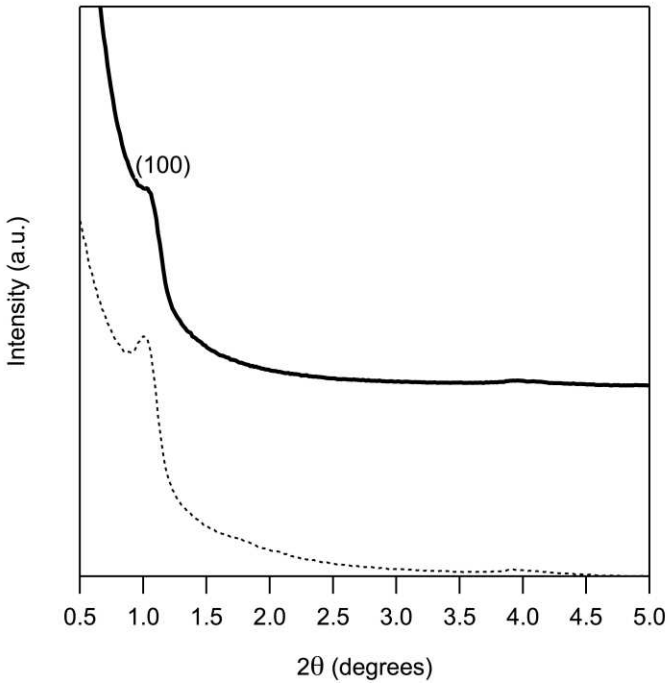

Figure 5.3 Low angle XRD patterns of OMC-l-MSN (solid lines) and CMK-3 type OMC (dotted line)

Thermogravimetric analysis. The TGA results for five OMC samples are shown in Figure 4 and Table 2. For the four OMC-*l*-MSN samples shown, the HDEHP was loaded in either a single addition (OMC-a, OMC-c, and OMC-d, Figure 5.4) or in three instalments (OMC-b, Figure 4a) This was done to investigate the effect of loading methodology. The OMC-a was loaded with 6.6% (v/v) HDEHP in hexanes. All other OMC-*l*-MSN samples were loaded using 20% (v/v) HDEHP in hexanes. CMK-3 type OMC (red dotted line, Figure 5.4) was loaded in a single addition using 20% (v/v) HDEHP in hexanes, allowing for a comparison between the two different OMC materials. Loading ranged between 33 and 63 wt% or 1.5 to 4.7 mmol HDEHP g^{-1} OMC as compared to 2.1 mmol HDEHP g^{-1} LN Resin Table 5.2

As expected, using a more dilute HDEHP solution (6.7% (v/v) in hexanes) resulted in a lower ligand loading (33 wt%) than the 20% (v/v) HDEHP in hexanes loading solution (46-63

wt%). Adding the HDEHP to the OMC material in multiple additions also resulted in a higher loading of 63 wt% HDEHP than the single ligand additions (46-55 wt%). However, it should be noted that the samples OMC-b and OMC-d were not washed, resulting in additional, loosely physisorbed HDEHP.

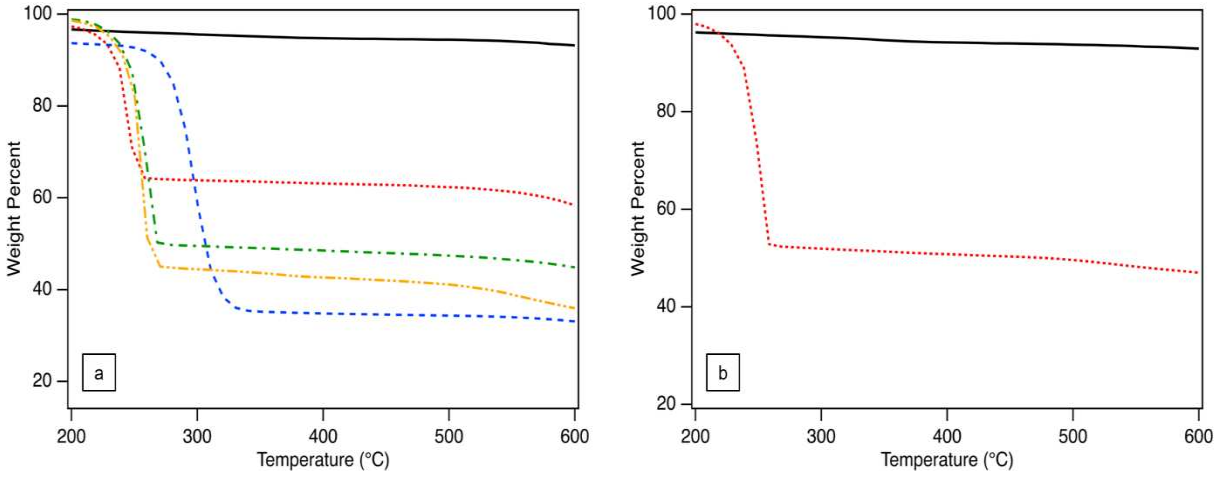

Figure 5.4 TGA data for the physisorption of HDEHP onto (a) OMC-l-MSN and (b) CMK-3 type OMC.

The sharp decrease in mass around 250 °C is due to combustion of HDEHP on the OMC surface. Shown from top to bottom at 400 °C are: (a) blank OMC-l-MSN (black solid line), 33 wt% HDEHP-OMC-a (red dotted line), 49 wt% HDEHP-OMC-c (green dash-dotted line), 55 wt% HDEHP-OMC-d (gold dash-double-dotted line), 63 wt% HDEHP-OMC-b (blue dashed line) (b) blank CMK-3 type OMC (black solid line) and 46 wt% HDEHP-CMK-3 type OMC. The OMC-a was loaded with 6.6% (v/v) HDEHP in hexanes. All other OMC-*l*-MSN samples were loaded using 20% (v/v) HDEHP in hexanes**.** CMK-3 type OMC was loaded in a single addition using 20% (v/v) HDEHP in hexanes, allowing for a comparison between the two different OMC materials

Table 5.2 HDEHP loading of OMC samples determined by TGA

		HDEHP loading				
Carbon sample	Sample identifier	Loading additions	(v/v) % HDEHP in hexanes	HDEHP wt%	g HDEHP/ g OMC	mmol HDEHP/ g OMC
OMC-*l*-MSN[a]	OMC-a	1	6.7	33	0.49	1.5
OMC-*l*-MSN[b]	OMC-b	3	20	63	1.5	4.7
OMC-*l*-MSN[c]	OMV-c	1	20	49	0.96	3.0
OMC-*l*-MSN[d]	OMC-d	1	20	55	1.2	3.8
CMK-3 type OMC	-	1	20	46	0.85	2.6

5.6.2 Radiochemical analyses

Batch distribution experiments. The batch sorption experiments were done using HDEHP-OMC-b, HDEHP-CMK-3 type OMC, and LN Resin (40 wt% HDEHP). Higher K_d values represent a greater adsorption of Eu^{3+} by the sorbent material. As the HNO_3 concentration

is increased, the K_d value decreases for all materials reported (Table 5.5). Both HDEHP-OMC materials have larger K_d values than the LN Resin across all HNO_3 concentrations, even after the K_d values were corrected for the wt% HDEHP the materials contained. The higher distribution coefficients may imply that the increased surface area of the OMC materials plays a role in the uptake of Eu^{3+}.

Based on the distribution slope, the number of ligands required to extract the metal ion can be deduced.[35] This analysis suggests three ligands were involved in the uptake of each Eu^{3+} cation and is consistent with previous reports on trivalent metal recovery by HDEHP.[36-37] Despite both HDEHP-OMC materials providing higher K_d values, the CMK-3 type OMC wasn't further studied due to its irregular morphology. The Langmuir isotherm studies were completed using HDEHP-OMC-a and LN Resin (Figure 5.6). The HDEHP-OMC-a materials have a larger q_{max} value of 0.35 ± 0.06 mmol g^{-1} than that of LN Resin (0.17 ± 0.07 mmol g^{-1}, Table 3). The slopes of both materials are comparable, which is to be expected since both materials use HDEHP as an extractant. No corrections were made for the HDEHP content. The batch sorption experiments were done using HDEHP-OMC-b, HDEHP-CMK-3 type OMC, and LN Resin (40 wt% HDEHP). Both HDEHP-OMC materials have larger K_d values than the LN Resin across all HNO_3 concentrations, even after the K_d values were corrected for the wt% HDEHP the materials contained. The higher distribution coefficients may imply that the increased surface area of the OMC materials plays a role in the uptake of Eu^{3+}. This analysis suggests three ligands were involved in the uptake of each Eu^{3+} cation and is consistent with previous reports on trivalent metal recovery by HDEHP.

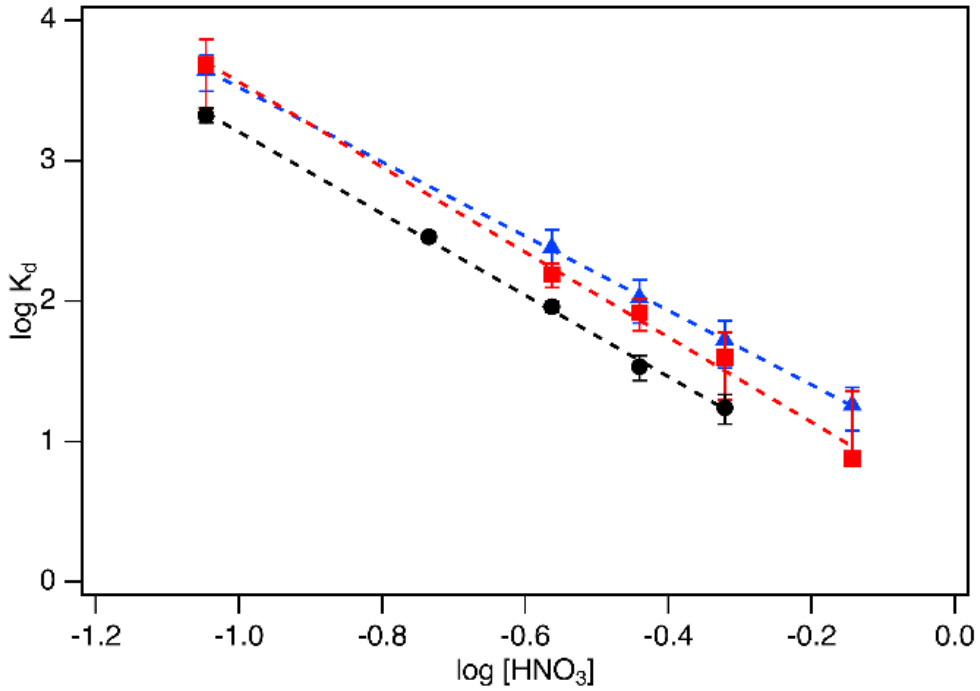

Figure 5.5 Uptake of Eu^{3+} as a function of HNO_3 concentration by LN Resin (black circles, bottom), HDEHP-OMC-b (red squares, middle), and HDEHP-CMK-3 type OMC (blue triangles, top). The slopes for the LN Resin, HDEHP-OMC-b, and HDEHP-CMK-3 type OMC are -2.91 ± 0.06, -3.0 ± 0.1, and -2.66 ± 0.03, respectively

Europium adsorption isotherms. The Langmuir isotherm studies were completed using HDEHP-OMC-a and LN Resin (Figure 5.6). The HDEHP-OMC-a materials have a larger q_{max} value of 0.35 ± 0.06 mmol g^{-1} than that of LN Resin (0.17 ± 0.07 mmol g^{-1}, Table 3). The slopes of both materials are comparable, which is to be expected since both materials use HDEHP as an extractant. No corrections were made for the HDEHP content. Although the OMC material contained less HDEHP than the LN Resin it provided twice the maximum adsorption capacity of its analogue. Data for the isotherms can be found in Tables S1 and S2. The maximum adsorption capacities for Eu^{3+} by other carbonaceous materials are presented in Table 5.4 for comparision

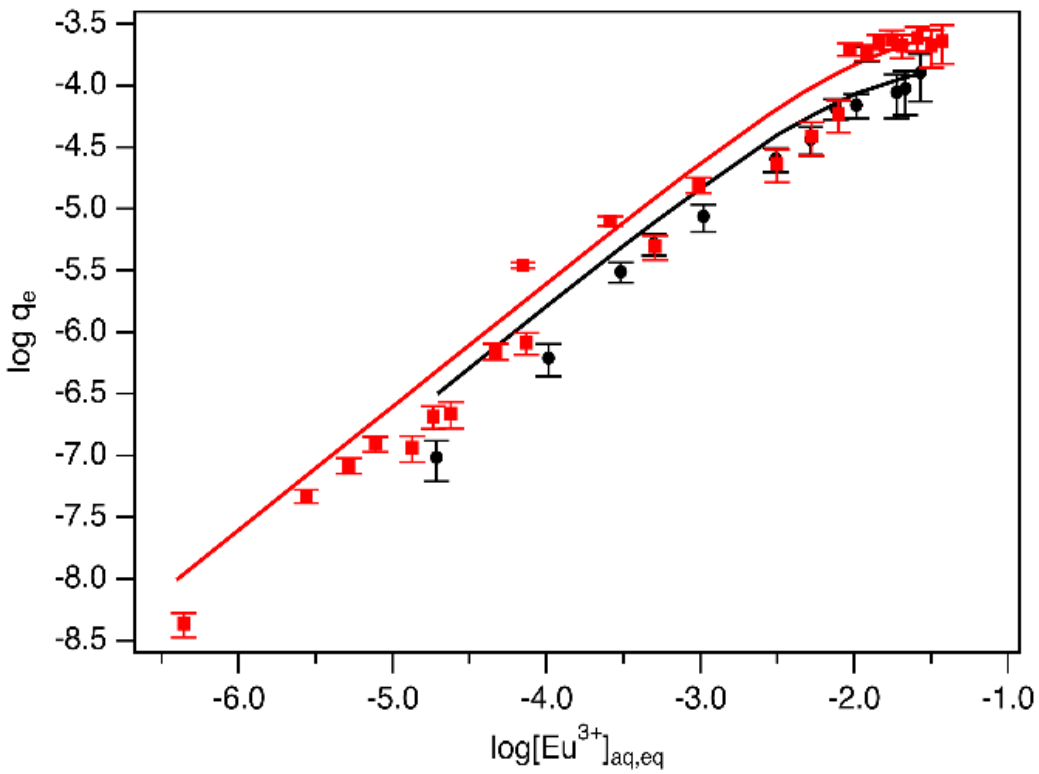

Figure 5.6 Langmuir adsorption isotherms for LN Resin (black circles) and OMC-l-MSN materials (red squares)

Breakthrough curves were used to find the maximum adsorption capacity of the chromatographic material under dynamic conditions using HDEHP-OMC-c and LN Resin. The *Q(m)* values were 0.11 ± 0.01mmol g^{-1} and 0.32 ± 0.04 mmol g^{-1} for LN Resin and HDEHP-OMC-c, respectively. Each breakthrough curve was done twice and *V(50)* was found by using a best fit line between approximately 10% and 90% breakthrough. Errors reported are the relative difference between the two measurements of *Q(m)*. Representative breakthrough curves are shown in Figure 5.7

Table 5.3 Maximum Eu^{3+} adsorption capacity comparison of selected functionalized and pristine carbonaceous materials

Carbon Sample	q_{max} (mmol g^{-1})	Ionic strength (M)	Reference
HDEHP-OMC-*l*-MSN	0.35(6)	1	This work
Oxidized MWCNTs	2.87×10^{-8}	0.1	[38]
C-CS-type OMCs	0.910	0.1	[14]
N,N-dihexyl amide MWCNTs	0.536	-	[39]
1st generation poly(amidoamine) dendrimer CNTs	0.544	-	[40]
2nd generation poly(amidoamine) dendrimer CNTs	0.976	-	[40]

5.6.3 Europium breakthrough curves

Breakthrough curves were used to find the maximum adsorption capacity of the chromatographic material under dynamic conditions using HDEHP-OMC-c and LN Resin. The *Q(m)* values were 0.11 ± 0.01mmol g^{-1} and 0.32 ± 0.04 mmol g^{-1} for LN Resin and HDEHP-OMC-c, respectively. Each breakthrough curve was done twice and *V(50)* was found by using a best fit line between approximately 10% and 90% breakthrough. Errors reported are the relative difference between the two measurements of *Q(m)*. Representative breakthrough curves are shown in Figure 7. Additional breakthrough curves and data can be found in Table S3 and Figure

S1. Because the q_{max} and $Q(m)$ values for both the LN Resin and HDEHP-OMC-c agree within error, Table 5.4

It was assumed that equilibrium was reached. It should be noted that the HDEHP-OMC materials used for the breakthrough curve and adsorption isotherm had different ligand loadings. The agreement in q_{max} and $Q(m)$ between the samples containing different HDEHP loadings may imply that there is a limit in ligand loading capacity where additional loading does not aid the in adsorption capacity. This could be a result of HDEHP being loaded into regions of the OMC material that limits the accessibility for the metal ions.

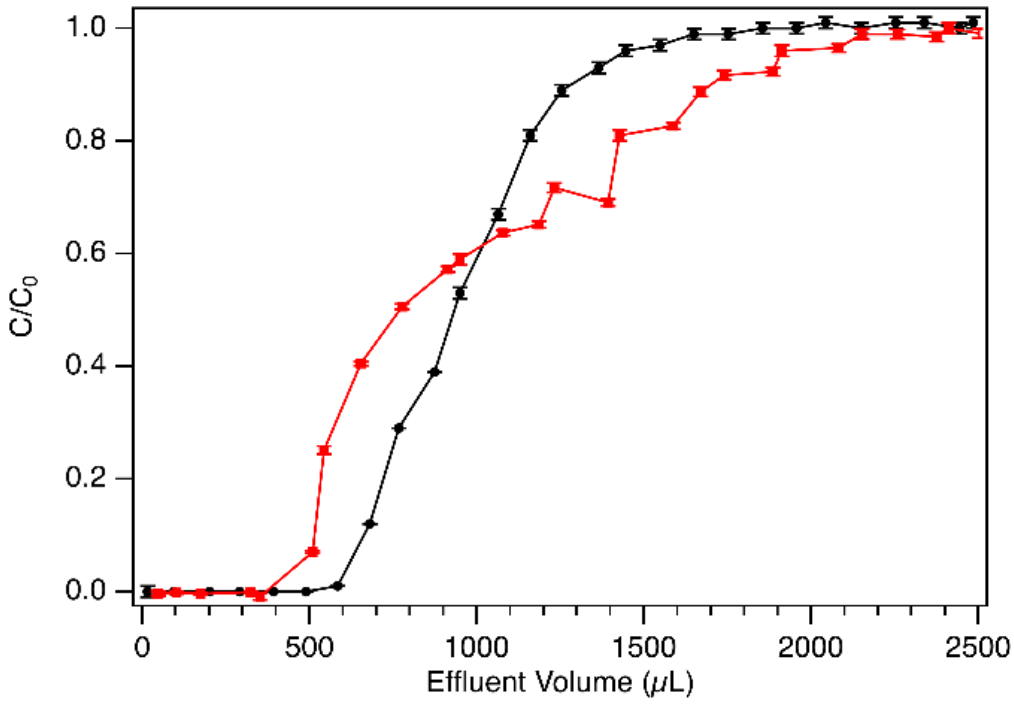

Figure 5.7 Europium breakthrough curves for LN Resin (black circles) and HDEHP-OMC-c (red squares). The plots show the ratio of the concentration of Eu^{3+} with in fraction, C, to the initial concentration of Eu^{3+} in the loading solution, C_0, as a function of the effluent volume (µL)

Table 5.4 Maximum adsorption capacities for LN Resin and OMC-l-MSN under static and dynamic conditions

	q_{max} (mmol g^{-1})	$Q(m)$ (mmol g^{-1})
LN Resin	0.17 ± 0.07	0.11 ± 0.01
OMC-*l*-MSN	0.35 ± 0.06	0.32 ± 0.04

Europium/nedymium separations. To investigate the *f*-element separation capability of HDEHP-OMC-*l*-MSN, the separation of Nd^{3+} and Eu^{3+} was attempted using HDEHP-OMC-d and compared to LN Resin. Although both columns were prepared to approximately half column height, the mass of the LN Resin was considerably lower than the HDEHP-OMC-d; however, the FCV were quite similar (Table 5.5). Well-packed particles with smaller diameters should diminish the free volume within the column. While the density of the OMC particles is greater, likely owing to the better packing of smaller particles, the FCV stayed nearly the same as the LN Resin. This could be due to the availability of the pore volumes within the OMC material.

Table 5.5 The mass and FCV for half columns used in Eu and Nd separations

	Mass (g)	FCV (μL)
LN Resin	0.1059(1)	135.2(1)
OMC-*l*-MSN	0.1669(1)	134.9(1)

No metal breakthrough was observed during the loading and washing steps. The activites of $^{147}Nd^{3+}$ and $^{154}Eu^{3+}$ were corrected to reflect the varying volumes contained in each of the fractions. No separation was observed using LN Resin, while separation was achieved using the OMC material (Figure 5.8 and Figure 5.9). Additional presentations of the separations can be found in Figures S2 and S3. A resolution of 0.58 ± 0.02 was obtained for the HDEHP-OMC-d column and was determined using the volume corrected elution curves. Gaussian curves were generated in QtiPlot for each peak to determine the width at half the peak height maximum. The error in the resolution represents $\pm 1\sigma$ through propagation of error in the resolution calculation.

Approximately 56% of the Nd^{3+} can be recovered with less than 6% contamination from the Eu^{3+}. Conversely, about 50% of the Eu^{3+} can be recovered with less than a 7% Nd^{3+} contamination.

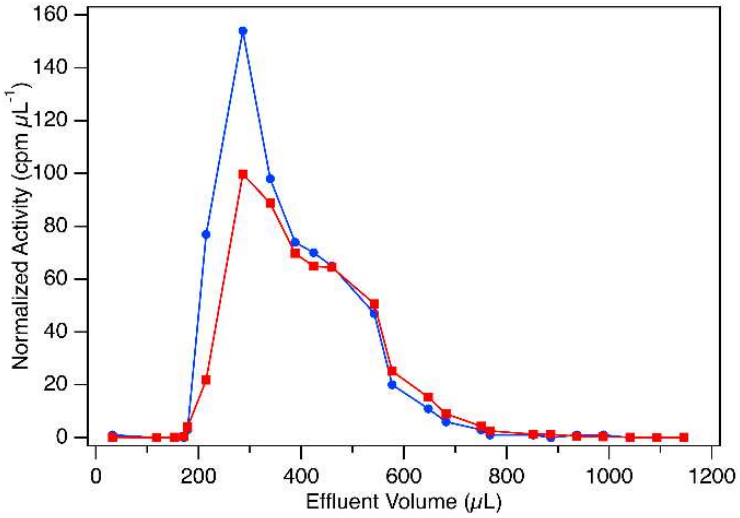

Figure 5.8 Separation of $^{147}Nd^{3+}$ (blue circles) and $^{154}Eu^{3+}$ (red squares) by LN Resin. Activities have been normalized to the volume the fraction contained

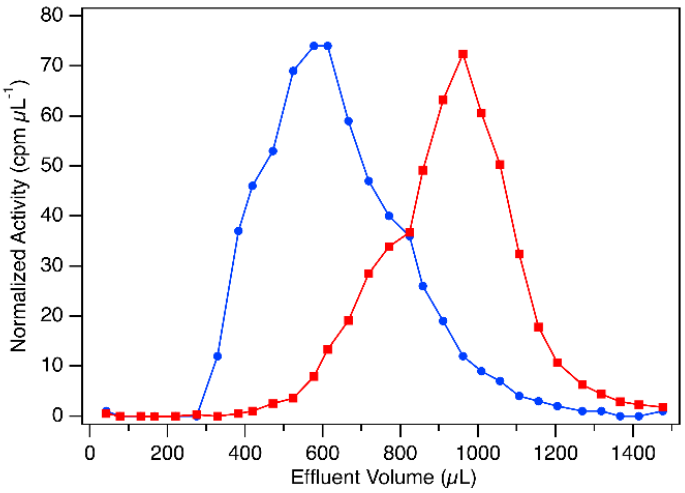

Figure 5.9 Separation of $^{147}Nd^{3+}$ (blue circles) and $^{154}Eu^{3+}$ (red squares) by HDEHP-OMC-l-MSN. Activities have been normalized to the volume the fraction contained

5.7 Conclusions

Two OMC materials with different morphologies, OMC-*l*-MSN and CMK-3 type OMC, were synthesized and modified with HDEHP for Eu^{3+} and Nd^{3+} recovery. HDEHP loadings varied depending on the concentration, number of HDEHP additions and the material being loaded. higher loading of the OMC-*l*-MSN material was accomplished through multiple HDEHP additions.

The Eu^{3+} uptake by these materials was compared against the industry standard lanthanide extraction chromatographic material, LN Resin. Both HDEHP-OMC materials showed higher distribution values than the LN Resin. Furthermore, HDEHP-CMK-3 type OMC showed improvement in performance over HDEHP-OMC-*l*-MSN and LN Resin at the higher acid concentrations, but displayed a less ordered morphology. The batch Langmuir isotherm and breakthrough column studies of the LN Resin and HDEHP-OMC-*l*-MSN demonstrated that the OMC materials have at least double the maximum adsorption capacity.

This study is the first to report a separation of the *f*-elements Nd and Eu using MCs as a chromatographic material. The HDEHP-OMC-*l*-MSN material successfully separated trivalent Nd and Eu using an unpressurized system and a small compact column. This preliminary examination of the HDEHP physisorbed OMC materials has confirmed their potential as solid-phase sorbents for *f*-element recovery and separation. Additional studies need to be completed to determine the maximum amount of HDEHP-OMC material that can be packed into a column before back-pressure issues arise. This would allow for resolution optimization of the HDEHP-OMC-*l*-MSN columns. Furthermore, studies utilizing OMC materials functionalized with other ligands have begun.

5.8 References

1. Ansari, S. A.; Mohapatra, P. K., A review on solid phase extraction of actinides and lanthanides with amide based extractants. *Journal of Chromatography A* **2017,** *1499*, 1-20.

2. Zakharchenko, E.; Mokhodoeva, O.; Malikov, D.; Molochnikova, N.; Kulyako, Y.; Myasoedova, G., Novel Sorption Materials for Radionuclide Recovery from Nitric Acid Solutions: Solid-Phase Extractants and Polymer Composites based on Carbon Nanotubes. *Procedia Chemistry* **2012,** *7*, 268-274.

3. Mokhodoeva, O. B.; Myasoedova, G. V.; Zakharchenko, E. A., Solid-phase extractants for radionuclide preconcentration and separation. New possibilities. *Radiochemistry* **2011,** *53* (1), 35-43.

4. Florek, J.; Giret, S.; Juère, E.; Larivière, D.; Kleitz, F., Functionalization of mesoporous materials for lanthanide and actinide extraction. *Dalton Transactions* **2016,** *45* (38), 14832-14854.

5. Veliscek-Carolan, J., Separation of actinides from spent nuclear fuel: A review. *Journal of Hazardous Materials* **2016,** *318*, 266-281.

6. Carboni, M.; Abney, C. W.; Taylor-Pashow, K. M. L.; Vivero-Escoto, J. L.; Lin, W. B., Uranium Sorption with Functionalized Mesoporous Carbon Materials. *Industrial & Engineering Chemistry Research* **2013,** *52* (43), 15187-15197.

7. Górka, J.; Mayes, R. T.; Baggetto, L.; Veith, G. M.; Dai, S., Sonochemical functionalization of mesoporous carbon for uranium extraction from seawater. *Journal of Materials Chemistry A* **2013,** *1*, 3016-3016.

8. Nie, B. W.; Zhang, Z. B.; Cao, X. H.; Liu, Y. H.; Liang, P., Sorption study of uranium from aqueous solution on ordered mesoporous carbon CMK-3. *Journal of Radioanalytical and Nuclear Chemistry* **2013,** *295* (1), 663-670.

9. Tian, G.; Geng, J.; Jin, Y.; Wang, C.; Li, S.; Chen, Z.; Wang, H.; Zhao, Y.; Li, S., Sorption of uranium(VI) using oxime-grafted ordered mesoporous carbon CMK-5. *Journal of Hazardous Materials* **2011,** *190* (1–3), 442-450.

10. Wang, Y. Q.; Zhang, Z. B.; Liu, Y. H.; Cao, X. H.; Liu, Y. T.; Li, Q., Adsorption of U(VI) from aqueous solution by the carboxyl-mesoporous carbon. *Chemical Engineering Journal* **2012,** *198-199*, 246-253.

11. Yue, Y.; Sun, X.; Mayes, R. T.; Kim, J.; Fulvio, P. F.; Qiao, Z.; Brown, S.; Tsouris, C.; Oyola, Y.; Dai, S., Polymer-coated nanoporous carbons for trace seawater uranium adsorption. *Science China Chemistry* **2013,** *56* (11), 1510-1515.

12. Zhang, Z. B.; Yu, X. F.; Cao, X. H.; Hua, R.; Li, M.; Liu, Y. H., Adsorption of U(VI) from aqueous solution by sulfonated ordered mesoporous carbon. *Journal of Radioanalytical and Nuclear Chemistry* **2014,** *301* (3), 821-830.

13. Parsons-Moss, T.; Tüysüz, H.; Wang, D.; Jones, S.; Olive, D.; Nitsche, H., Plutonium sorption to nanocast mesoporous carbon. 2014; Vol. 102, pp 489-504.

14. Parsons-Moss, T.; Wang, J.; Jones, S.; May, E.; Olive, D.; Dai, Z.; Zavarin, M.; Kersting, A. B.; Zhao, D.; Nitsche, H., Sorption interactions of plutonium and europium with ordered mesoporous carbon. *Journal of Materials Chemistry A* **2014,** *2* (29), 11209-11209.

15. Jung, Y.; Lee, H. I.; Kim, J. H.; Yun, M.-H.; Hwang, J.; Ahn, D.-H.; Park, J.-N.; Boo, J.-H.; Choi, K.-S.; Kim, J. M., Preparation of polypyrrole-incorporated mesoporous carbon-based composites for confinement of Eu(iii) within mesopores. *Journal of Materials Chemistry* **2010,** *20* (22), 4663-4663.

16. Perreault, L. L.; Giret, S.; Gagnon, M.; Florek, J.; Larivière, D.; Kleitz, F., Functionalization of Mesoporous Carbon Materials for Selective Separation of Lanthanides under Acidic Conditions. *ACS Applied Materials & Interfaces* **2017,** *9* (13), 12003-12012.

17. May, M.; Abedin-Zadeh, R.; Barr, D.; Carnesale, A.; Coyle, P. E.; Davis, J.; Dorland, W.; Dunlop, W.; Fetter, S.; Glaser, A.; Hutcheon, I. D., *Nuclear Forensics: Role, State of the Art, Program Needs*. Washington, DC, 2008.

18. Kristo, M. J., Chapter 21 . Nuclear Forensics in Radiometric Methods of Detection. 2011.

19. Zhang, J.; Zhao, B.; Schreiner, B., *Separation Hydrometallurgy of Rare Earth Elements*. Springer International Publishing Switzerland: 2016; p 1-259.

20. Starý, J., Separation of Transplutonium Elements. *Talanta* **1966,** *13*, 421-437.

21. Horwitz, E. P.; Bloomquist, C. A. A., Chemical Separations for Super-Heavy Element Searches in Irradiated Uranium Targets. *Journal of Inorganic and Nuclear Chemistry* **1975,** *37* (2), 425-434.

22. McAlister, D. R.; Horwitz, E. P., Characterization of Extraction of Chromatographic Materials Containing Bis(2-ethyl-1-hexyl)Phosphoric Acid, 2-Ethyl-1-Hexyl (2-Ethyl-1-Hexyl) Phosphonic Acid, and Bis(2,4,4-Trimethyl-1-Pentyl)Phosphonic Acid. *Solvent Extraction and Ion Exchange* **2007,** *25* (6), 757-769.

23. Pin, C.; Santos Zalduegui, J. F., Sequential separation of light rare-earth elements, thorium and uranium by miniaturized extraction chromatography: Application to isotopic analyses of silicate rocks. *Analytica Chimica Acta* **1997,** *339* (1-2), 79-89.

24. Braley, J. C.; McAlister, D. R.; Philip Horwitz, E.; Nash, K. L., Explorations Of Talspeak Chemistry In Extraction Chromatography: Comparisons of TTHA with DTPA and HDEHP with HEH[EHP]. *Solvent Extraction and Ion Exchange* **2013,** *31* (2), 107-121.

25. Valenstein, J. S.; Kandel, K.; Melcher, F.; Slowing, I. I.; Lin, V. S. Y.; Trewyn, B. G., Functional mesoporous silica nanoparticles for the selective sequestration of free fatty acids from microalgal oil. *ACS Applied Materials and Interfaces* **2012,** *4* (2), 1003-1009.

26. Joglekar, M.; Pylypenko, S.; Otting, M. M.; Valenstein, J. S.; Trewyn, B. G., Universal and Versatile Route for Selective Covalent Tethering of Single-Site Catalysts and Functional Groups on the Surface of Ordered Mesoporous Carbons. *Chemistry of Materials* **2014,** *26* (9), 2873-2882.

27. Jun, S.; Joo, S. H.; Ryoo, R.; Kruk, M.; Jaroniec, M.; Liu, Z.; Ohsuna, T.; Terasaki, O., Synthesis of New, Nanoporous Carbon with Hexagonally Ordered Mesostructure. *Journal of the American Chemical Society* **2000,** *122* (43), 10712-10713.

28. Zhao, D.; Feng, J.; Huo, Q.; Melosh, N.; Fredrickson, G. H.; Chmelka, B. F.; Stucky, G. D., Triblock Copolymer Syntheses of Mesoporous Silica with Periodic 50 to 300 Angstrom Pores. *Science* **1998,** *279* (5350), 548-552.

29. Drader, J. A.; Zhu, L.; Smith, P.; McCann, K.; Boyes, S.; Braley, J. C., Assessment of monoamide extractants and solid supports as new extraction chromatographic materials. *Separation and Purification Technology* **2016,** *163*, 352-356.

30. Vasilef, I., QtiPlot: Data Analysis and Scientific Visualization. Universitet Utrecht, Utrecht, Netherlands, 2013.

31. Shafer, J. C.; Sulakova, J.; Ogden, M. D.; Nash, K. L., Remediation of potentially acidified Hanford wastes using tri-n-octyl phosphine oxide extraction chromatographic materials. *Separation and Purification Technology* **2018,** *202* (November 2017), 157-164.

32. Sing, K. S. W.; Williams, R. T., Physisorption Hysteresis Loops and the Characterization of Nanoporous Materials. *Adsorption Science & Technology* **2004,** *22* (10), 773-782.

33. Shin, H. J.; Ryoo, R.; Kruk, M.; Jaroniec, M., Modification of SBA-15 pore connectivity by high-temperature calcination investigated by carbon inverse replication. *Chemical Communications* **2001,** (4), 349-350.

34. Xin, W.; Song, Y., Mesoporous carbons: recent advances in synthesis and typical applications. *RSC Advances* **2015,** *5* (101), 83239-83285.

35. Zhang, Y.; Yang, S.; Yuan, X.; Zhao, Y.; Tian, G., Separating lanthanides and actinides from nitric acid solutions by using N,N-di(2-ethylhexyl)-diglycolamic acid (HDEHDGA). *Chem. Commun.* **2017,** *53* (48), 6421-6423.

36. Pierce, T. B.; Hobbs, R. S., The separation of the rare earths by partition chromatography with reversed phases: Part I. Behaviour of column material. *Journal of Chromatography A* **1963,** *12*, 74-80.

37. Mason, G. W.; Metta, D. N.; Peppard, D. F., The extraction of selected M(III) metals by bis 2-ethylhexyl phosphoric acid in n-heptane. *Journal of Inorganic and Nuclear Chemistry* **1976,** *38* (11), 2077-2079.

38. Fan, Q. H.; Shao, D. D.; Hu, J.; Chen, C. L.; Wu, W. S.; Wang, X. K., Adsorption of humic acid and Eu (III) to multi-walled carbon nanotubes: EFFECT of pH, ionic strength and counterion effect. *Radiochimica Acta* **2009,** *97* (3), 141-148.

39. Gupta, N. K.; Sengupta, A., Understanding the sorption behavior of trivalent lanthanides on amide functionalized multi walled carbon nanotubes. *Hydrometallurgy* **2017,** *171* (February), 8-15.

40. Kumar, P.; Sengupta, A.; Singha Deb, A. K.; Ali, S. M., Poly(amidoamine) Dendrimer Functionalized Carbon Nanotube for Efficient Sorption of Trivalent f-Elements: A Comparison Between 1stAnd 2ndGeneration. *ChemistrySelect* **2017,** *2* (3), 975-985.

CHAPTER 6 SUMMARY AND OUTLOOK FOR THE FUTURE

6.1 Summary

Therapeutic proteins have been a significant promise for the treatment of diseases like cancer and diabetes. Proteins are highly specific in their action and cause minimal adverse side effect compared to low molecular weight drugs. Delivery of proteins have been demonstrated using various delivery systems such as polymers, liposomes and carbon nanotubes. As compared to these delivery systems, MSN have been demonstrated as an ideal candidate for the effective delivery of proteins to its target site under physiological conditions and protection from proteases and denaturation chemicals. MSN exhibit high loading capacity, tunable pore size and morphology as well as biocompatibility. The surface of MSN can be decorated by a variety of functional groups which serves to control the movement of molecules in and out of the pores. Thus, the entrapping guest molecules can be released upon exposure to a specific stimulus. MCM-41 type MSN have successfully loaded and delivered only small proteins due to the synthetic limitation of its pore size. Therefore, the delivery of large multi-subunit proteins still remains a substantial challenge.

A versatile and facile method have been manifested to load homomeric proteins into MSN with potential applications in enhancing the delivery of large therapeutic proteins. Concanavalin A (*Con A*) and Yeast alcohol dehydrogenase, with a mass of 104 kDa and 145 kDa, were chosen as a model homomeric proteins. Mesoporous silica nanoparticles (MSN) with enlarged pores were successfully synthesized and characterized, and reversibly dissociated subunits of model large homomeric protein molecules were entrapped in the mesopores. This was confirmed by multiple biochemical and material characterization. When loaded in the MSN, protein stability

from proteases and, upon release, the subunits reconstituted into active proteins was demonstrated.

In Chapter 5, synthesis of two OMC materials using different silica template, OMC-*l*-MSN and CMK-3 type OMC, was succesfully demonstrated. OMC materials were physisorbed with HDEHP for Eu^{3+} and Nd^{3+} recovery. Depending on the concentration and number of HDEHP additions, loading on the marterial was varied. Higher loading of the OMC-*l*-MSN material was accomplished through multiple HDEHP additions comapred to single addition. The uptake of Eu^{3+} by these materials was compared against commercially available polyacrylic ester-based LN Resin. HDEHP-OMC materials showed high loading capacities and distribution coefficients than the LN Resin. The batch Langmuir isotherm and breakthrough column studies showed greater maximum adsorption capacity for HDEHP-OMC-*l*-MSN comapred to the LN Resin. The OMC materials have at least double the maximum adsorption capacity.

6.2 Future work

The studies described herein, demonstrated in-vitro release of protein from MSN. To execute effective intracellular delivery, in-vivo studies must be conducted. The method of therapeutic protein delivery may be expanded to include heteromeric proteins and larger, multi-subunit enzymes in the future. Due to different multiple subunits in heteromeric protein, its adsorption and desorption rates can vary and therefore could be more challenging; however, re-association of dissociated heteromeric proteins may still be possible to recover active protein.

In Chapter 5, separation of the *f*-elements Nd and Eu using HDEHP physisorbed OMC as a chromatographic material was successfully demonstrated. The separation of elements was carried out using an unpressurized system and a small comact column. Further research is needed to find the maximum amount of HDEHP-OMC material that can accommodate into a column

before back-pressure issues arise which would lead toresolution optimization of the HDEHP-OMC-*l*-MSN columns. The preliminary studies of the HDEHP physisorbed OMC materials indicates that they are prime candidates as solid-phase sorbents for *f*-element recovery and separation. Hence, further studies with covalent attachment of other ligands using OMC materials can be studied for lanthanides separation.

Gauri Deodhar
<gdeodhar@mymail.mines.edu>

Permission to use our Langmuir paper

7 messages

Gauri Deodhar Sun, Jul 29, 2018 at
<gdeodhar@mymail.mines.edu> 9:58 AM
To: Marisa Adams <madams2@mymail.mines.edu>, sutapa joardar <sutapajor@yahoo.co.in>, joglekarmadhura1@gmail.com, Sydney Toler <stoler410@gmail.com>, Maddie Mettler <maddiekm0320@gmail.com>, Fiona Davies <fdavies@mines.edu>
Cc: Brian Trewyn <btrewyn@mines.edu>

Hi all,

Will you please grant me your permission to use our Langmuir paper titled 'Conserved activity of re-associated homotetrameric protein subunits released from mesoporous silica nanopartciles' as one of my thesis chapter?

Thanks,
Gauri

Sydney Toler Sun, Jul 29, 2018 at
<stoler410@gmail.com> 10:32 AM
To: Gauri Deodhar <gdeodhar@mymail.mines.edu>

Hi Gauri,

I give you my permission to use this paper as one of your thesis chapters! Good luck with it!

Sydney Toler
[Quoted text hidden]

Fiona Davies <fdavies@mines.edu> Sun, Jul 29, 2018 at 2:39 PM
To: Gauri Deodhar <gdeodhar@mymail.mines.edu>

Hi Gauri,

Yes, you have my permission to use our paper as a chapter in your thesis.

All the best,
Fiona
[Quoted text hidden]

Madhura Joglekar <joglekarmadhura1@gmail.com> Sun, Jul 29, 2018 at 11:03 PM
To: Gauri Deodhar <gdeodhar@mymail.mines.edu>
Cc: Marisa Adams <madams2@mymail.mines.edu>, sutapa joardar <sutapajor@yahoo.co.in>, Sydney Toler <stoler410@gmail.com>, Maddie Mettler <maddiekm0320@gmail.com>, Fiona Davies <fdavies@mines.edu>, Brian Trewyn <btrewyn@mines.edu>

Hi gauri congrats on your defense date. Sure, you can use this paper for your reference .
Thanks,
Madhura
[Quoted text hidden]

---

sutapa joardar <sutapajor@yahoo.co.in> Mon, Jul 30, 2018 at 8:44 AM
To: Gauri Deodhar <gdeodhar@mymail.mines.edu>, Madhura Joglekar <joglekarmadhura1@gmail.com>
Cc: Marisa Adams <madams2@mymail.mines.edu>, Sydney Toler <stoler410@gmail.com>, Maddie Mettler <maddiekm0320@gmail.com>, Fiona Davies <fdavies@mines.edu>, Brian Trewyn <btrewyn@mines.edu>

Hi Gauri,
Congratulations for thesis. Sure, you can incorporate the paper in the thesis. Wish you best luck.
Best,

Sutapa Joardar
Assistant Professor, Department of Biotechnology, Neotia Institute of Technology, Mangaement and Science (NITMAS), Jhinga,South 24 Parganas
West Bengal, india

To: Gauri Deodhar <gdeodhar@mymail.mines.edu>

Gauri,

Of course! Congratulations!

Maddie

> On Jul 29, 2018, at 9:58 AM, Gauri Deodhar <gdeodhar@mymail.mines.edu> wrote:
>

[Quoted text hidden]

Marisa Adams <madams2@mymail.mines.edu> Mon, Jul 30, 2018 at 10:05 AM
To: sutapa joardar <sutapajor@yahoo.co.in>
Cc: Gauri Deodhar <gdeodhar@mymail.mines.edu>, Madhura Joglekar <joglekarmadhura1@gmail.com>, Sydney Toler <stoler410@gmail.com>, Maddie Mettler <maddiekm0320@gmail.com>, Fiona Davies <fdavies@mines.edu>, Brian Trewyn <btrewyn@mines.edu>

You also have my permission to use the paper as a thesis chapter!

[Quoted text hidden]

Gauri Deodhar
<gdeodhar@mymail.mines.edu>

Permission to use our Biotechnology review paper

2 messages

Gauri Deodhar <gdeodhar@mymail.mines.edu> Sat, Jul 28, 2018 at 6:15 PM
To: Marisa Adams <madams2@mymail.mines.edu>
Cc: Brian Trewyn <btrewyn@mines.edu>

Hi Marisa,

Will you please grant me your permission to use our biotechnology review paper titled 'Controlled release and intracellular protein delivery from mesoporous silica nanoparticles' as one of my thesis chapter?

Thank you,
Gauri

Marisa Adams <madams2@mymail.mines.edu> Sat, Jul 28, 2018 at 6:17 PM
To: Gauri Deodhar <gdeodhar@mymail.mines.edu>
Cc: Brian Trewyn <btrewyn@mines.edu>

Sure thing! You have my permission.

JOHN WILEY AND SONS LICENSE TERMS AND CONDITIONS

AL

This Agreement between Gauri Deodhar ("You") and John Wiley and Sons ("John Sons") consists of your license details and the terms and conditions provided by Jc and Sons and Copyright Clearance Center.

License Number	4402020060826
License date	Aug 04, 2018
Licensed Content Publisher	John Wiley and Sons
Licensed Content Publication	Biotechnology Journal
Licensed Content Title	Controlled release and intracellular protein delivery from mesoporous silica nanoparticles
Licensed Content Author	Gauri V Deodhar, Marisa L Adams, Brian G Trewyn
Licensed Content Date	Dec 14, 2016
Licensed Content Volume	12
Licensed Content Issue	1
Licensed Content Pages	13
Type of use	Dissertation/Thesis
Requestor type	Author of this Wiley article
Format	Print and electronic
Portion	Full article
Will you be translating?	No
Title of your thesis / dissertation	Loading and release of large protein molecules using mes silica nanoparticles
Expected completion date	Aug 2018
Expected size (number of pages)	130
Requestor Location	Gauri Deodhar 17611 W 16th Ave Apt 201 GOLDEN, CO 80401 United States Attn: Gauri Deodhar

Publisher Tax ID	EU826007151
Total	0.00 USD

Terms and Conditions

TERMS AND CONDITIONS

This copyrighted material is owned by or exclusively licensed to John Wiley & So one of its group companies (each a"Wiley Company") or handled on behalf of a so which a Wiley Company has exclusive publishing rights in relation to a particular (collectively "WILEY"). By clicking "accept" in connection with completing this l transaction, you agree that the following terms and conditions apply to this transac (along with the billing and payment terms and conditions established by the Copyr Clearance Center Inc., ("CCC's Billing and Payment terms and conditions"), at the you opened your RightsLink account (these are available at any time at http://myaccount.copyright.com).

Terms and Conditions

- The materials you have requested permission to reproduce or reuse (the "Wi Materials") are protected by copyright.
- You are hereby granted a personal, non-exclusive, non-sub licensable (on a s alone basis), non-transferable, worldwide, limited license to reproduce the W Materials for the purpose specified in the licensing process. This license, an **CONTENT (PDF or image file) purchased as part of your order**, is for a use only and limited to any maximum distribution number specified in the li The first instance of republication or reuse granted by this license must be co within two years of the date of the grant of this license (although copies prep before the end date may be distributed thereafter). The Wiley Materials shall used in any other manner or for any other purpose, beyond what is granted in license. Permission is granted subject to an appropriate acknowledgement gi author, title of the material/book/journal and the publisher. You shall also du copyright notice that appears in the Wiley publication in your use of the Wil Material. Permission is also granted on the understanding that nowhere in th previously published source acknowledged for all or part of this Wiley Mate third party content is expressly excluded from this permission.
- With respect to the Wiley Materials, all rights are reserved. Except as expres granted by the terms of the license, no part of the Wiley Materials may be co modified, adapted (except for minor reformatting required by the new Publi translated, reproduced, transferred or distributed, in any form or by any mea derivative works may be made based on the Wiley Materials without the pri permission of the respective copyright owner.**For STM Signatory Publishe clearing permission under the terms of the STM Permissions Guideline**